The Second Realization of the International Celestial Reference Frame by Very Long Baseline Interferometry

Presented on behalf of the IERS[1]/ IVS[2] Working Group
Chair: C. Ma (CM)
and
Members: F. Arias (FA), G. Bianco, D. Boboltz (DB), S. Bolotin (SB1), P. Charlot (PC), G. Engelhardt, A. Fey (AF), R. Gaume, A.-M. Gontier (AMG), R. Heinkelmann, C. Jacobs (CJ), S. Kurdubov (SK), S. Lambert (SL1), Z. Malkin, A. Nothnagel (AN), L. Petrov, E. Skurikhina, J. Sokolova, J. Souchay, O. Sovers, V. Tesmer, O. Titov (OT), G. Wang, V. Zharov
and
Contributors: S. Böckmann (SB2), A. Collioud (AC), J. Gipson, D. Gordon (DG), S. Lytvyn (SL2), D. MacMillan (DM), R. Ojha (RO)
and
Editors: A. Fey (AF), D. Gordon (DG)

DRAFT: July 14, 2009

ABSTRACT

This Technical Note describes the generation of a second realization of the International Celestial Reference Frame (ICRF2) at radio wavelengths using nearly 30 years of very long baseline interferometry (VLBI) observations, by an international team. ICRF2 contains precise positions of 3414 compact radio astronomical sources, more than five times the number as in the first ICRF, hereafter ICRF1. Further, the ICRF2 is found to have a noise floor of only ≈ 40 μas, some $5-6$ times better than ICRF1, and an axis stability of ≈ 10 μas, nearly twice as stable as ICRF1. Alignment of ICRF2 with the International Celestial Reference System (ICRS) was made using 138 stable sources common to both ICRF2 and ICRF-Ext2. Future maintenance of ICRF2 will be made using a set of 295 new "defining" sources selected on the basis of positional stability and the lack of extensive intrinsic source structure. The stability of these 295 defining sources, and their more uniform sky distribution eliminates the two largest weaknesses of ICRF1.

---

[1]International Earth Rotation and Reference System Service (IERS)

[2]International VLBI Service for Geodesy and Astrometry (IVS)

Contents

List of Tables

List of Figures

1. Introduction (DG, CM)

The International Celestial Reference Frame (hereafter referred to as ICRF1) was the realization of the International Celestial Reference System (ICRS) at radio frequencies (Ma et al. 1997). It was defined by the very long baseline interferometry (VLBI) positions of 212 "defining" compact radio sources. These positions were independent of the equator, equinox, ecliptic, and epoch, but were made consistent with the previous stellar and dynamical realizations within their respective errors. The usage of VLBI for celestial reference frames was outlined by Gontier, Feissel & Ma (1997). The ICRF1 used most geodetic/astrometric VLBI data taken between August 1979 and July 1995, and contained 608 sources. It was adopted by the IAU in 1997 and became official on 1 January 1998. Two extensions, adding 109 additional sources (Fey et al. 2004) were later made using several years of newer VLBI data, including the first of a series of Very Long Baseline Array (VLBA) Calibrator Surveys (VCS) (Beasley et al. 2002).

ICRF1 had an estimated noise floor of 250 micro-arc-seconds (μas) and an estimated axes stability of ≈ 20 μas. This represented roughly an order of magnitude improvement over the previous stellar celestial reference frame, the FK5 (Fricke et al. 1988). Even so, it had its limitations and deficiencies. The distribution of defining sources was very nonuniform, with most being in the northern hemisphere. Additionally, several of the original defining sources have been found to be unstable (showing significant systematic position variations).

Significant developments and improvements in geodetic/astrometric VLBI have been made since the generation of ICRF1. Geodetic/astrometric VLBI sensitivity and quality have improved significantly due to developments such as wider single channel bandwidths, wider spanned bandwidths, receiver improvements, and better observing strategies. Also, the use of newer and more sensitive antennas and arrays, such as the 10 station VLBA, has greatly improved the sensitivity and quality of the data as well. And additional new observing programs, such as the VLBA Research and Development VLBI (RDV) sessions, the southern hemisphere celestial reference frame (CRF) sessions, the weekly large network R1 and R4 Earth Orientation Parameter (EOP) sessions, and the VCS sessions have greatly improved the quality and quantity of the available VLBI data. Also, better geophysical modeling and faster computers have allowed for significant improvements in the data analysis. The additional 14 years of data now allow us to select a set of stable sources distributed more uniformly on the sky to more precisely define the axes. The additional data also allows us to filter out the most unstable sources for special handling, avoiding possible distortion of the frame that might occur otherwise. Additionally, there is now also a large amount of imaging data (e.g., the USNO Radio Reference Frame Image Database[3] and the Bordeaux VLBI Image Database [4]), mostly from analysis of the RDV sessions. Sources with extensive structure can thus be identified and eliminated from use in defining a reference frame. The ICRF1 used $\sim$1.6 million group delay measurements. At the current time, there are $\sim$6.5

[3]http://rorf.usno.navy.mil/RRFID/

[4]http://www.obs.u-bordeaux1.fr/BVID/

million VLBI S/X-band group delay measurements available for use. The number of sources has also increased substantially. The ICRF1 contained 608 sources and was later expanded to 717. There are currently over 1200 sources whose positions can be obtained from the regular geodetic/astrometric sessions, and the number of far-southern sources has increased greatly. When we include the purely astrometric VCS sessions, nearly 2200 additional sources can be added, for a total of over 3400 sources. As previously mentioned, the sensitivity and quality of the data has also improved, and a conservative estimate is that the current noise floor has been reduced by a factor of 5 or more over ICRF1. Thus, there are many reasons for a new realization of the ICRF.

Greater accuracy and stability of the ICRF would have benefits in at least two areas. It would allow improvements in spacecraft navigation using differential VLBI relative to a nearby ICRF source. Also benefiting would be the VLBI monitoring of Earth orientation parameters, particularly of precession/nutation and UT1, which are the unique domain of VLBI. Enhanced stability and accuracy are needed for studies of the small, variable effects of deep structures of the Earth. Also, the upcoming Gaia mission will require much more precise positions of bright quasars in order to get the best optical-radio registration.

Since the adoption of ICRF1 by the IAU in 1997, the work of maintaining the ICRS was given to the IERS, with the International VLBI Service for Geodesy and Astrometry (IVS) having operational responsibility for the VLBI realization. An IERS/IVS Working Group was established specifically for the second realization of the ICRF. This Working Group is truly an international team, with members in the USA, France, Germany, Italy, Russia, Ukraine, Australia, and China. This report describes the work of that team towards the generation of the second realization of the ICRF, hereafter referred to as ICRF2¡. In the following sections we will present details of the preliminary work towards picking unstable sources, various model and data comparisons, the data used, comparisons of preliminary catalog solutions, the configuration of the catalog solution, an evaluation of the realistic uncertainties, selection of the final axes-defining sources, the presentation of the ICRF2 catalog, and prospects for the future.

The Working Group studied the VLBI data using several independent software analysis packages, including Calc/Solve, OCCAM, SteelBreeze, and Quasar, all of which will be described briefly later in this report. Preliminary work with all the software packages included the generation and study of source position time series to identify stable and unstable sources, the generation and inter-comparison of preliminary catalogs, and the creation and study of a combination catalog. In the end, it was decided to use a single catalog rather than a combination for several reasons. The solutions going into the combination catalog all had some small differences in geophysical modeling, in editing criteria, and/or in data used. Also a combination catalog loses certain information, such as the full covariance matrix, and the links to the EOP and the Terrestrial Reference Frame (TRF) solutions. Although the final ICRF2 catalog is based on a single solution done at the NASA Goddard Space Flight Center (GSFC), the generation of ICRF2 has truly been an international group effort. The ICRF2 could not have been realized as accurately and with as much understanding of the limiting errors and noise levels without the participation of all the analysis centers and

software packages involved.

2. The Data (DG)

The celestial reference frame results presented in this Technical Note come from nearly 30 years of accumulated geodetic/astrometric VLBI sessions organized and scheduled by many groups in many regional and worldwide campaigns. The major organizers have included the GSFC, the NASA Jet Propulsion Laboratory (JPL), the National Geodetic Survey (NGS), the US Naval Observatory (USNO), the Naval Research Lab (NRL), the Geodetic Institute University of Bonn, Bundesamt für Kartographie und Geodäsie (BKG), and the Geographic Survey Institute (GSI) of Japan. The International VLBI Service (IVS) was formed in 1999, and took over coordination of the geodetic/astrometric campaigns, but the scheduling and analysis of individual sessions is still done by the individual member groups.

The earliest data used in this report is from 1979 August 3 and the latest is from 2009 March 16. All sessions used were dual frequency S/X-band (2.3/8.4 GHz) VLBI sessions taken either with the Mark III, Mark IV, VLBA, K4, K5, or combinations of these VLBI hardware/software systems. The participating antennas were all either dedicated geodetic stations or radio astronomical telescopes which spend most of their time doing astronomical research. The fixed antennas used here are located on all continents – with antennas in Antarctica, Australia, Brazil, Canada, Chile, China, Germany, Italy, Japan, Norway, Russia, Spain, South Africa, Sweden, Ukraine, and the USA. Most of the VLBI data used here was taken primarily for geodetic purposes, but is also well suited for astrometric analysis. A typical VLBI geodetic/astrometric experiment uses several antennas during a typical 24-hr data taking session.

The S/X-band systems record simultaneously several narrow channels ($2 - 8$ MHz) spanning broader bandwidths ($\sim 100 - 700$ MHz). The combination of both bands allows for a first order correction for the dispersive effects of the Earth's ionosphere. In most of the VLBI sessions used, there were eight individual channels at X-band and six at S-band. Exceptions are the VLBA sessions, which use only four channels each at of S- and X-bands.

There were a total of 4540 sessions used for the final ICRF2 catalog, with approximately 6.5 million S/X-band ionosphere-corrected group delay measurements. The VLBI sessions used for ICRF2 include:

- Most fixed station sessions that are 18 hours or longer.
- Most of the Western U.S. and Alaska Crustal Dynamics Project (CDP) Mobile sessions, plus other sessions with mobile antennas – provided at least two large fixed antennas also participated. The three mobile systems were small transportable antennas of 3, 5, and 9 meter aperture. The two smaller systems occupied several dozen sites in the U.S., Canada, the Caribbean, and Europe during the 1980's and early 1990's.

- Most VLBA correlated and AIPS fringed S/X-band VLBA and VLBA+Mark IV sessions, a total of 168 such sessions. This includes 72 RDV sessions (January 1997 - December 2008) and 24 VCS sessions (August 1994 - January 2007).

- Most one-baseline southern hemisphere Celestial Reference Frame sessions, coordinated by USNO.

- 74 one-baseline NASA Deep Space Network sessions from 1988 August 20 – 1994 September 04 that were used in ICRF1 for consistency with ICRF1, even though some are of shorter duration than 18 hrs.

Sessions that were not used include various small and regional sessions (JADE, Canadian regional, most European mobiles), various "ties" sessions, several short one-baseline sessions, and other special sessions not suitable for astrometric analysis. Also, no single band data (X-band only, S-band only, K-band, Q-band, Ka-band, etc.) was used.

It is important to note that the data used in this work is a very heterogeneous data set. The networks involved ranged from as little as 2 stations (1 baseline) to as large as 20 stations (190 baselines). Antenna sizes ranged from 3 meters up to 100 meters. The distribution of the fixed antennas was also very uneven. Out of some 53 antennas used over the past 30 years, only 10 have been in the southern hemisphere. Currently, there are some 34 fixed antennas that regularly or occasionally participate in geodetic/astrometric sessions, but only seven of those are in the southern hemisphere. This distribution directly affects the data available for the ICRF2. The amount of data begins to drop off quickly for sources south of around -30° declination. In recent years, the USNO has made great efforts to observe new sources in the far south using the HARTRAO and HOBART antennas, and this has added several dozen such sources. But with the mechanical failure of HARTRAO in 2008, further progress in this area has been severely curtailed.

Worth mentioning is the contribution of the VLBA in improving the precision of the ICRF2. The VLBA[5] is an astronomical VLBI array of ten 25-meter antennas, all on U.S. territory. The VLBA antennas are some of the most sensitive and phase stable systems available. Details of their geodetic/astrometric use are given by Petrov et al. (2009). Use of the Pietown VLBA antenna began in 1988 followed by the Los Alamos (LA-VLBA) antenna in 1991. Use of all 10 VLBA antennas, and correlation on the VLBA correlator began in 1994. In a 2004 study, Gordon (2004) found that the regular VLBA (non-VCS) observations accounted for some 30% of the available geodetic/astrometric VLBI data and its usage improved the TRF at non-VLBA sites by typically 10-40% and reduced the average source position formal errors by ∼62% in R.A. and ∼54% in declination for sources north of -30° declination. This means the formal errors are roughly cut in half by a combination of more data and higher data quality due to VLBA usage. Currently, VLBA data comprises ∼28% of all the data used in this report.

[5]The VLBA is operated by the National Radio Astronomy Observatory, which is a facility of the National Science Foundation, and operated under cooperative agreement by Associated Universities, Inc.

The VCS were a series of six multi-session S/X-band astrometry campaigns designed to map and find precise positions of as many new compact radio sources as possible for use as phase referencing calibrators by the radio astronomical community. The first of these, VCS-1, was observed $1994-1997$, and its 10 sessions are described and analyzed by Beasley et al. (2002). An eleventh VCS-1 session, initially considered a failure, was later found and analyzed successfully. Five follow up VCS campaigns were made between 2002 and 2007 by Fomalont et al. (2003), Petrov et al. (2005), Petrov et al. (2006), Kovalev et al. (2007), and Petrov et al. (2008). These added another 13 VCS sessions for a total of 24. The observing mode was much different from regular geodetic/astrometric sessions. The VCS sessions concentrated on making short observations of many new sources. They were not optimized for full sky coverage or atmospheric calibration, although the later ones were better calibrated than the first. The VCS sessions add nearly 2200 additional sources to the catalog, with most of those observed in only one VCS session. In spite of that, many of the VCS source positions are as precise as many non-VCS sources.

3. VLBI Analysis Software (DG)

Several software packages have been developed over the years for VLBI processing and/or analysis. All have been developed independently by different groups. Four such software packages were used in studying the data included in ICRF2 and in generating preliminary and final solutions. In the following sections, we briefly describe each one.

3.1. Calc/Solve (DG)

The Calc/Solve analysis package has been under development and in use for over 30 years, with most of the development work being done by the VLBI group at the GSFC. It is the oldest, and most complete of the VLBI geodetic/astrometric analysis packages. It is composed of over one hundred different programs used for the creation and calibration of database session files, the analysis of individual sessions or mass analysis of multiple sessions, and many other assorted tasks. Calc/Solve was built around the original Mark III database handler, which dates back to the late 1970's. Calc/Solve is the only analysis package which allows for single session editing and updating of individual VLBI sessions. As such, Calc/Solve provides the analyzed database versions which the other analysis packages depend on for their analysis.

Program Calc contains most of the geophysical models and computes a theoretical VLBI delay and delay rate for each observation in a session, consistent with the IERS Conventions (2003) (McCarthy & Petit 2004). Calc also computes many of the partial derivatives of the delay and delay rates with respect to various parameters (such as nutation, polar motion, UT1, site positions, source coordinates, etc), which are used in the analysis to solve for adjustments of those parameters. Calc also has an active role in the VLBI correlation process, as it is used at most of the world's VLBI geodetic and astronomical correlators (the three Mark IV correlators, the VLBA correlator, the JIVE correlator, the ATNF correlator,

and the DiFX software correlator) to compute the correlator model delays for offsetting the bit streams from the different antennas.

Solve is made up of a large family of programs for both single session analysis and multiple session analysis. It performs a least-squares fit and parameter adjustments using the Calc theoretical delays and partial derivatives, the observed delays, and additional models and partials. Solve has two modes, an interactive single session analysis mode and a non-interactive global analysis mode. In the single session analysis mode, the analyst reads in the Calc'ed and calibrated X-band and S-band databases. They then perform ambiguity resolution (either automatically or manually); perform the ionosphere calibration; set the clock, atmosphere, and other parametrization; edit the data on each baseline (either automatically or manually); and update the X-band database. The analyzed, updated session version can then be used in the global analysis mode. In the non-interactive, global analysis mode, Solve is used to analyze large groups of sessions. It uses the arc-parameter elimination method described in Ma et al. (1990). It can solve for various arc parameters (adjusted for each session) and global parameters (adjusted once for the entire data set). The use of Solve for generation of the ICRF2 solution is described in §7.

Calc/Solve was originally written in Fortran 77, and ran on a variety of HP machines for many year. Several years ago, it was converted to Fortran 90 and Linux. It is now most commonly used on Linux PC's under a variety of Linux operating systems.

3.2. SteelBreeze (SB1)

Software SteelBreeze was developed from scratch as a tool for geodetic VLBI data analysis at the Main Astronomical Observatory of the National Academy of Sciences of Ukraine. It performs a least-squares estimation of various geodynamical parameters using the Square Root Information Filter (SRIF) algorithm (Biermann 1977). SRIF allows the introduction of stochastic models for parameter estimation.

The software imports geodetic VLBI observations in known formats (NGS cards and Mark III databases). It stores observations as well as catalogs of radio sources, stations, EOP, ephemerides, and some other data sets in its own inner binary formats.

SteelBreeze analyzes VLBI data (group delays) of single and multiple sets of sessions. The time delay is modeled according to the IERS Conventions (2003) (McCarthy & Petit 2004), and other additional models (tectonic plate motions, nutation models, wet and hydrostatic zenith delay, mapping function, etc). The software makes estimations of the following parameters: Earth orientation parameters, coordinates and velocities of selected sets of stations, coordinates of selected sets of radio sources, clock functions and wet zenith delays and gradients, axis offsets, Love numbers, etc.

The SRIF algorithm allows estimations of unbiased parameters as well as stochastic ones. In SteelBreeze, each estimated parameter can be one of the following types:

- Global parameter: unbiased estimation for an entire set of selected sessions (typically applied for source and station coordinates estimation, etc.).

- Local parameter: unbiased estimation at each session. The estimates on different sessions are considered to be independent (e.g., EOP).
- Local parameter with time propagation: unbiased estimation at each session, the estimates on adjacent sessions are dependent according to a given rule.
- Stochastic parameter: the behavior of the estimated parameter is assumed to be varying with time with a given rule (implemented: white noise, 2^{nd} order Markov process, random walk). This type is useful for estimation of clock parameters and wet zenith delays.
- Stochastic parameter with time propagation: the same as above, but adjacent estimations for different sessions are tied with the same rule.

SteelBreeze is written in C++, uses the Qt user interface library and runs on Linux/GNU system.

3.3. OCCAM (OT)

The OCCAM software package (Titov et al. 2004a) analyzes VLBI data by the least-squares collocation method (LSCM) (Titov et al. 2004b). The LSCM minimizes a function similar to the conventional least-squares method and, additionally, it takes into account intra-day correlations between observations. These correlations are calculated from external data, in the case of VLBI, from the data about stochastic behavior of hydrogen maser clocks and wet components of troposphere delays and gradients. All estimated parameters are split into three groups based on their properties: stochastic, estimated for every epoch (clock functions and wet troposphere delays); daily or 'arc' parameters to be approximately constant within a 24-hour session; and so-called 'global' parameters, which are constant over the total period of observations.

3.4. QUASAR (SK)

QUASAR is the VLBI analysis software package developed by the Institute of Applied Astronomy of the Russian Academy of Sciences. It uses the least-squares collocation technique. Most of the reduction calculations are implemented according to the IERS Conventions (2003) (McCarthy & Petit 2004). QUASAR software supports both single and multi-session adjustment. There is a wide list of parameters which have partials and can be estimated. Every parameter can be estimated as a global, arc or stochastic parameter. Every parameter can be represented as a polynomial function over the span of one session or the entire observation period. The Vienna Mapping Function (VMF1) (Boehm, Werl, & Schuh 2006) is used for the tropospheric delay. QUASAR has two options for atmospheric loading: a one-dimensional regression model and a three dimensional numerical model. Antenna and axis offset thermal deformation are also accounted for. Celestial Intermediate Pole (CIP)

formalism is used for Celestial pole coordinates and derivations. For nutation adjustments, QUASAR estimates the new CIP-X and CIP-Y instead of $d\psi$, $d\epsilon$.

For the iaa008c catalogue, VLBI observations from 1980 to 2009.03.30 (mostly from the GSFC list) were used. There were a total of 6353387 group delays. The celestial reference frame was defined by no-net-rotation (NNR) constraints on the coordinates of 203 sources from the ICRF1 "defining" list. The VTRF2008 catalog was used for *a priori* station positions. No-net-translation and no-net-rotation constraints were applied for the coordinates and velocities of 11 stations: MATERA, KOKEE, WETTZELL, FORTLEZA, WESTFORD, ALGOPARK, NYALES20, NOTO, ONSALA60, LA-VLBA, MK-VLBA. Coordinates of all radio sources, and positions and velocities of all stations were estimated as global parameters. EOP's were estimated as local parameters. Clock functions were estimated as the sum of a quadratic polynomial and a stochastic function. Tropospheric wet zenith delays were estimated as the sums of linear and stochastic parts. Total tropospheric gradients were estimated as local parameters with no constraints and no *a priori* model applied. For coordinates of sources that were observed fewer than 5 times, a soft 10 cm constraint was applied. For velocities of stations participating in fewer than 5 session or time spans less than one year, a soft 10 cm constraint was applied. Atmospheric pressure loading was applied using the Petrov & Boy (2004) 3D model and the Vienna Mapping Function (VMF1) (Boehm, Werl, & Schuh 2006) was used.

4. Selection and Treatment of Special Handling Sources (DG, DM)

The radio sources observed were, in most cases, distant compact quasars or other active galactic nuclei. The positions of most of the sources were treated as global parameters in the least-squares solutions. This means that all the observations of each source in all the sessions were combined to estimate a single average position. For these global sources, the amount of data varied from as little as 3 observations in one session, to as many as ∼337300 observations in 4068 sessions (source 0552+398, which was observed in 89.6% of the sessions).

Studies of source positional stability were carried out by running solutions which generated time series of the source positions, i.e., a separate position for each observing session. Various statistics of the right ascension (RA) and declination of the sources were examined, such as weighted root-mean-square (wrms) variations about the mean, χ^2 per-degree-of-freedom, smoothed 2-year slopes, and other statistics. Some of these statistics were later used to identify the most stable sources, discussed later in this report. Smoothed and unsmoothed time series plots were also studied. One goal was to identify sources so unstable as to require special handling. Special handling sources were to be treated as arc parameters, with their positions estimated once for each session. A further goal was to keep this list as small as possible. Some 39 sources were selected for special handling. Most of these are sources that were observed in many sessions and which show significant positional instability in either RA and/or Declination. Some of these are strong sources that have been observed sparingly in recent years because of known adverse source structure effects on geodetic solutions (such as 3C84, 3C273B, 3C279, 3C345, and 3C454.3). A few

are sources that have not been observed heavily, but still show convincing systematic position variations. Estimating the positions of these problem sources globally would yield grossly underestimated position uncertainties and could possibly distort the overall reference frame. Therefore they were treated as arc parameters. The positions given for them in the catalogs are the weighted means of their time series positions and the uncertainties are the wrms positions about the weighted means. Seven of these special handling sources were original ICRF1 defining sources (0014+813, 0235+164, 0637−752, 0738+313, 1308+326, 1448+762, and 2145+067). The 39 special handling sources are: 0014+813, 0106+013, 0202+149, 0208−512, 0212+735, 0235+164, 0238−084 (NGC1052), 0316+413 (3C84), 0430+052 (3C120), 0438−436, 0451−282, 0528+134, 0607−157, 0637−752, 0711+356, 0738+313, 0919−260, 0923+392 (4C39.25), 0953+254 (OK290), 1021−006, 1044+719, 1226+023 (3C273B), 1253−055 (3C279), 1308+326, 1404+286 (OQ208), 1448+762, 1458+718 (3C309.1), 1611+343, 1610−771, 1641+399 (3C345), 1739+522, 2121+053, 2128−123, 2134+004 (2134+00), 2145+067, 2201+315, 2234+282, 2243−123, and 2251+158 (3C454.3). Time series plots of these 39 special handling sources are shown in Figure 1 to Figure 10. The plotted points are 45-day averages.

It should not be assumed that there are only 39 unstable sources among the ∼3400 available sources. The vast majority of the sources have not been observed with the frequency necessary to detect the type of small systematic position variations seen, for example in sources like 0014+813, 0235+164, 0528+134, or 1044+719. Many other sources showed smaller position variations, but at a level that did not cause concern.

There were also many sources that were excluded from the solutions for various reasons. Included in this category were three known gravitational lenses and six known radio stars. The gravitational lenses present analysis problems in assigning a single position and the radio stars were too weak to be used. Also excluded from the solution were 795 sources which had either zero or only one or two good group delay observations. A reliable position cannot be determined from only one or two observations. Most of these were sources either too weak or too spatially extended to be detected in the VCS sessions.

5. Characterization of Source Structure (PC, AC, AF, RO, DB)

As noted above, there is now a large amount of imaging data which can be used to both filter out the most extended sources and identify the most compact sources for defining the ICRF2 frame. In order to assess the astrometric quality of the sources, we used the so-called "structure index" (SI) defined by Fey & Charlot (1997), modified as to obtain a continuous structure index scale as described below. The structure index indicates the expected magnitude of the effects of intrinsic source structure on VLBI delay observations according to the median value of the structure delay corrections, $\tau_{\rm median}$, calculated for all projected VLBI baselines that could be observed with Earth–bound VLBI, using the algorithm devised by Charlot (1990). While Fey & Charlot (1997) separated the sources into four categories, with values of the structure index ranging from 1 to 4, we adopted a

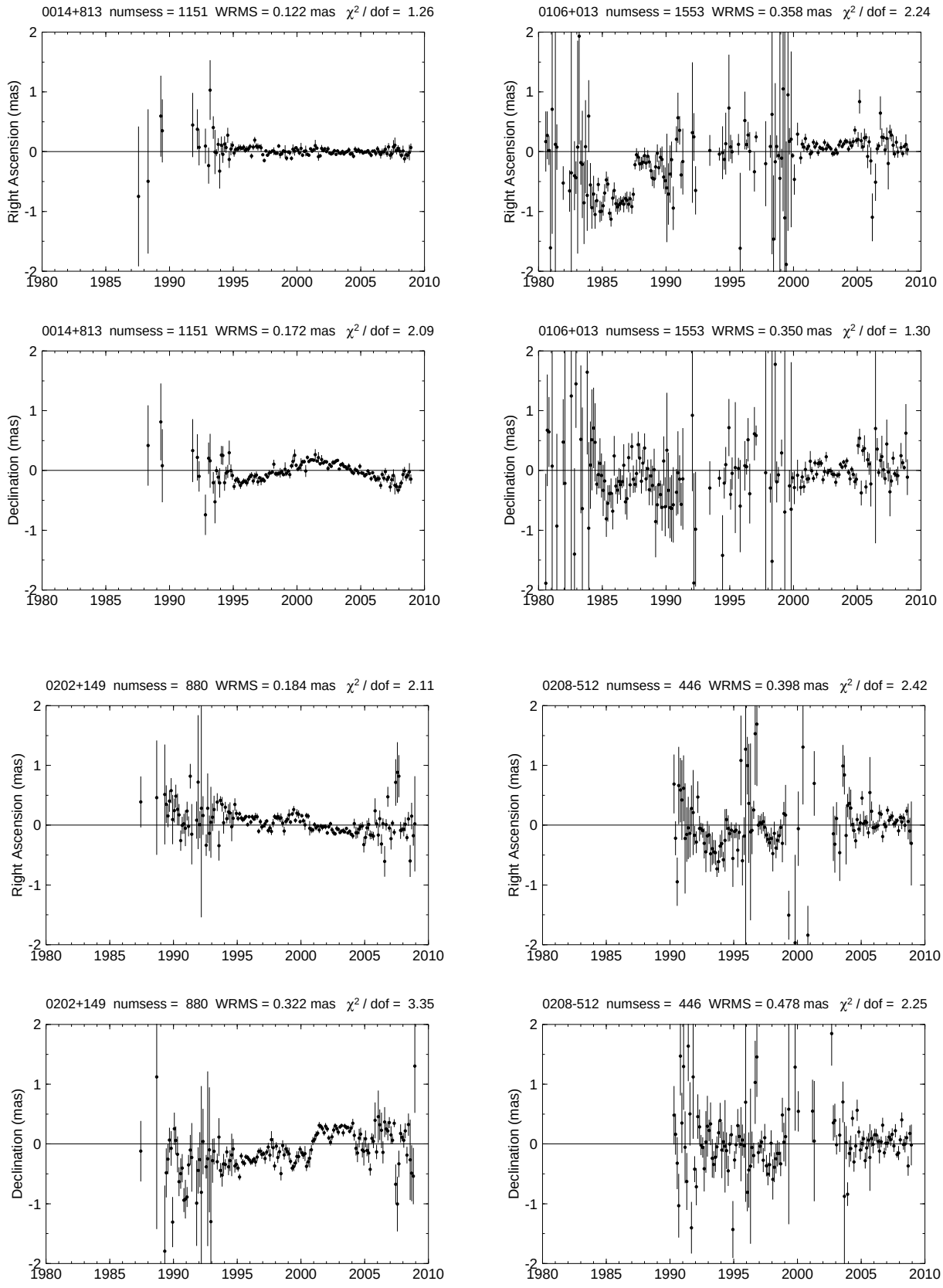

Fig. 1.— Time series plots of the 39 special handling sources.

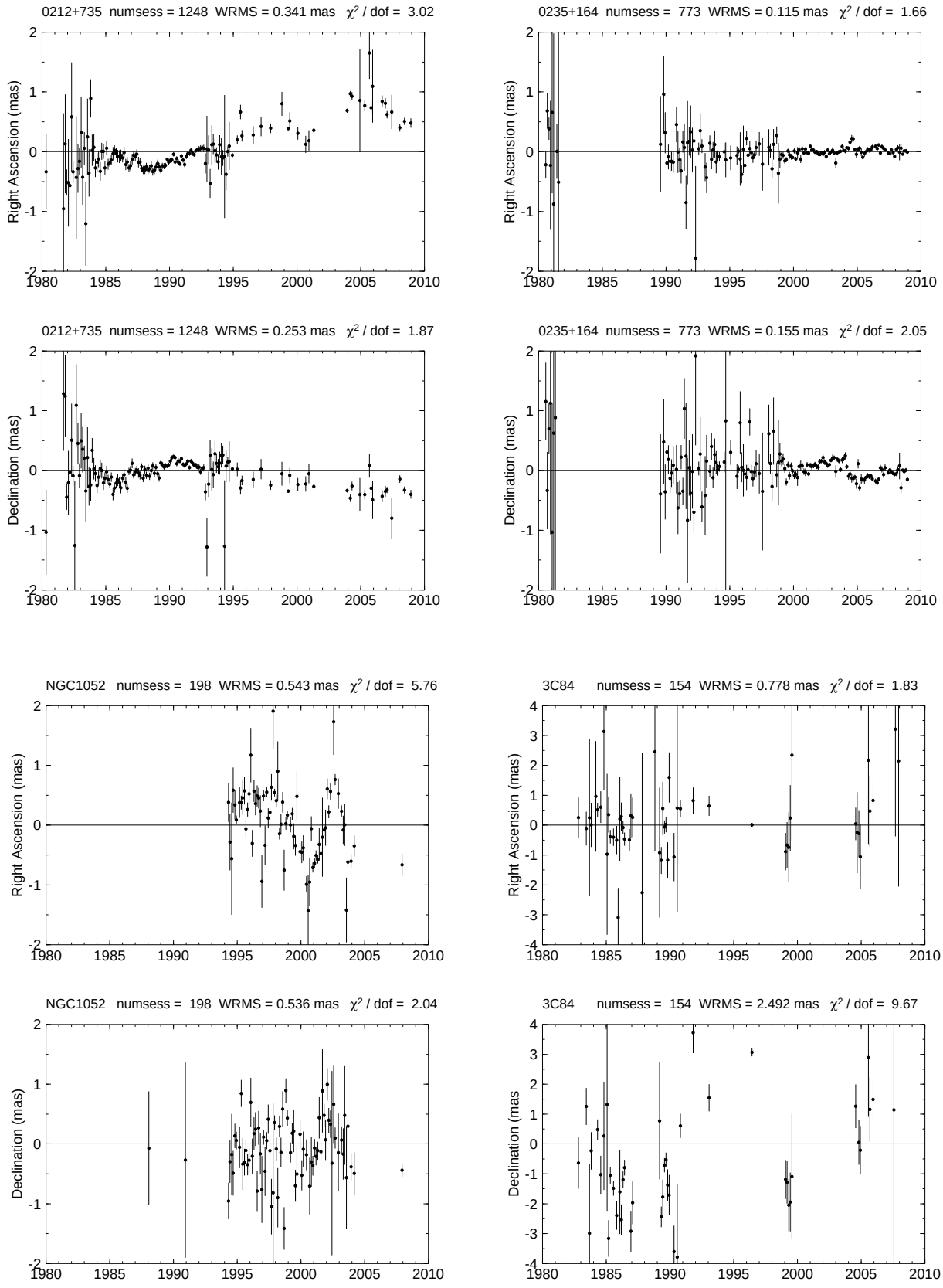

Fig. 2.— Time series plots of the 39 special handling sources – continued.

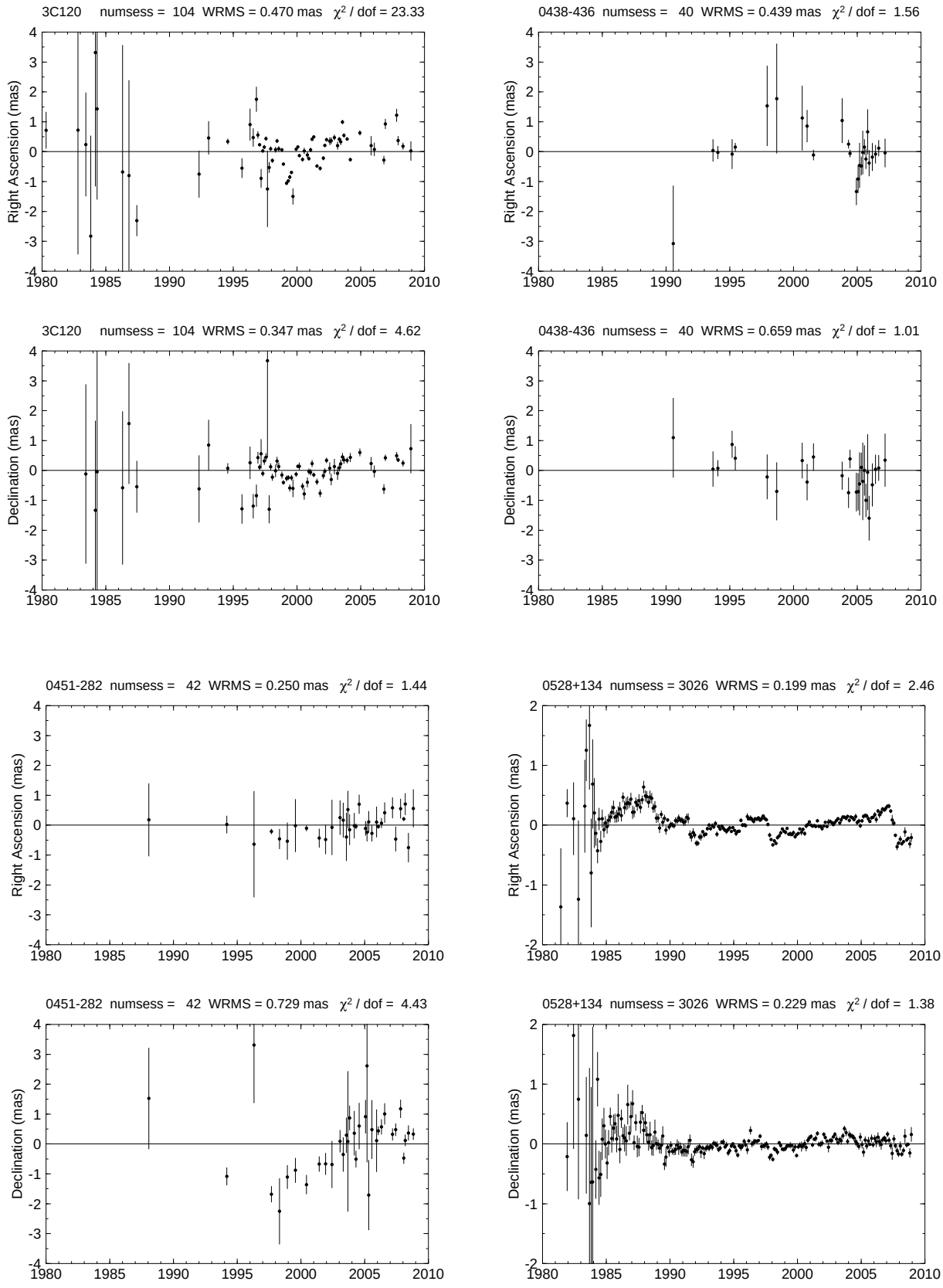

Fig. 3.— Time series plots of the 39 special handling sources – continued.

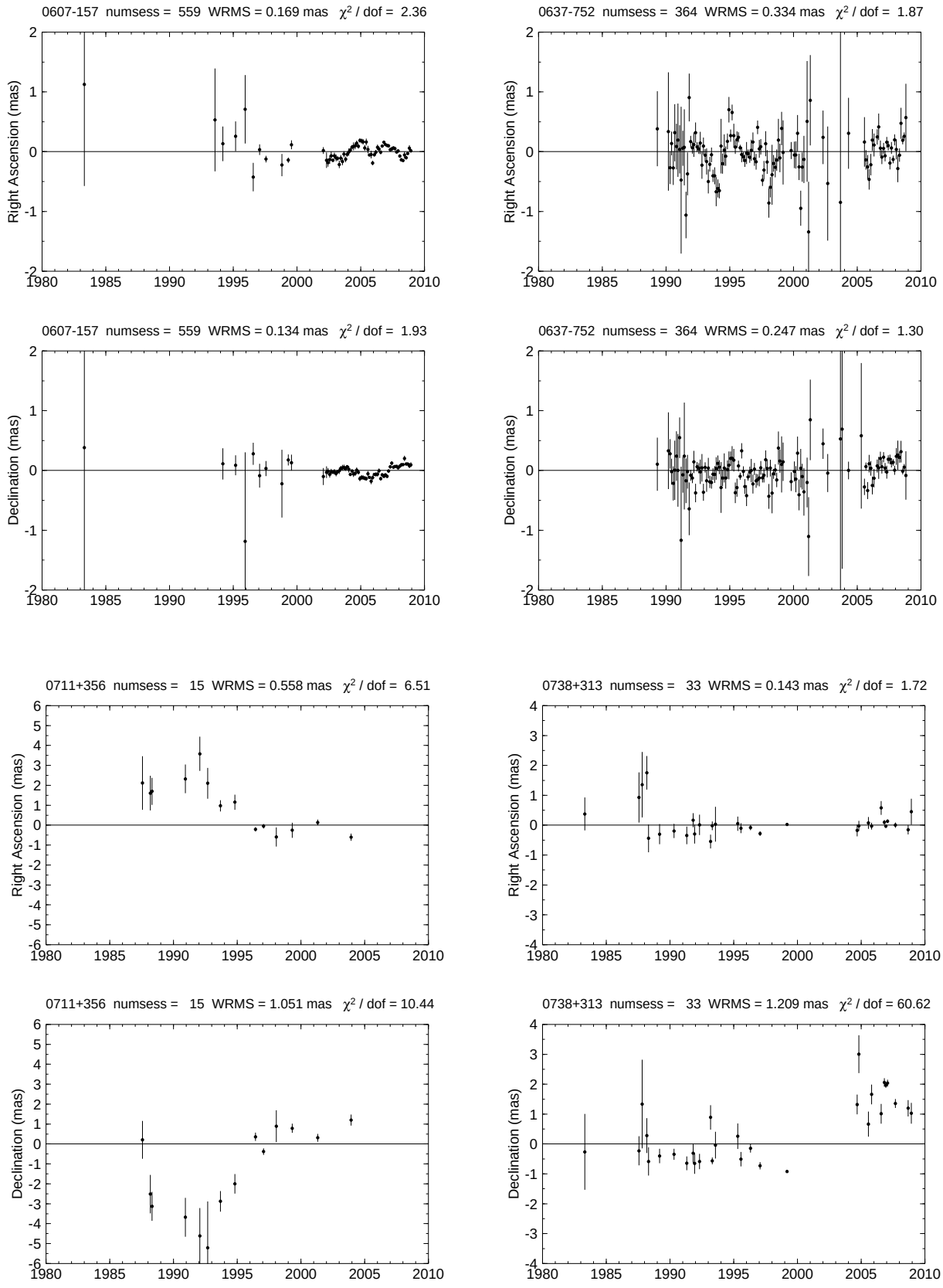

Fig. 4.— Time series plots of the 39 special handling sources – continued.

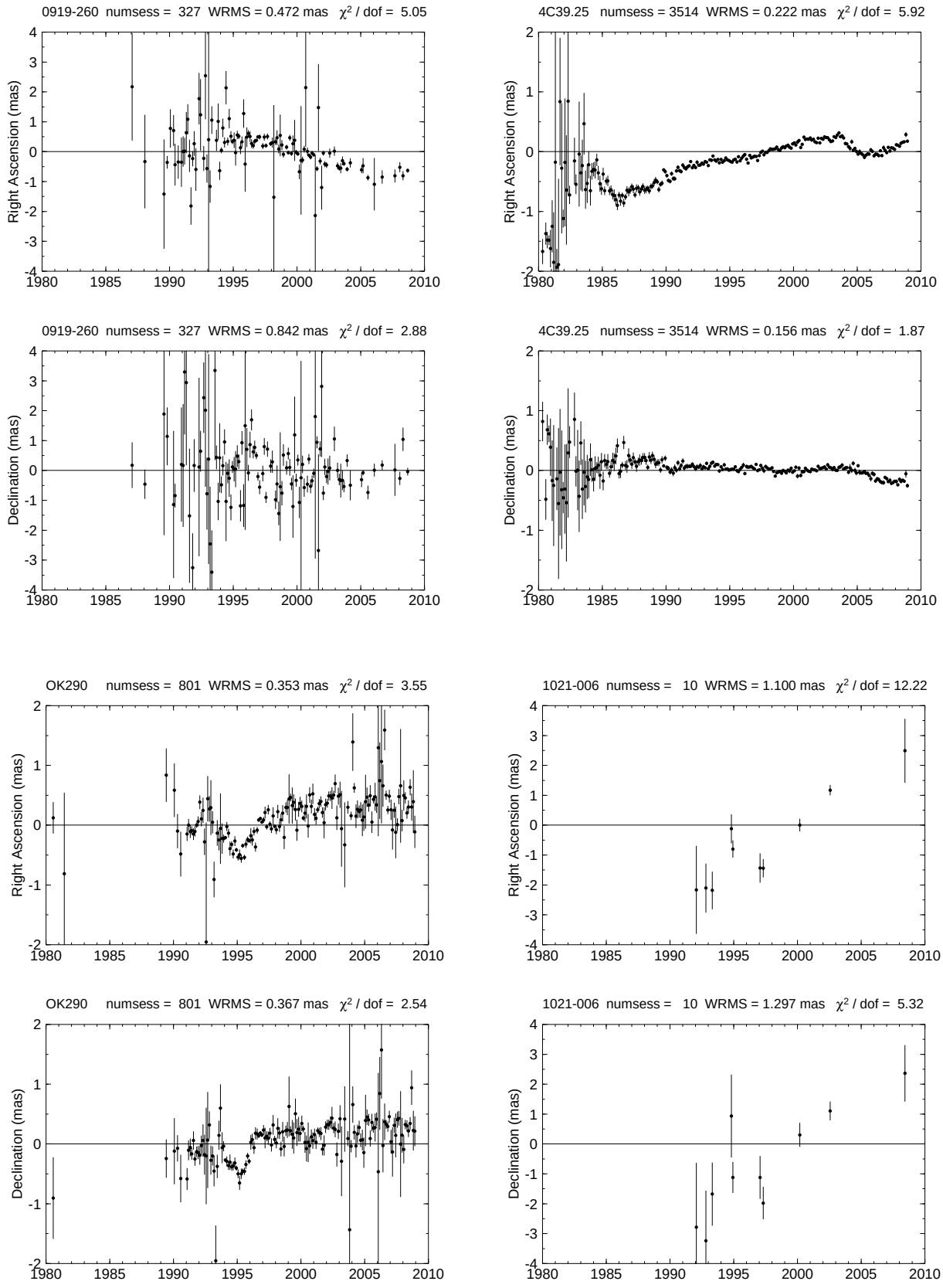

Fig. 5.— Time series plots of the 39 special handling sources – continued.

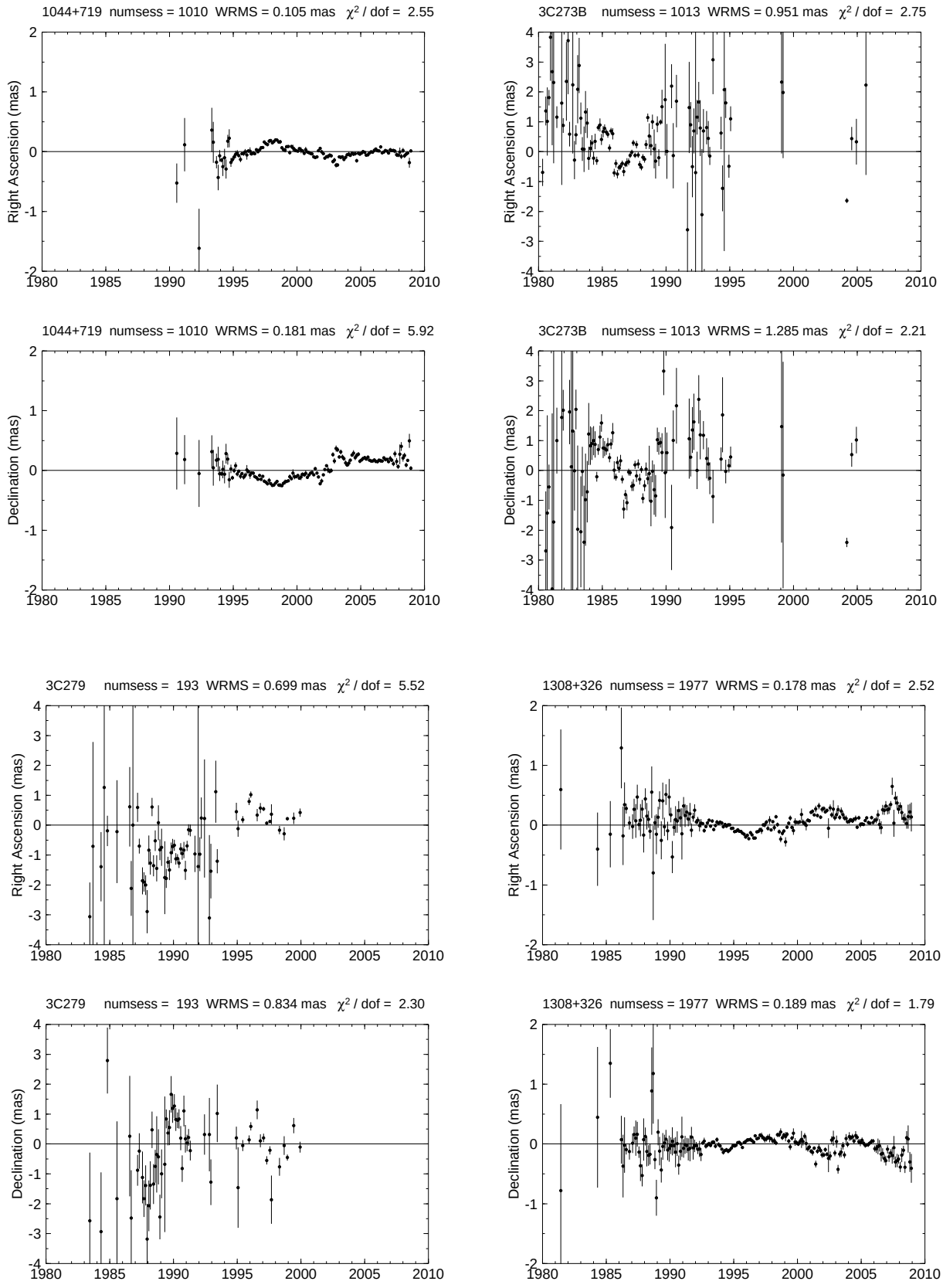

Fig. 6.— Time series plots of the 39 special handling sources – continued.

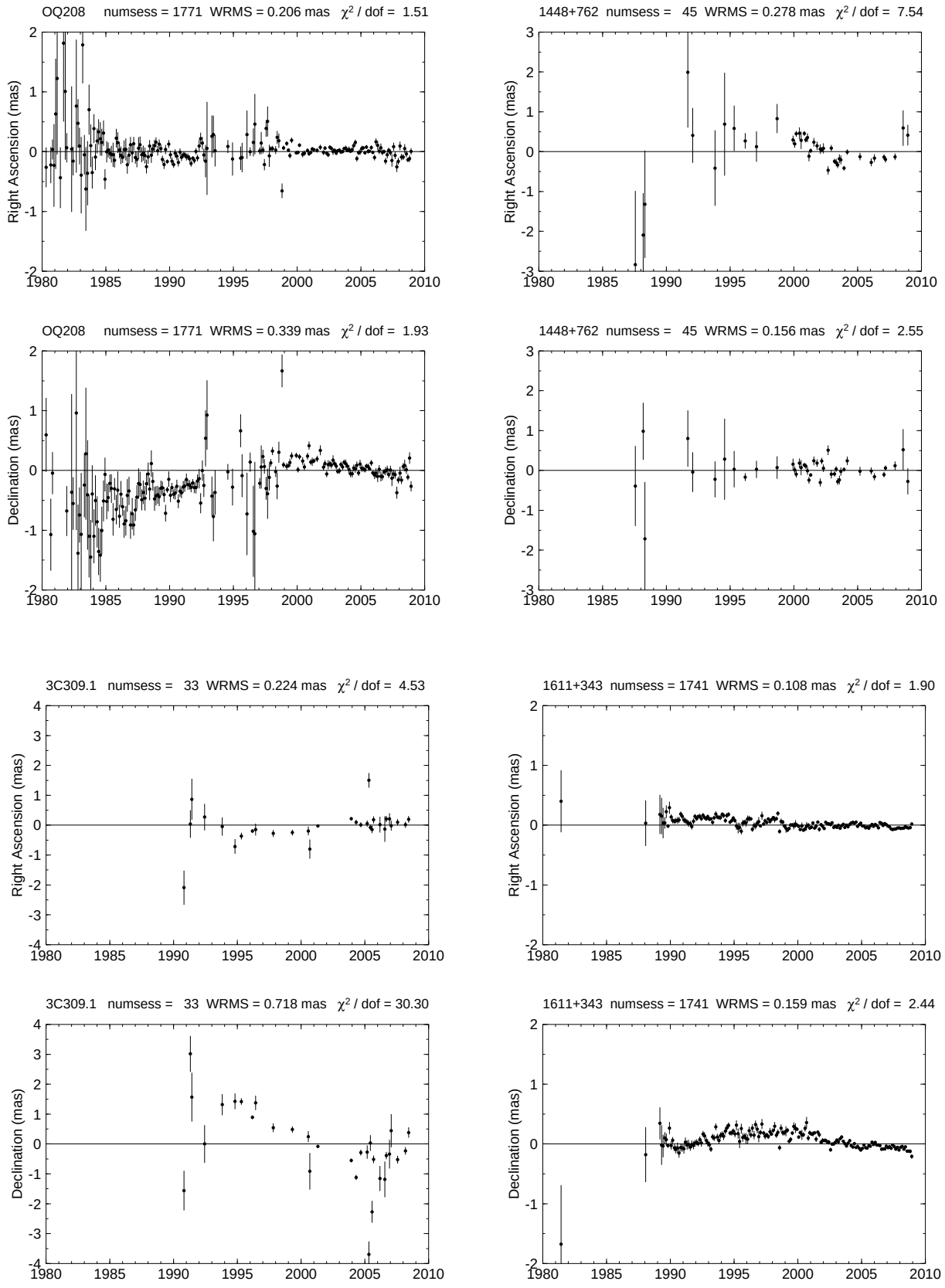

Fig. 7.— Time series plots of the 39 special handling sources – continued.

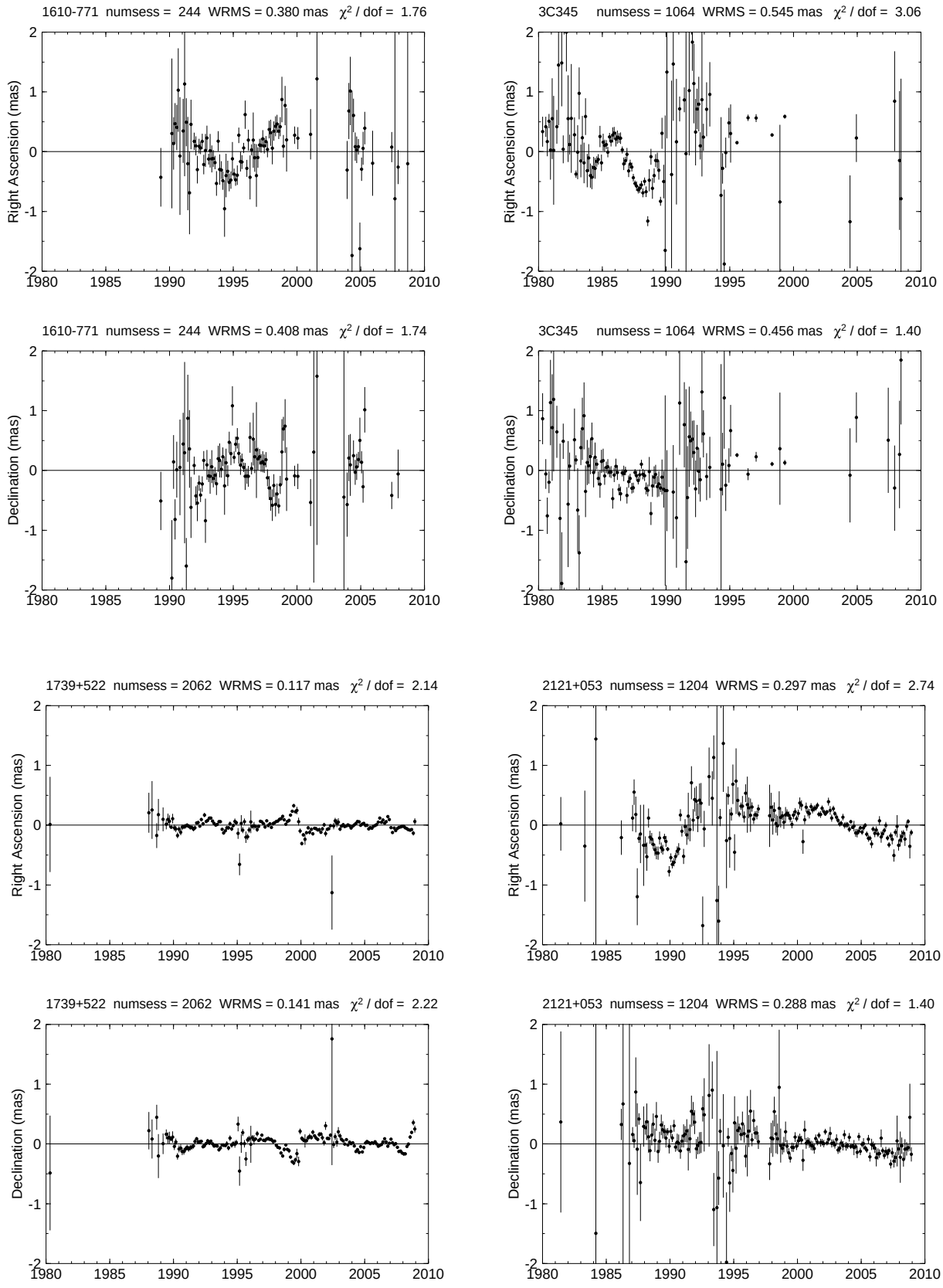

Fig. 8.— Time series plots of the 39 special handling sources – continued.

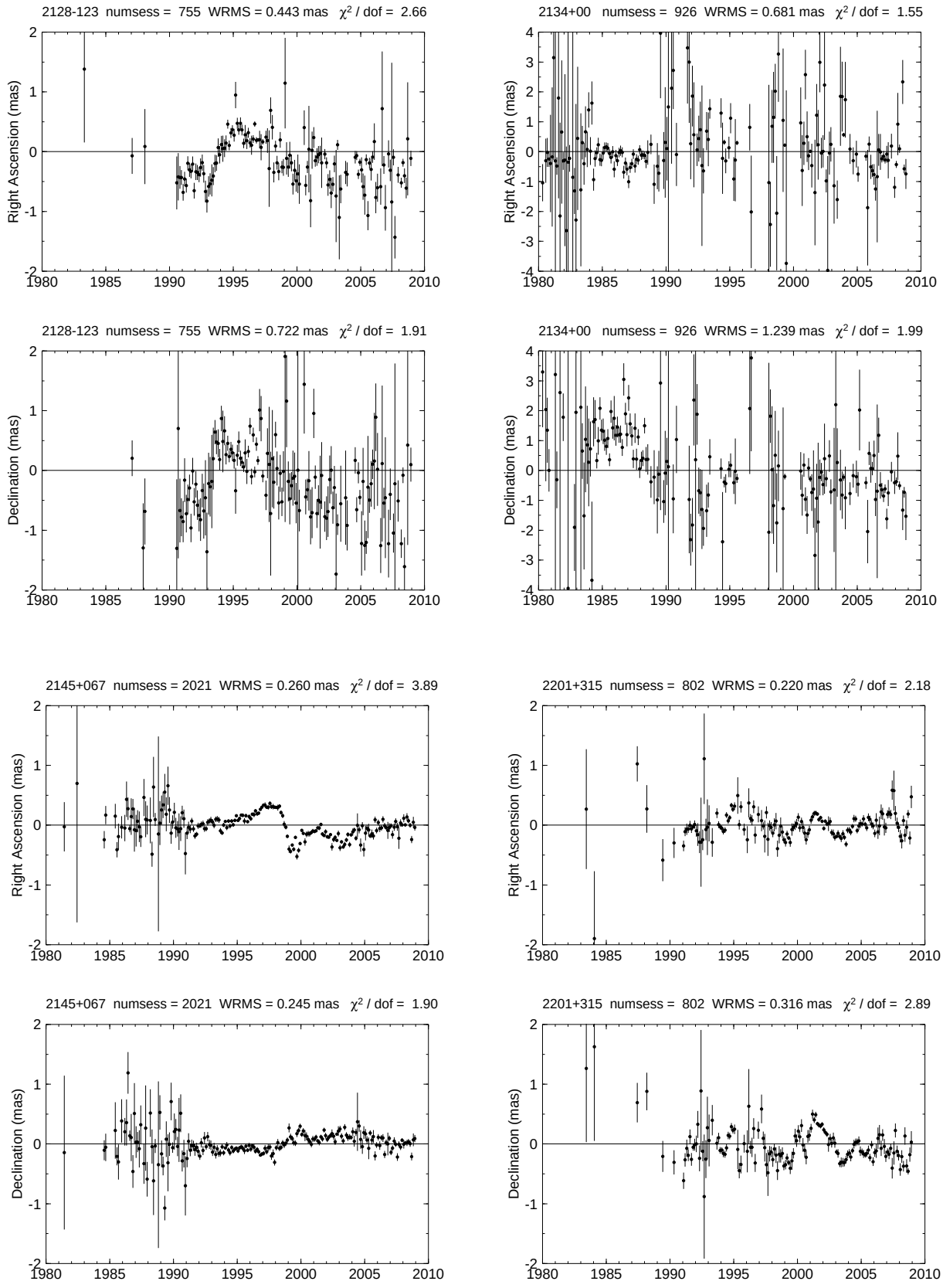

Fig. 9.— Time series plots of the 39 special handling sources – continued.

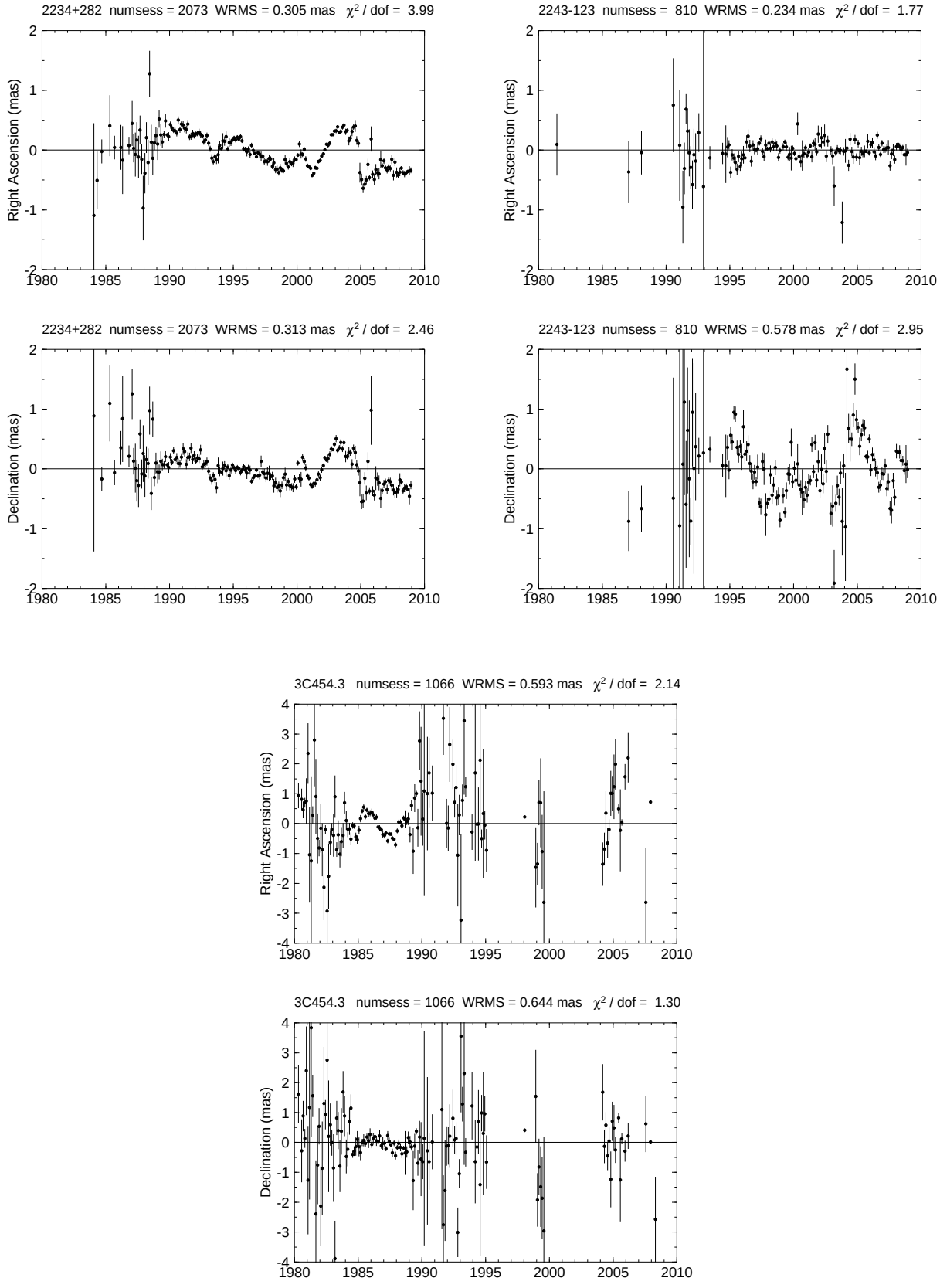

Fig. 10.— Time series plots of the 39 special handling sources – continued.

continuous scale for the present work and defined the structure index SI as follows:

$$\mathrm{SI} = 1 + 2\log\left(\tau_{\mathrm{median}}\right) \tag{1}$$

where τ_{median} is expressed in picoseconds (ps). Additionally, we constrained SI values to remain always positive by setting SI = 0 when $\log\left(\tau_{\mathrm{median}}\right) < -0.5$ (i.e., $\tau_{\mathrm{median}} <\sim 0.3$ ps). As shown in Figure 11, there is close correspondence at the (discrete) SI boundaries between the continuous SI values defined here and the values defined in Fey & Charlot (1997) (SI = 1.95 vs 2 for $\tau_{\mathrm{median}} = 3$ ps, SI = 3.00 vs 3 for $\tau_{\mathrm{median}} = 10$ ps, SI = 3.95 vs 4 for $\tau_{\mathrm{median}} = 30$ ps). Therefore, the recommendation of Fey & Charlot (1997) that sources with SI values of 3 or 4 should preferably not be used for high-precision VLBI astrometry remains largely valid with this new definition of the structure index.

Based on the above definition, structure indices were derived for 707 different sources by using a total of 3052 X-band VLBI images from the USNO Radio Reference Frame Image Database and Bordeaux VLBI Image Database for epochs between 1994 and 2008. The vast majority of the images for the sources north of about $-40°$ declination were obtained from RDV sessions or from earlier VLBA sessions (Fey et al. 1996; Fey & Charlot 1997, 2000). For the sources in the far south, the images are from dedicated southern-hemisphere VLBI sessions (Ojha et al. 2004, 2005). Nearly half of the sources (337 sources) have been imaged at only a single epoch whereas the most-intensively observed source (0727−115) has 32 images available. For the sources imaged at more than one epoch, an additional step was taken and the mean SI over all epochs was calculated. The time series of structure indices were also scrutinized to check for outliers, possibly caused by images with low dynamic range or poor resolution, which may affect the mean SI values, and for SI variability over time, which is indicative of astrophysical instabilities.

All source structure indices derived in this way, including the number of images on which the mean SI values are based, are reported in Table 1. Sources with good structure index (SI < 3.0) but which show significant SI variations over time or have bad structure at S band are also marked in the table. The distribution of the mean SI values is plotted in Figure 12. These values peak at about 2.75, corresponding to a value of 7.5 ps for the delay structure correction. Also marked in Figure 12, are the special handling sources discussed in the previous section, all of which but 0438−436 have a structure index available. Based on our calculation, it is found that 26 sources of these have a SI value larger than 3.0, which is an indication of extended emission. In addition, 6 of the remaining 12 sources that have a mean SI smaller than 3.0 (0528+134, 0919−260, 0923+392, 1044+719, 2145+067, 2234+282) are marked as variable in Table 1, which indicates that they are likely to show positional instabilities. Overall, more than 80% of the special handling sources are thus found to be unsuitable for the highest astrometric accuracy when considering solely their structure, in agreement with the findings in the previous section.

Finally, it is to be noted that the structure index values listed in Table 1 represent a snapshot of the imaging data available at the time this work was carried out and that these values may evolve with time. While sources with already many images are likely to show

only small variations of structure index in the future, those with only a single image may in some cases show larger variations due to temporal changes in their structure.

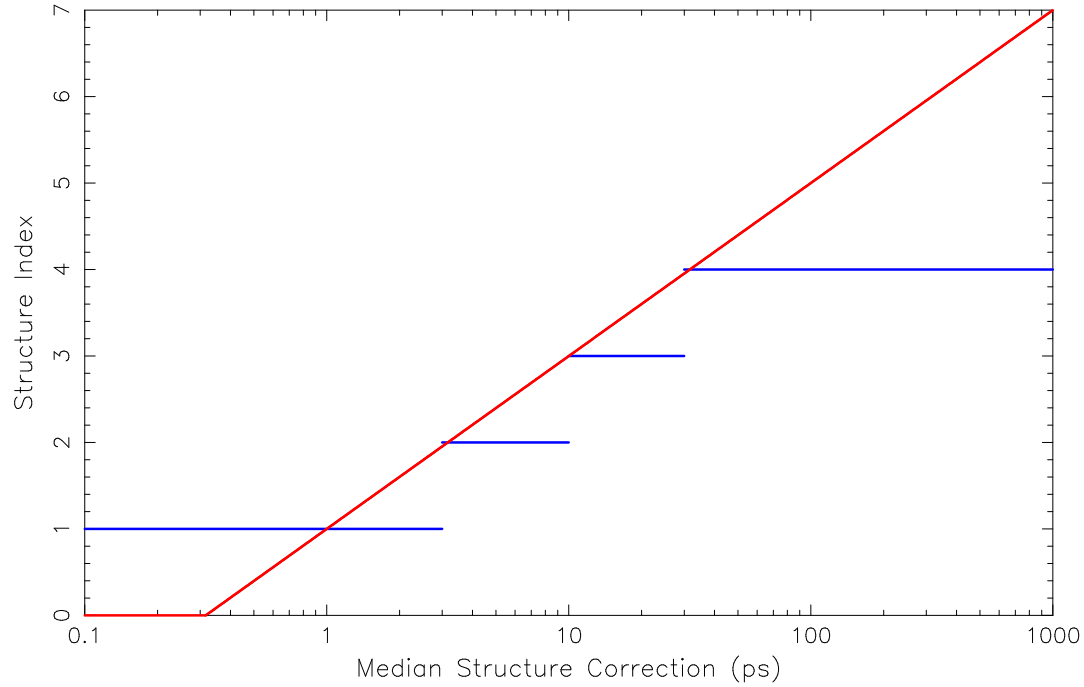

Fig. 11.— Correspondence between the discrete structure index defined by Fey & Charlot (1997), plotted in blue, and the continuous structure index from Equation 1, plotted in red.

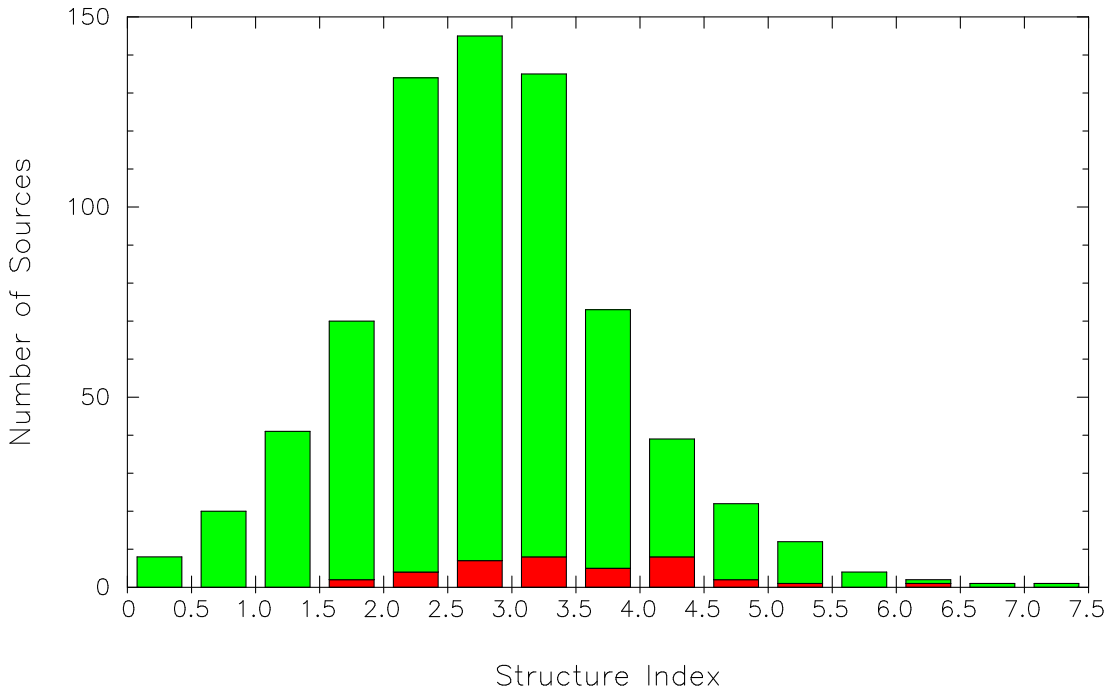

Fig. 12.— Distribution of the mean structure index for 707 sources with VLBI images available from the USNO Radio Reference Frame Image Database or Bordeaux VLBI Image Database. The special handling sources discussed in §4 are color-coded in red.

Table 1. Mean source structure index values at X-band (8.4 GHz) for 707 sources with VLBI images available from the USNO Radio Reference Frame Image Database (RRFID) or Bordeaux VLBI Image Database (BVID).

Source name	Number of maps	Structure Index	Source name	Number of maps	Structure Index	Source name	Number of maps	Structure Index
0003+380	3	3.4	0149+218	5	2.9‡	0333+321	2	3.7
0003−066	25	3.1	0150−334	1	4.5	0335−364	1	3.6
0007+106	3	0.9	0151+474	2	2.2	0336−019	28	3.0†
0007+171	3	3.7	0153+744	2	5.0	0338−214	1	3.4
0008−264	1	1.6	0159+723	3	1.9	0340+362	1	2.5
0009+081	1	0.6	0159−117	1	3.4	0341+158	1	2.5
0010+405	2	2.6	0201+113	21	3.1	0342+147	2	2.9
0013−005	2	2.2	0202+149	21	3.1	0345+460	1	3.1
0014+813	22	2.5	0202+319	4	1.8	0346−279	1	2.3
0016+731	2	2.1†	0202−172	1	3.2	0347−211	1	2.4
0017+200	1	2.2	0202−765	1	3.4	0350+465	1	2.4
0019+058	3	1.4	0208−512	1	2.3	0355+508	2	2.0
0025+197	1	1.6	0209+168	1	3.2	0358+040	1	1.4
0026+346	1	5.0	0211+171	1	0.8	0358+210	1	0.8
0035+413	1	2.8	0212+735	6	3.1	0400+258	4	3.0
0035−252	1	1.8	0215+015	1	1.4	0400−319	1	3.0
0039+230	3	4.2	0219+428	4	3.1	0402−362	19	2.4
0046+316	5	3.1	0220−349	2	3.2	0403−132	1	0.6
0047−579	1	3.8	0221+067	4	2.4	0405+304	1	1.8
0048−097	28	1.1	0224+671	4	3.3	0405−123	4	3.1
0048−427	1	1.8	0229+131	20	2.4	0405−385	9	2.3
0054+161	1	1.2	0234+285	18	2.6	0406+121	3	2.9
0055+300	1	3.6	0235+164	13	1.8	0406−127	2	3.1
0056−001	1	4.3	0237+040	1	2.4	0409+229	2	3.4
0056−572	1	5.0	0237−027	2	2.0	0410+110	1	2.5
0059+581	29	1.6	0237−233	2	5.6	0414−189	3	1.8
0103+127	1	3.6	0238−084	16	4.4	0415+398	1	1.6
0104−408	25	1.3	0239+108	3	3.0	0420+417	4	3.3
0106+013	6	3.2	0239+175	1	3.0	0420−014	3	2.5†
0108+388	1	5.1	0241+622	2	2.9†	0422+004	4	2.0
0109+224	2	2.0	0244−452	1	3.6	0422−380	1	4.1
0111+021	11	3.4	0248+430	4	4.3	0423+051	1	3.4
0111+131	1	2.4	0252−712	1	6.6	0423+237	1	2.7
0112−017	1	4.2	0256+075	2	3.1	0425+048	1	3.2
0113−118	2	3.4	0256−005	1	2.5	0426+273	4	2.6
0115−214	1	2.5	0259+121	2	3.9	0426−380	1	4.1
0118−272	1	5.0	0300+470	5	2.5	0430+052	16	4.3
0119+041	20	2.9†	0302+625	2	2.7	0434−188	5	3.3
0119+115	25	2.3	0305+039	2	3.1	0437−454	2	2.2
0123+257	4	3.0	0306+102	2	2.8	0440+345	1	2.8
0130−171	1	4.0	0307+380	1	0.0	0440−003	2	2.9
0131−450	1	0.9	0308−611	1	1.4	0442+389	1	2.4
0131−522	1	2.4	0309+411	2	2.1	0444+634	1	2.0
0133+476	26	2.0	0312+100	1	2.5	0446+112	4	2.4
0134+311	1	2.7	0316+413	1	4.4	0451−282	1	3.3
0135−247	2	3.2	0316−444	1	2.5	0454+844	11	2.9
0137+012	1	1.5	0317+188	2	3.0	0454−234	27	1.9
0137+467	1	1.2	0319+121	2	4.0	0454−463	1	1.2
0138−097	5	2.6	0322+222	1	1.8	0454−810	1	2.5
0144+209	1	4.6	0325+395	1	0.9	0457+024	2	4.2
0146+056	4	3.3	0326+277	1	4.3	0458+138	2	2.9
0148+274	1	3.8	0332−403	1	2.3	0458−020	30	2.6
0459+060	1	3.5	0645+209	1	3.1	0821+394	4	2.4‡

Table 1—Continued

Source name	Number of maps	Structure Index	Source name	Number of maps	Structure Index	Source name	Number of maps	Structure Index
0459+252	1	3.0	0646−306	3	2.7	0823+033	27	2.7
0500+019	1	4.3	0648−165	5	1.8	0823−223	1	1.8
0502+049	1	3.4	0648−287	1	0.8	0823−500	1	6.0
0506+056	1	2.3	0650+371	1	3.2	0826−373	1	4.2
0506+101	2	1.3	0654+244	1	3.5	0827+243	3	2.4
0506−612	1	2.7	0656+082	9	2.9	0828+493	1	2.3
0507+179	3	2.9	0657+172	4	2.2	0828−222	1	2.1
0511−220	1	2.8	0707+476	2	2.5	0829+046	3	3.0
0518+165	1	4.1	0710+439	4	5.7	0831+557	3	5.1
0519+142	1	3.3	0711+356	2	4.6	0833+585	2	3.3
0521−365	1	3.6	0716+714	2	1.9	0834+250	1	2.8
0522−611	2	2.8	0718+793	8	2.5	0834−201	2	2.3
0524+034	1	1.1	0721−071	1	2.4	0836+710	3	3.6
0528+134	29	2.6†	0722+145	2	2.7	0838+133	1	3.2
0528−250	1	2.9	0723+219	1	0.6	0839+187	3	4.3
0529+075	1	4.0	0723−008	1	3.3	0850+581	3	3.2
0530−727	1	3.9	0725+219	1	2.1	0851+202	32	2.6†
0536+145	3	1.4	0727−115	32	2.0	0859+470	2	3.1
0537−158	1	3.4	0727−365	1	3.7	0859−140	3	3.8
0537−286	1	0.8	0728+249	1	2.3	0906+015	1	3.1
0537−441	22	2.7	0729+259	1	3.4	0906−048	1	2.2‡
0538+498	5	4.4	0733−174	2	4.9	0912+029	2	2.3
0539−057	2	2.8	0735+178	2	3.4	0912+297	3	2.5
0544+273	5	2.1	0736+017	3	2.3	0917+449	3	3.1
0547+234	1	2.0	0736−332	1	4.3	0917+624	3	3.1
0548+378	1	1.8	0738+313	2	4.1	0918−297	1	3.6
0552+398	31	2.5	0738+491	5	1.4	0919−260	18	2.7†
0554+242	2	2.9†	0738−674	2	3.1	0920+390	1	1.1
0556+238	14	1.3	0742+103	10	3.9	0920−397	16	2.5
0558−396	1	2.3	0743+259	9	2.1	0923+392	23	2.8†
0600+177	2	2.8	0743+277	1	1.5	0925−203	2	2.2
0601+245	1	3.1	0743−006	2	1.9	0927+469	1	3.4
0602+673	10	3.5	0743−673	1	4.2	0942+358	1	3.3
0605−085	3	3.4	0745+241	3	2.5	0945+408	3	3.6
0606−223	1	2.9	0746+483	1	2.7	0949+354	2	2.6
0607−157	15	2.2	0747+185	1	0.7	0951+268	1	1.8
0609+607	3	3.3	0748+126	6	2.1	0951+693	3	2.7
0611+131	2	2.2	0749+540	9	2.7†	0952+179	3	3.0
0615+820	2	3.5	0754+100	4	3.1	0953+254	16	3.2
0620+389	1	2.5	0759+183	1	2.4	0954+658	4	2.6
0625−354	1	3.1	0804+499	20	1.8	0955+326	4	2.8
0627−199	1	2.5	0805+410	11	2.1	0955+476	24	1.2
0629+160	1	4.6	0805−077	2	3.3	0958+346	1	2.1
0632−183	1	1.3	0808+019	4	1.6	1003+351	1	3.4
0636+680	1	1.7	0809−493	1	3.9	1004+141	10	3.5
0637−337	1	2.8	0812+020	1	1.9	1004−500	1	2.6
0637−752	1	4.3	0812+367	1	2.8	1011+250	2	3.2
0639−032	1	2.7	0814+425	2	2.3	1012+232	4	2.8
0641+392	1	2.6	0818−128	1	3.5	1013+127	1	1.1
0642+214	1	3.8	0820+560	3	3.2	1013+208	1	3.7
0642+449	24	1.5	0821+248	1	1.7	1020+400	1	3.1
1021−006	2	4.6	1148−001	1	4.6	1334−127	27	2.3
1022+194	5	2.6	1150+497	2	3.2	1338+381	3	3.8

Table 1—Continued

Source name	Number of maps	Structure Index	Source name	Number of maps	Structure Index	Source name	Number of maps	Structure Index
1030+415	1	0.6	1150+812	3	3.2	1342+662	2	1.9
1032−199	2	3.2	1155+251	3	4.7	1342+663	3	2.8
1034−293	31	2.4	1156+295	26	2.5†	1345+125	1	5.4
1038+064	4	3.5	1156−094	1	3.6	1347+539	4	3.0‡
1038+528	1	2.8	1212+171	1	2.2	1348+308	1	2.1
1039+811	1	2.3	1213+350	2	3.3	1349−439	1	2.2
1039−474	1	5.0	1213−172	2	2.2	1351−018	17	2.3
1040+123	1	3.9	1215+303	2	2.5	1352−104	2	2.6†
1040+244	1	1.6	1216+487	3	3.1	1354+195	1	3.7
1042+071	1	2.5	1218+339	1	2.0	1354−152	3	1.7
1044+719	23	2.2†	1219+044	15	1.9	1357+769	22	0.7
1045−188	4	3.0	1219+285	1	3.8	1402+044	2	3.0
1046−026	1	1.4	1221+809	3	2.6	1404+286	24	3.6
1046−409	1	1.6	1221−829	1	2.7	1406−076	3	2.3
1047+147	1	2.4	1222+037	1	4.5	1409+218	2	2.5
1048−313	1	4.3	1222+131	1	2.2	1412+461	1	3.3
1049+215	2	3.0	1223−188	2	2.6	1413+135	3	1.9‡
1053+704	3	1.8	1226+023	1	5.5	1416+067	3	3.1
1053+815	13	2.3†	1226+373	2	1.5	1417+273	4	2.6
1054+004	1	2.9	1228+126	21	3.6	1417+385	10	1.9
1055+018	5	2.8	1236+077	3	2.8	1418+546	20	3.0
1056+212	1	1.9	1237−101	1	4.3	1418−192	1	0.8
1057−797	2	3.4	1240+381	3	2.8	1420+326	1	1.0
1059+282	1	1.4	1241+166	1	2.0	1424+240	1	2.1
1100+122	1	2.1	1243−072	1	2.1	1424+366	1	2.6
1101+384	22	2.3	1244−255	1	0.2	1424−418	18	2.5
1101−325	1	3.0	1246+489	1	2.3	1428+422	1	1.6
1104+728	1	2.1	1251−197	1	2.5	1430−178	1	3.9
1105−680	1	4.9	1251−713	1	2.8	1432+200	3	2.3
1107+485	1	1.5‡	1252+119	3	2.9	1433+304	1	2.4
1111+149	3	2.5	1253−055	3	4.1	1435+638	1	4.2
1116+128	3	3.3	1255−316	15	3.2	1435−218	1	4.5
1119+183	1	3.8	1256−220	1	1.9	1441+252	1	1.6
1123+264	2	2.4	1257+145	1	2.1	1442+101	2	3.6
1124−186	27	1.5	1300+580	17	1.3	1443−162	1	2.8
1125+366	1	1.0	1302−102	2	3.3	1445−161	2	3.5
1127−145	2	4.3	1306+360	1	1.6	1448+762	6	2.7
1128+385	22	2.0	1307+121	1	3.6	1451−375	16	3.0
1128−047	1	3.3	1308+326	23	3.3	1458+718	3	4.0
1130+009	1	2.4	1308+328	3	2.7	1459+480	3	2.6
1142+052	1	3.0	1308+554	1	2.1	1502+036	3	1.7
1143−245	3	3.5	1313−333	18	2.7	1502+106	4	2.9
1143−332	1	2.8	1315+346	3	3.5	1504+377	1	2.0
1144+402	3	1.5	1323+321	1	4.6	1504−166	3	3.5
1144−379	26	2.2	1324+224	2	0.3	1505+428	1	3.4
1145+268	1	3.3	1328+307	1	5.7	1508−055	1	3.0‡
1145−071	17	2.8	1330+022	1	2.9	1510−089	3	2.9
1146+596	1	4.1	1330+476	1	0.8	1511−100	2	2.6
1147+245	2	2.6	1333−152	2	2.3	1514+004	1	3.1
1147−192	1	3.0	1333−337	1	2.5	1514+197	2	2.0
1514−241	16	3.5	1705+018	2	2.6	1856+736	2	3.6
1519−273	12	1.8	1705+456	3	3.3	1901+319	2	3.9
1520+319	1	1.8	1706−174	4	2.4	1903−802	1	4.6

Table 1—Continued

Source name	Number of maps	Structure Index	Source name	Number of maps	Structure Index	Source name	Number of maps	Structure Index
1531−352	1	1.2	1710−323	1	3.7	1908+484	1	0.7
1532+016	2	4.1	1717+178	3	2.8	1908−201	25	2.5
1538+149	2	2.4	1718−259	1	2.2	1909+161	1	2.7
1540−828	1	7.2	1718−649	1	5.4	1910+052	1	2.6
1541+050	1	3.4	1722+330	1	2.0	1920−211	2	2.5
1546+027	4	2.7	1725+044	3	3.2	1921−293	24	2.8
1547+507	3	3.3	1725+123	1	2.5	1922+155	1	2.3
1548+056	2	2.9	1726+455	15	2.2	1923+210	11	3.3
1549−790	1	4.8	1729−373	1	5.2	1925−206	2	2.1
1555+001	2	1.8	1730−130	3	2.5	1926+087	1	3.2
1555−140	1	4.0	1732+389	3	1.7	1928+738	4	3.9
1557+032	1	2.1	1736+324	1	1.5	1929+226	2	2.5
1600+335	2	4.0	1738+476	2	2.7	1932+204	3	2.1
1600−294	2	2.8	1738+499	3	2.3	1934−638	2	6.4
1604−333	1	2.8	1739+522	21	1.5	1936−155	4	2.1
1606+106	30	2.5	1741−038	28	1.9	1937−101	2	3.6
1607+268	1	4.4	1742−078	1	3.3	1943+228	1	1.3
1608+243	1	1.5	1743+173	1	2.6	1947+079	1	5.1
1610−771	1	6.4	1744+557	1	3.5	1951+355	1	2.7
1611+343	24	3.2	1745+624	22	1.7	1954+513	2	2.6
1614+051	1	3.0	1745+670	1	3.5	1954−388	22	2.6
1616+063	2	2.8	1746+470	4	1.1	1955+335	1	1.4
1617+229	1	2.2	1748−253	1	3.9	1958−179	10	1.5
1622−253	25	2.0	1749+096	31	1.3	2000+148	1	0.7
1622−297	2	3.8	1749+701	2	3.0	2000+472	1	2.1
1624+416	1	3.7	1751+288	2	2.3	2000−330	2	4.1
1627+476	1	2.0	1751+441	2	3.2	2005+403	1	3.6
1633+382	1	3.4	1754+155	1	2.1	2005−489	1	4.1
1636+473	1	2.5	1758+388	2	2.2	2007+777	2	3.4
1637+574	3	2.5	1758−651	1	1.7	2008−068	3	4.1
1637+826	7	3.7	1759−396	1	2.4	2008−159	4	1.6
1638+398	22	1.6	1800+440	4	2.2	2013+163	1	1.4
1639+230	2	1.3	1803+784	22	2.5†	2017+743	4	2.2
1639−062	1	2.3	1805−214	1	1.3	2018+282	1	0.0
1639−200	1	1.8	1806+456	1	0.0	2021+317	4	3.3
1640−231	1	3.7	1807+698	4	3.2	2021+614	1	4.8
1641+399	2	4.1	1814−637	1	5.5	2023+336	2	3.4
1642+690	5	3.0	1817−254	1	3.5	2029+024	1	0.4
1645+271	1	2.9	1821+107	3	3.2	2029+121	2	2.7
1645−329	1	3.7	1822+033	1	2.1‡	2030+547	1	4.1
1647−296	1	2.3	1823+568	3	2.5†	2037+511	14	3.3
1648+084	1	0.0	1826+796	1	4.4	2037−253	1	3.3
1651+391	1	1.0	1829−207	1	4.8	2048+312	4	3.0
1652+398	4	3.4	1830+285	2	3.6	2052−474	12	2.4
1655+077	3	3.2	1842+681	3	1.9	2054−377	1	3.1
1656+053	2	3.2	1845+797	2	3.9	2056−369	1	3.1
1656+348	3	3.1	1845−273	1	0.0	2059+034	1	2.1
1656+477	1	4.0	1846+322	1	1.0	2059−786	1	4.1
1657−261	6	2.1	1849+670	3	1.5	2101−490	1	3.1
2106+143	1	2.6	2205+743	1	3.1	2300−683	1	2.1
2109−811	1	3.6	2209+236	9	1.9	2309+454	1	2.8
2113+293	11	2.8	2210−257	1	3.1	2312−319	1	3.1
2120+099	1	4.7	2211−388	1	4.5	2314−409	1	2.8

6. Data and Modeling Comparisons (DG, DM)

One of the requirements for ICRF2 is that it should be consistent with the current realization of the International Terrestrial Reference Frame (ITRF) and EOP products. In practice, this means that it should be consistent with the VLBI contribution to ITRF2008, which is called VTRF2008 (Böckmann, Nothnagel, & Artz 2009). Thus, it was necessary for the ICRF2 solution to also solve for site positions, site velocities, and EOP. The level of agreement with VTRF2008 and EOP comparisons are discussed later in §10. The generation of ICRF2 is also required to use the best current state-of-the-art astronomical and geophysical models. Thus, the solution should use atmosphere gradients, the VMF1 troposphere mapping function model (Boehm, Werl, & Schuh 2006), antenna thermal deformation, and the other standard VLBI models. Specifically, it should also use corrections for atmosphere pressure loading, even though they were not used for VTRF2008, since pressure loading is one of the state-of-the-art geophysical models that has become a standard VLBI analysis tool.

Some of the newer models have only recently become available in the analysis, such as the VMF1 model and the thermal deformation model. There was a desire to understand the effects of using different models, and to validate the newer models. Therefore, a number of model comparisons and tests were made. Tests were also made comparing subsets of the data, on the types of data, and on the data span. It was hoped that these tests and comparisons would help in determining the best data subset, the best analysis strategy, to identify and understand any systematic errors, and to help determine the noise floor. Some of these tests (decimation) are discussed later in §9. These tests were done at GSFC using the Calc/Solve analysis package. Most were made using preliminary catalog solutions, before the session and source lists were finalized. All the comparison tests except the VCS vs. non-VCS comparison used solutions without the 24 VCS sessions. In the discussions below of solution differences, the RA differences are always scaled by the cosine of the declination to give true arc lengths. A good summary of additional and complimentary comparisons using the OCCAM software can also be found in Tesmer (2007). Their results generally agree with the results presented here.

6.1. Data Start Time Tests

The chronologically earlier VLBI data is known to be considerably noisier than later data. This has been due to many improvements over the past 30 years, such as: increased individual channel bandwidths, increased spanned bandwidths, improved electronics, new and more sensitive stations, larger networks, improved scheduling methods, and other factors. A question posed was whether to use data going back to the beginning of the Mark III era (August 1979), or to throw away the first few years of data. Alternate start times suggested were 1990 and 1993. One thought was, that although the earlier data is noisier, the formal errors are also larger, and with proper weighting, the earlier data should not degrade the reference frame. Three tests were made to study this issue, using data start times of Aug. 1979, Jan. 1990, and Jan. 1993.

Table 1—Continued

Source name	Number of maps	Structure Index	Source name	Number of maps	Structure Index	Source name	Number of maps	Structure Index
2121+053	4	3.0	2214+350	1	1.9	2318+049	12	2.6
2126−158	10	2.4	2216+178	1	0.9	2318−195	1	1.4
2127−096	1	2.9	2216−038	2	3.3	2319+272	4	3.1
2128−123	6	4.2	2223−052	13	2.3	2319+317	1	1.7
2131−021	2	2.8	2227−088	2	1.6	2320+506	3	3.6
2134+004	6	3.5	2227−399	1	3.8	2320−035	2	3.2
2135−184	1	2.0	2229+695	1	2.6	2325+093	1	1.9
2136+141	19	2.8	2229−172	1	3.4	2325−150	1	2.5
2142+110	2	2.7	2230+114	6	4.2	2328+107	1	3.9
2143−156	3	3.1	2233−148	2	3.3	2329−162	3	3.7
2144+092	2	3.4	2234+282	20	2.4[†]	2329−415	1	2.7
2145+067	26	2.8[†]	2235+731	2	3.2	2331−240	1	3.5
2145+082	1	2.8	2239+096	1	2.9	2335−027	2	3.0
2147+077	1	4.9	2243−123	24	3.8	2337+264	2	4.8
2149+056	3	2.6	2245−328	1	2.8	2344+092	2	3.4
2149−306	2	3.6	2250+194	5	2.3	2345−167	1	3.8
2150+173	3	2.8	2251+158	4	3.7	2351+456	3	3.4
2152−699	1	4.5	2252−089	3	3.3	2351−154	2	2.5
2155+312	1	1.3	2253+417	2	3.6	2353+816	1	2.7
2155−152	2	3.7	2254+024	3	1.0	2353−686	1	2.9
2155−304	1	2.1	2254+074	2	2.2	2355−106	1	0.7
2200+420	18	3.5	2255−282	22	1.9	2356+385	11	1.9
2201+315	5	3.2	2259−375	1	4.9	2358+189	1	1.9
2205+166	1	2.5	2300−307	1	3.8			

[‡] Source has very extended S band structure (information provided only for sources with SI $\leq$ 3.0).

[†] Time series of structure indices or maps indicate variability (information provided only for sources with SI $\leq$ 3.0).

When the start time is delayed from 1979 to 1990, there are some small differences in RA and declination for some sources, with some as large as ∼0.5 milli-arc-seconds (mas,) but most much smaller. The formal uncertainties also increase slightly. The wrms differences between the ensemble of source positions estimated with and without the earlier data are 11 and 8 micro-arc-seconds (μas) in RA and declination, respectively. When the start time is delayed from 1979 to 1993, the differences are more dramatic. Large differences are seen for some sources, with a dozen or so between 1 and 10 mas. The formal uncertainties for some sources also increase, some by ∼0.1 mas. Presumably, this is due to a greater emphasis on some sources in the earlier years. The wrms differences are 18 and 14 μas in RA and declination, respectively. From these comparisons, it was concluded that, the earlier data, though noisier, will not degrade the reference frame, so it was used for ICRF2.

6.2. Data Type Comparisons

Another question was which types of sessions should be used. The earlier VLBI sessions were more concerned with plate tectonic and regional tectonic motion and less on Earth orientation and astrometry than the later sessions. Also, from 1982 until 1991 the Crustal Dynamics Project sponsored the Western U.S. and Alaska mobile VLBI campaigns. These used three small mobile VLBI systems (of 3, 5, and 9 meter diameter aperture), and the two smaller systems made repeated measurements at several dozen sites in California, Nevada, Arizona, Colorado, Alaska, and Canada to measure regional plate tectonics (see Clark et al. (1987) and Ma et al. (1990)). Data from the small mobile systems would not be expected to contribute to the celestial reference frame. However, most of these mobile sessions also used several large fixed antennas, such as OVRO130 (40 meter), Hatcreek (26 meter), Mojave12 (12 meter), Gilcreek (26 meter), and Westford (18.3 meter). These larger antennas would be expected to contribute to the celestial reference frame. A comparison was made of two solutions, one using only fixed station sessions (no mobile sessions) and one with mobile sessions added. When mobile sessions were added, very little difference in source positions were seen. The wrms differences are only 2 μas, and the average differences are only 1 μas in both RA and declination. Only one difference was larger than 0.1 mas, for a source observed in only a few sessions. There were no significant changes in formal errors and no significant rotation of the frame.

There was another class of sessions whose use was questionable. These were the small, regional sessions, like the JADE sessions, the Canadian regional sessions, most of the European mobile sessions, various “ties” sessions, and an assortment of special sessions not considered suitable for most VLBI analysis. Although these sessions were useful for their own purposes, they are made up of small or geometrically weak networks, usually with only one large antenna and one or more small antennas. As such, they would not be expected to contribute much to the celestial reference frame. We made a comparison solution in which these sessions were added. When they were added in, the average position differences were not large, but some individual position differences were large, up to ∼1.6 mas, with 41 differences larger than 0.1 mas.

From these two comparison tests, it was decided to use most of the regular mobile sessions (with at least two well-separated fixed antennas) since they would add a considerable amount of data and could contribute to the reference frame, but not to use the smaller regional sessions, the ties sessions, or other special sessions.

6.3. Type of Solution: TRF vs. Baseline

There are two basic ways of treating the antenna positions in a solution. In a terrestrial reference frame (TRF) solution they are solved globally, and the result is a set of antenna site positions and velocities at a specified epoch, based on the entire observing history. In a baseline solution, site positions are treated as local (arc) parameters, and separate positions are obtained for each session. In a TRF solution, one can apply no-net-rotation and no-net-translation constraints on the positions and velocities of a set of core sites to align the TRF with an *a priori* reference frame. EOP are estimated for each session, except usually for 1-baseline sessions. Some sites show discontinuities, due to earthquakes or mechanical movement of the antenna, which must be modeled into the solution. In a baseline solution, no-net-translation constraints can be applied for the estimation of site coordinates for each experiment session. EOP is normally fixed to an *a priori* EOP series for a baseline solution.

For ICRF1 and its extensions, baseline solutions were made. However, for consistency with ITRF2008, ICRF2 must be generated as a TRF solution. Tests were made to see what effect this might have on the reference frame. Matching TRF and baseline solutions were made and compared. For both, the *a priori* TRF was VTRF2008 (Böckmann, Nothnagel, & Artz 2009). Comparison of these two solutions allows us to assess how much unmodeled site position noise in the TRF solution propagates to other parameter estimates, specifically the source position estimates. The two solutions show mostly only noise-like differences with wrms of 10-12 μas, and with no differences greater than around 0.6 mas. There are no declination-dependent systematic variations in the differences. Plots of the RA and Declination differences vs. Declination are shown in Figure 13. This comparison gives us confidence that the TRF requirement will not have any adverse effect on ICRF2.

6.4. Gradient Tests

The troposphere above VLBI sites is known to be azimuthally asymmetric, i.e. there are atmosphere gradients. In general, all stations have an average North-South gradient, which increases towards the equator, due to the pole-to-equator temperature gradient. East-West gradients also exist, but vary considerably over periods of days or less, due to weather patterns. East-West gradients are expected to average out to near zero for most sites. If the refractive effects of atmospheric gradients are not accounted for, the radio source positions will be biased. This bias would be mainly seen in declination. For northern hemisphere stations, the N-S gradient will make lower declination sources appear higher in the sky, thus increasing their apparent declination. For southern hemisphere stations, the apparent declinations of higher declination sources will decrease. The northern hemisphere networks

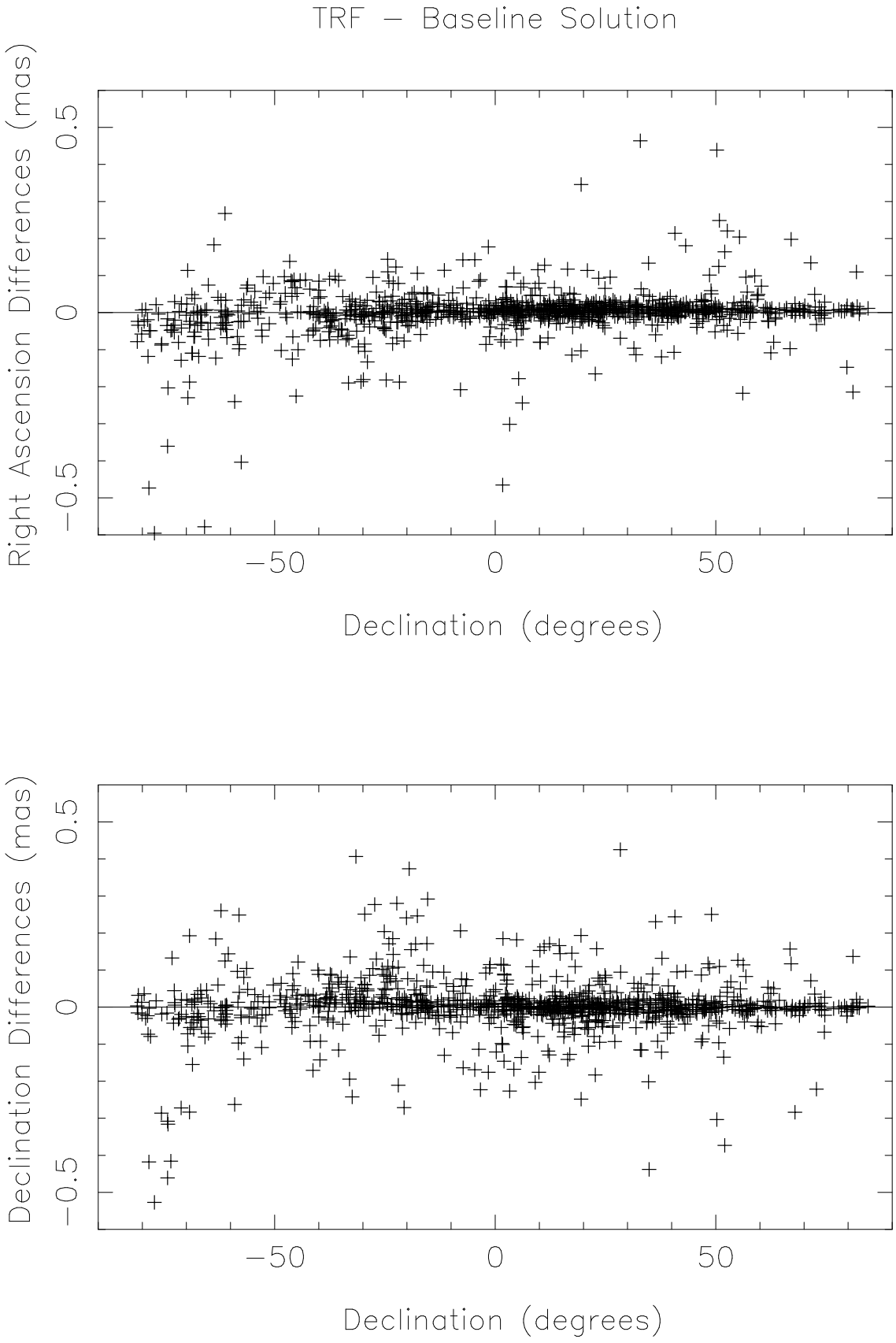

Fig. 13.— Differences between a TRF and a baseline solution. Sources with formal errors greater than 0.6 mas are not plotted.

dominate though so that the maximum effect on declinations occurs south of the celestial equator. The end result is that, if gradients are not accounted for, the apparent declinations would increase by a maximum of ∼0.5 mas at ∼ −10° declination.

The standard method of estimating gradients in program Solve has been to apply an *a priori* gradient model and solve for residual gradients. The *a priori* model of MacMillan & Ma (1997) was derived from a numerical weather model, and essentially gives a fixed N-S gradient for each site. The residuals can be solved for either by applying constraints or not. For a base solution, constraints of 0.5 mm and 2.0 mm/day on offsets and rates were imposed. Comparison tests were made in which: a) no *a priori* gradients were applied and no residual gradients were estimated; b) the *a priori* gradient model was applied, but no residuals were estimated; and c) no *a priori* model was applied, but total gradients were estimated.

As expected, a no gradients solution, compared to the standard gradients solution, shows a strong declination dependence, as was seen for ICRF1 (Ma et al. 1997). Without gradients, apparent declinations increase from the poles to a maximum of ∼0.5 mas at around -10° declination. If only mean *a priori* gradients are used, apparent declinations decrease by ∼0.05 mas for declinations south of around +10°. The *a priori* models thus appear to be statistically accurate at about the 10% level.

A second method for estimating gradients is to estimate total gradients, without the use of an *a priori* file. This is the method that was used for ICRF1 and its extensions, so a comparison of these two methods is very important. When a comparison was initially done, it was found that the constraints were too restrictive when used to estimate total gradients. Further tests were done in which the constraints were weakened four-fold and ten-fold. With these solutions, the agreement is very good, and all differences are less than ≈2.1 times their formal errors. Figure 14 shows the comparison plots for this case.

6.5. Pressure Loading Tests

Atmospheric pressure loading has become a standard VLBI analysis model over the past few years. Pressure loading corrections have been shown to improve VLBI baseline repeatability (Petrov & Boy 2004), therefore it is desirable to use pressure loading for the ICRF2 solution. Pressure loading was *not* used for ITRF2008, at the request of the IERS, mainly because the other geodetic techniques were not using it. However, its use would not be expected to cause any adverse effects on the celestial or terrestrial reference frames or the EOP solution. Further, pressure loading is considered a current "state-of-the-art" geophysical model which thus should be used in the generation of ICRF2. Comparison solutions were made with pressure loading applied and not applied. Only small differences are seen in source positions, mostly less than 0.2 mas, and nothing systematic. Formal errors are unchanged. This test indicates that pressure loading corrections will have no adverse effect on the celestial reference frame.

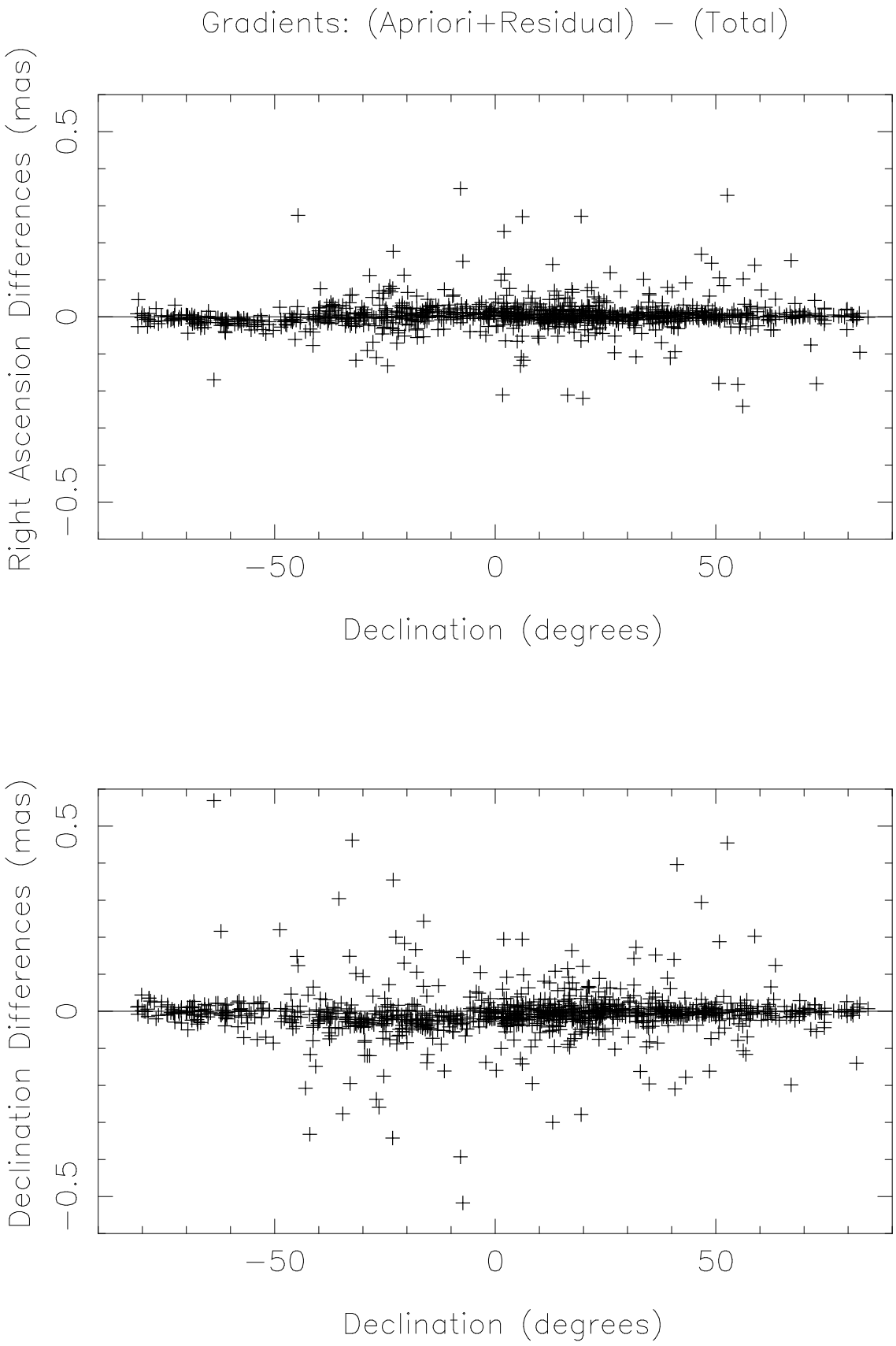

Fig. 14.— Differences between solving for gradients with an *a priori* mean gradient applied versus no mean gradient applied and using weak gradient constraints. Sources with formal errors greater than 0.6 mas are not plotted.

6.6. Vienna Mapping Function vs. Niell Mapping Function

The VLBI contribution to ITRF2008 used the VMF1 mapping function (Boehm, Werl, & Schuh 2006) for tropospheric delays, and it is considered the best current "state-of-the-art" model. Therefore it should also be used for ICRF2. The previous standard was the Niell Mapping Function (NMF) (Niell 1996). We made comparison solutions using VMF1 and NMF. Catalog position differences are mostly small, but some as large as 0.8 mas are seen. There are only small, insignificant increases in uncertainties. VMF1 is derived from the ECMWF numerical weather model. Figure 15 shows the differences between using the two troposphere mapping functions, in units of formal errors. There are no differences greater than $0.9\,\sigma$.

6.7. VCS Test

The VLBA Calibrator Survey (VCS) sessions were VLBA only observing campaigns begun by Beasley et al. (2002) to obtain precise positions and snapshot maps of several thousand compact radio sources to increase the number of calibrator sources available for VLBI phase referencing. Five additional VCS campaigns were later carried out: Fomalont et al. (2003), Petrov et al. (2005), Petrov et al. (2006), Kovalev et al. (2007), and Petrov et al. (2008). There were 24 successful VCS sessions. Use of these 24 sessions adds nearly 2200 additional sources to the catalog. Most of the VCS sources were scheduled for two scans (90 baseline observations) in only one session. A few sources were observed in two sessions. For many of the sources there are only a few good observations and their uncertainties are large. But also for many of them, there are many good observations, and their uncertainties are small. Therefore, it is desirable to include them in ICRF2, as long as doing so will not distort the frame. Comparisons were made with and without the 24 VCS sessions. Mostly just small differences are seen. However, a few sparsely observed sources show large position changes (up to $\sim$200 mas) when the VCS sessions are added, due to a large increase in the number of observations, and presumably a better position. No systematic effects are seen. Figure 16 shows the position differences for cases where the number of observations (without VCS) is greater than four and the formal errors (non VCS) are less than 1 mas.

6.8. Thermal Deformation Test

The use of an antenna thermal deformation model was used for ITRF2008. Therefore it should also be used for ICRF2. The thermal deformation model described in Nothnagel (2008) accounts for the change in the position of the reference point of an antenna as a function of temperature relative to a specified reference temperature for each site. Specific information for each antenna (structural dimensions, expansion coefficients, reference temperature) are provided in Nothnagel (2008). A comparison of source catalogs was made using thermal deformation and not using thermal deformation. Mostly small random differences are seen, up to $\sim$0.1 mas. Formal uncertainties are virtually unchanged. Figure 17

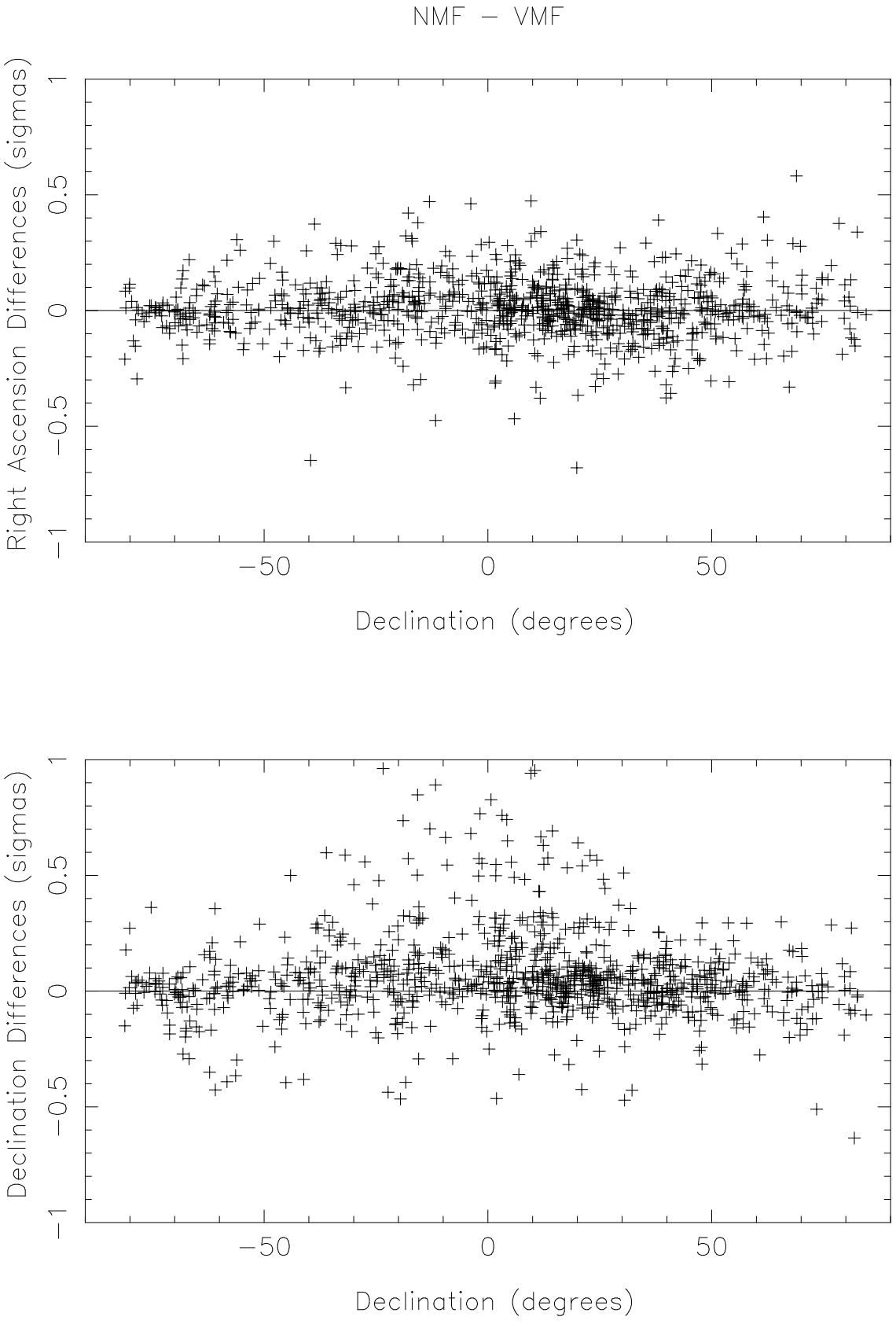

Fig. 15.— Differences between using the Niell Mapping Function (NMF) versus the Vienna Mapping Function (VMF1), in formal error units.

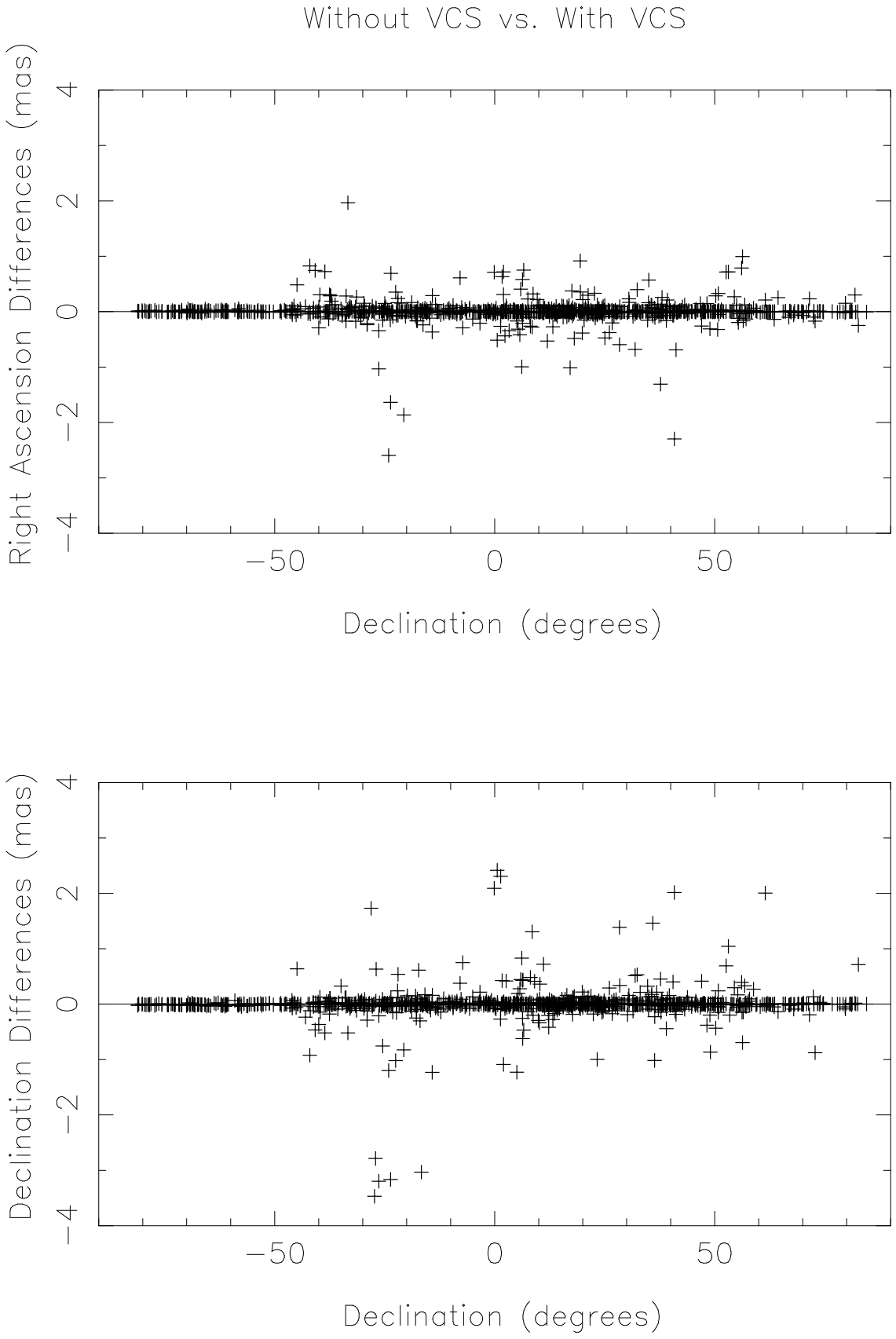

Fig. 16.— Solutions with and without the VCS sessions. Sources with fewer than four observations or formal errors greater than 4 mas are not plotted.

shows the differences, in formal error units.

6.9. Summary of Data and Model Comparisons

Table 2 summarizes the results of the various data and model comparisons. We present the weighted means of the differences and their wrms in Right Ascension and declination, as well as the overall rotation angles between the pairs of solutions. It will be seen that any uncertainties due to the data or model options are all smaller than the estimates that will be presented later for the ICRF2 noise floor and axes stability.

Table 2: Summary of Data and Model Comparisons

Data/Model Comparison	$\Delta\alpha \cos\delta$		$\Delta\delta$		Rotation Angles		
	mean (μas)	wrms (μas)	mean (μas)	wrms (μas)	X (μas)	Y (μas)	Z (μas)
Start Time: 1979 vs. 1990	1	8	1	11	0	2	1
Start Time: 1979 vs. 1993	0	14	0	18	-1	5	4
Session Type: Fixed vs. Fixed+Mobile	-1	2	-1	2	0	0	-1
Session Type: Fixed vs. Fixed+Mobile+Regionals	0	5	-2	5	2	-1	-3
TRF vs. Baseline	-1	10	0	12	2	2	2
Gradients: *a priori* vs. No *a priori*	0	7	6	12	8	5	3
Pressure Loading: On vs. Off	0	2	0	3	2	1	0
VMF1 vs. NMF	-1	3	-3	5	-1	2	-1
VCS vs. No VCS	2	17	1	18	-7	1	1
Thermal Deformation: On vs. Off	0	0	0	1	0	0	0

7. The ICRF2 Solution (DG, DM)

7.1. Configuration

The solution used for generating ICRF2 is the "gsf008a" solution. It was run by the VLBI group at GSFC using the Calc/Solve analysis package, in its global solution mode. The solution used a total of 4540 VLBI sessions observed between 1979 August 3 and 2009 March 16. The solution used group delays only (no phase delay rates). Parameters were estimated using the arc-parameter elimination method described in Ma et al. (1990), where arc-parameter refers to those parameters that are estimated for each experiment session (arc) in a solution. Global parameter adjustments are based on data from the entire set of VLBI data in the solution. The specific parameters falling into these two general classes are as

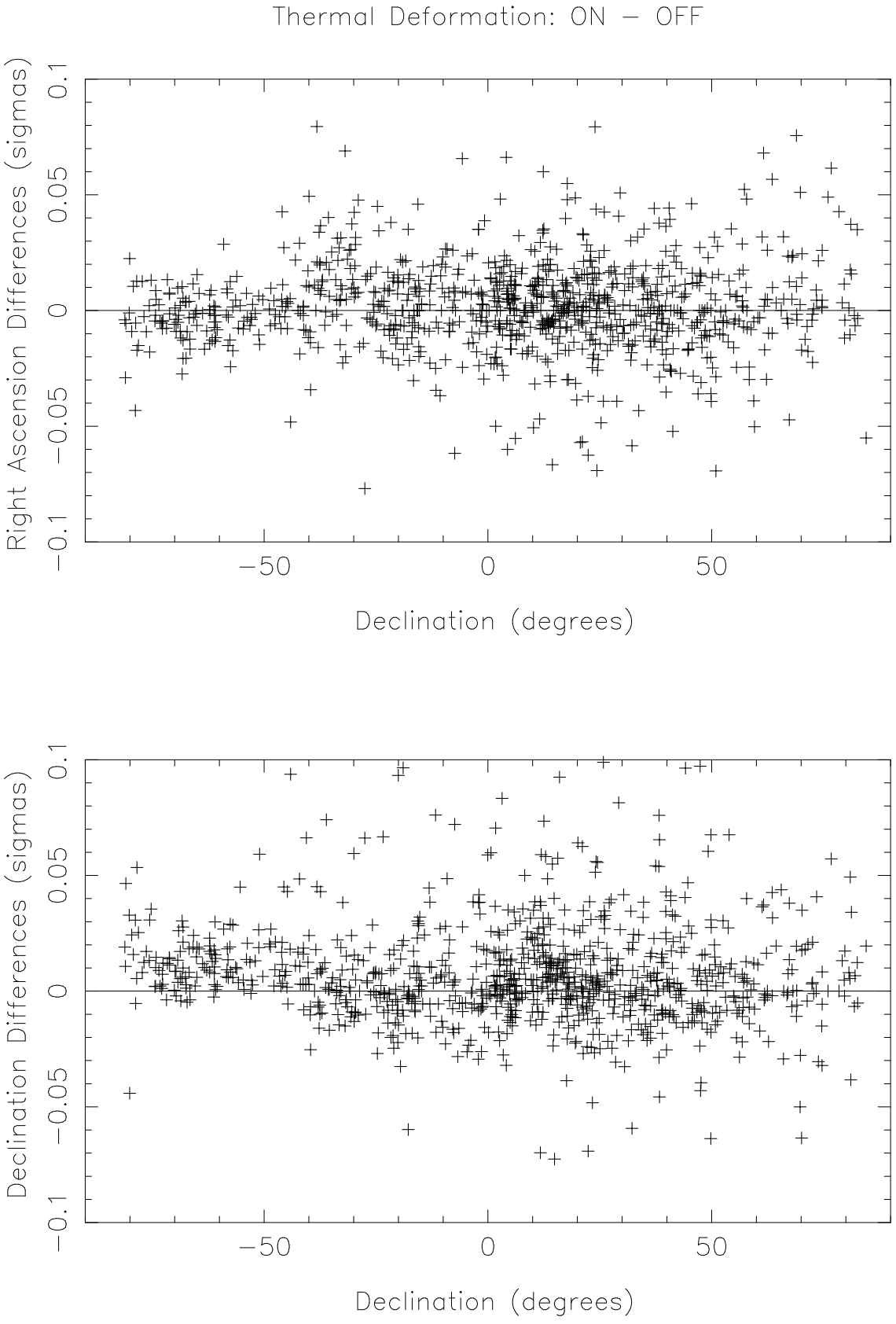

Fig. 17.— Differences between applying antenna thermal deformation and not applying antenna thermal deformation, in formal error units.

follows:

1) Arc parameters adjusted for each observing session:

- Station clocks were estimated as quadratic clock polynomials for the slowly varying clock behavior. Short-term behavior was estimated as piecewise linear continuous functions at 60 minute intervals.
- Station wet troposphere zenith delays were estimated as piecewise linear continuous functions at 20 minute intervals.
- Atmosphere gradient residuals in the N-S and E-W directions were estimated at 6 hour intervals. These residuals were adjustments from an *a priori* gradient model (MacMillan & Ma 1997).
- UT1 and polar motion offsets and rates were estimated at the midpoint of each session.
- Nutation offsets were estimated at the midpoint of each session.
- Source positions were estimated for a set of 39 "special handling" sources whose time series exhibited clear systematic variations (see §4).

2) Global parameters adjusted based on the entire data set:

- Station positions and velocities were estimated, for reference epoch 2000.01.01. No-net-rotation and no-net-translation constraints were imposed on a set of 27 stations to align the estimated TRF with VTRF2008 (Nothnagel 2008).
- Station position harmonic variations were estimated for 41 stations at diurnal, semi-diurnal, annual, and semi-annual frequencies.
- Spline parameter estimation of nonlinear variation was made for sites Gilcreek, Pietown, and HRAS085.
- A discontinuous offset parameter was estimated for 12 stations at epochs corresponding to an identifiable effect, e.g., an earthquake or an antenna repair. These sites were: YAKATAGA, SOURDOGH, WHTHORSE, FORTORDS, PRESIDIO, MOJAVE12, DSS15, MEDICINA, EFLSBERG, DSS65, GGAO7108, and SINTOTU3.
- Source positions were estimated for all sources with three or more good S/X-band observations, except for three gravitational lenses and six radio stars. Positions were estimated globally (for the entire data span) for all but 39 special handling sources. Some 795 sources were excluded from the solution because there were fewer than three good S/X-band observations in at least one session. Most of these were from the VCS sessions. A no-net-rotation constraint was imposed on 205 of the 212 ICRF1 defining sources (seven are special handling sources) to align their positions with the original ICRF1 defining sources.

- Adjustments to the antenna axis offsets were estimated at all fixed sites.

The *a priori* models for geophysical effects and precession/nutation generally followed the IERS Conventions (2003) (McCarthy & Petit 2004). Specifically, corrections for solid Earth tides, the pole tide, ocean loading, and high frequency EOP variations were made using the IERS Conventions (2003) (McCarthy & Petit 2004). A 5° elevation cutoff was imposed. Other important effects were modeled using:

- Atmosphere pressure loading corrections according to Petrov & Boy (2004).
- The Vienna Mapping Function (VMF1) troposphere model of Boehm, Werl, & Schuh (2006).
- The antenna thermal deformation model of Nothnagel (2008), in which the antenna heights were adjusted in each session using the average temperatures during that session.

The weighting of data in the solution followed the usual procedure for GSFC solutions. For each experiment session, re-weighting noise is calculated for each baseline so that the reduced χ^2 is close to one when the re-weighted noise is added quadratically to the measurement uncertainty determined from the correlation, fringe-fitting, and ionosphere calibration process. Ionosphere corrections were made using the difference of the X-band and S-band group delay observables.

7.2. Statistics

The Solve/Global solution used a total of 4540 VLBI sessions and 6.495553 million observations. The sessions extended from 1979 August 3 to 2009 March 16. The overall wrms post-fit delay residual was 21.856 ps and the χ^2 per degree of freedom was 0.890. "Global" positions were obtained for 3375 sources, and "arc" positions (time series) positions were obtained for the 39 special handling sources. Weighted mean positions of these 39 sources were computed and added to the global catalog. For their formal errors, we assigned the wrms of their RA and Declination positions with respect to the weighted means. Catalog gsf008a thus has positions and formal errors for 3414 sources.

8. Combination and Comparison of Contributed Catalogs (SL2, SB1, DG)

The following section describes the preliminary catalogs submitted by seven different analysis centers using four independent software analysis packages, the construction of a combination catalog from seven contributed catalogs generated at seven different VLBI analysis centers, and comparisons of individual catalogs between themselves and the combined catalog. The main purpose of this analysis is to investigate systematic effects in individual solutions and estimate a precision of the combined and the individual realizations of the celestial reference frame.

8.1. Contributed Catalogs

The analysis centers involved in ICRF2 were asked to generate and submit two catalogs, one without the VCS sessions and one with the VCS sessions. The data and models used were to be as similar as possible. The VCS catalogs were to be used to construct a combination catalog at Main Astronomical Observatory. Lists of database sessions, sources to solve as arc parameters, and sources to exclude were distributed by GSFC. The solutions were to use group delays only, use only sources with more or more "good" observations, be a TRF solution using VTRF2008, and apply a no-net-rotation constraint using the 205 ICRF1 defining sources that were not classified as special handling sources. The solutions also were to solve for atmosphere gradients, apply pressure loading, use the VMF1 model, and apply thermal deformation. Seven analysis centers generated catalogs using four independent software analysis packages and submitted them in time for use in constructing a combination catalog. Table 3 lists the particulars of the contributed solutions. It can be seen that no two analysis centers used the same data span, the same sessions, or obtained the same number of estimated sources. One of the catalogs also had an editing problem and used some observations normally considered bad. Also, most analysis centers used different analysis models. Some did not use the thermal deformation model, or the VMF1 model, or pressure loading, or solved for baselines instead of the TRF. The model comparisons section showed that these analysis differences should not produce any significant systematic differences, but may increase the noise level of the differences between solutions. Seven contributed catalogs were used to produce the combined catalog, listed with an "*" in Table 3. Because of larger differences seen in the aus007a solution, the Geoscience Australia group produced two additional solutions, aus008a and aus009a, which are included in the comparisons later in this section. Later, in §10, we will present comparisons of the corresponding TRF and EOP solutions.

8.2. Creation of a Combined Catalog

The seven catalogs used to generate a combination catalog are given in Table 4. The first line is the combination catalog itself, designated maoC08a. There are two columns for the number of sources. The first gives the number of sources in the catalog and the second gives the number of sources included in the combination catalog and used in the comparisons.

In the combination procedure, only sources which were observed three or more times (number of group delays) were used. The procedure was performed recursively, eliminating outlier radio sources (5σ) from individual catalogs. The outliers are sources with small ($3 - 15$) numbers of observations in one or two sessions with poor network configuration (usually, one-baseline sessions). The combined catalog, maoC08a, consists of the coordinates of 3572 radio sources. The combined solution, maoC08a, was created using the arc-length method. The method of arc-lengths was developed at the Main Astronomical Observatory of the National Academy of Sciences of Ukraine and is described in Kur′yanova & Yatskiv (1993). The principles of the arc-length method are:

Table 3: Contributed Catalogs

Solution ID	# Sessions	# Sources	Time Range	Software	Analysis Center
aus007a*	3712	1564	1979.7-2008.7	OCCAM6.2	GA
aus008a	3774	2869	1979.7-2008.7	OCCAM6.2	GA
aus009a	3774	537	1979.7-2008.7	OCCAM6.2	GA
bkg001a*	3823	3039	1984.0-2009.2	CALC 10, SOLVE rev. 2007.10.31	BKG
gsf007a	4516	1219	1979.7-2009.2	CALC 10, SOLVE rev. 2008.12.05	GSFC
gsf007b*	4540	3414	1979.7-2009.2	CALC 10, SOLVE rev. 2008.12.05	GSFC
iaa008a	···	3009	1980.0-2009.2	QUASAR	IAA
iaa008b	···	3009	1980.0-2009.2	QUASAR	IAA
iaa008c*	···	3009	1980.0-2009.2	QUASAR	IAA
mao008a*	4541	3555	1979.7-2009.3	SteelBreeze	MAO
opa008b*	4528	3244	1979.7-2009.2	CALC 10, SOLVE rev. 2008.12.05	OP
opa008c	4434	1188	1979.7-2009.2	CALC 10, SOLVE rev. 2008.12.05	OP
usn010b*	4465	3414	1979.7-2009.2	CALC 10, SOLVE rev. 2007.11.08	USNO

Table 4: General characteristics of the combination catalog and the seven contributed solutions used to construct it.

Solution ID	Number of Sources		Software	Analysis Center
maoC08a	3572	3572	Combination	MAO
aus007a	1564	1516	OCCAM6.2	GA
bkg001a	3019	2978	CALC/SOLVE	BKG
gsf007b	3414	3378	CALC/SOLVE	GSFC
iaa008c	2961	2918	QUASAR	IAA
mao008a	3555	3512	SteelBreeze	MAO
opa008b	3244	3214	CALC/SOLVE	OP
usn010b	3414	3380	CALC/SOLVE	USNO

– calculation of the arc lengths (distances on the celestial sphere) of the common ICRF1 defining sources for all individual solutions;

– construction of an intermediate reference frame, with an orientation defined by the positions of two radio sources;

– building of a combined catalog in the intermediate reference frame;

– transition from the combined catalog frame of two sources to a frame given by the positions of the ICRF1 defining radio sources.

The list of ICRF1 defining sources used consisted of 204 objects. From the 212 ICRF1 defining sources we eliminated eight sources: seven are from the special handling sources list (0014+813, 0235+164, 0637−752, 0738+313, 1308+326, 1448+762 and 2145+067) plus the source 1903−802, which is missing in bkg001a solution.

8.3. Comparison of Individual Solutions

A comparison of catalogs was performed in the following way. First, the parameters of a transformation model between two catalogs were estimated with the least-squares method. Then, the model was applied to coordinates of one of the catalogs and wrms residuals for right ascension and declination were calculated. And lastly, from the comparison of three catalogs at a time (combined and the two individual ones), the so-called "external" dispersions have been evaluated.

8.3.1. Systematic Effects

For evaluation of systematic effects a transformation model was applied. The model assumes the following systematic effects: rotation of one catalog relative to another, slopes in right ascension and declination, a bias in declination, and harmonic terms in both coordinates (see Bolotin & Lytvyn (2008)). The differences in right ascension, $\Delta\alpha$, and declination, $\Delta\delta$, are presented as:

$$\Delta\alpha = A_1 \tan\delta \cos\alpha + A_2 \tan\delta \sin\alpha - A_3 + D_\alpha(\delta - \delta_0) + C_\alpha \sin(\alpha + \varphi_\alpha) \quad (2)$$

$$\Delta\delta = -A_1 \sin\alpha + A_2 \cos\alpha + D_\delta(\delta - \delta_0) + B_\delta + C_\delta \sin(\alpha + \varphi_\delta), \quad (3)$$

where A_1, A_2 and A_3 are the rotation angles about the three axes; D_α and D_δ are the slopes in right ascension and declination as functions of the declination; B_δ is a bias in declination; C_α, φ_α and C_δ, φ_δ are amplitudes and phases of harmonic oscillations in right ascension and declination.

To calculate the parameters of the model the coordinates of the common (for both catalogs) ICRF1 defining sources were used. Then, after the model was applied, the wrms was evaluated for the entire set of common radio sources. The numbers of common defining sources and all sources for each pair of catalogs are presented in Table 5.

Table 5: Number of common sources in the catalogs (all and defining).

ID	aus008a		aus009a		bkg001a		gsf007b		iaa008c		mao008a		opa008b		usn010b	
maoC08a	2847	203	536	177	2977	204	3375	204	2918	204	3505	204	3214	204	3377	204
aus008a			537	177	2736	203	2836	203	2583	203	2829	203	2804	203	2839	203
aus009a					536	177	536	177	536	171	536	177	536	177	536	177
bkg001a							2945	204	2747	204	2933	204	2883	204	2945	204
gsf007b									2897	204	3340	204	3202	204	3367	204
iaa008c											2899	204	2848	204	2898	204
mao008a													3193	204	3345	204
opa008b															3209	204

Table 6: Weighted post-fit residuals ($\Delta\alpha \cos\delta$, $\Delta\delta$), μas.

ID	aus008a		aus009a		bkg001a		gsf007b		iaa008c		mao008a		opa008b		usn010b	
maoC08a	103	127	57	59	39	37	27	30	45	42	43	54	27	39	27	41
aus008a			26	19	129	128	104	109	108	115	98	102	106	108	115	110
aus009a					66	68	58	58	60	69	53	56	58	58	64	62
bkg001a							40	39	47	46	59	61	42	42	42	69
gsf007b									49	64	41	46	15	15	24	29
iaa008c											59	52	46	40	49	49
mao008a													41	46	46	55
opa008b															24	28

Table 7: Comparison of catalogs: maoC08a vs individual solutions. The first row for each pair presents the estimated parameters of the transformation model. The second row present the corresponding standard deviations.

A_1	A_2	A_3	D_α	D_δ	B_δ	S_α	φ_α	S_δ	φ_δ
				maoC08a – aus008a					
290.5	111.4	−164.5	−37.8	37.8	−23.3	13.0	301.7	32.3	18.5
20.1	16.6	11.6	21.3	13.1	10.6	15.2	65.1	22.1	37.4
				maoC08a – aus009a					
29.0	8.1	−11.6	−26.1	−8.0	18.4	12.8	261.5	35.7	353.8
10.9	9.8	7.5	12.6	7.8	6.9	9.3	40.0	12.5	18.6
				maoC08a – bkg001a					
−34.2	13.9	−14.4	−5.2	13.0	−30.0	9.2	146.3	13.2	128.3
6.8	6.0	4.1	7.2	4.8	4.3	5.0	34.9	7.7	30.6
				maoC08a – gsf007b					
−1.2	−3.4	0.3	−0.9	11.2	−2.2	8.9	185.8	1.8	79.5
5.2	4.6	3.3	5.6	3.5	3.1	4.2	27.1	5.3	181.4
				maoC08a – iaa008c					
−7.1	11.9	5.0	21.3	−16.7	2.5	7.5	225.8	9.4	305.8
7.8	6.9	5.1	8.6	5.4	4.8	6.8	46.3	8.8	49.2
				maoC08a – mao008a					
8.8	−25.3	−6.6	1.1	−24.5	24.5	19.2	148.7	7.2	53.3
8.8	7.9	6.0	9.7	5.9	5.3	7.1	23.9	9.1	81.6
				maoC08a – opa008b					
9.6	−11.8	2.3	−0.8	18.6	−12.1	5.4	191.5	6.3	73.3
6.3	5.6	4.1	6.8	4.2	3.7	5.2	54.6	6.5	65.4
				maoC08a – usn010b					
−6.3	26.4	7.4	2.7	3.6	−1.6	33.7	350.5	18.2	259.5
6.5	5.7	4.2	7.0	4.5	4.0	5.2	9.2	6.7	23.3

Table 8. Comparison of catalogs: comparisons between individual solutions. The first rows of each comparison present the estimated parameters of the transformation model. The second rows present the corresponding standard deviations.

A_1	A_2	A_3	D_α	D_δ	B_δ	S_α	φ_α	S_δ	φ_δ
.				aus008a – aus009a					
−266.4	−109.7	146.7	11.0	−18.3	22.5	12.3	138.8	4.0	234.8
4.1	3.5	2.5	4.5	2.8	2.3	3.1	14.9	4.1	67.8
				aus008a – bkg001a					
−332.9	−106.2	155.3	39.1	−21.0	−9.9	27.2	118.7	43.4	167.2
21.9	18.4	12.7	23.4	14.6	11.8	16.6	34.1	25.5	28.9
				aus008a – gsf007b					
−289.4	−114.7	162.3	33.9	−22.5	19.8	16.0	154.5	28.4	190.6
18.1	15.1	10.5	19.3	11.9	9.7	13.3	49.8	20.4	37.9
				aus008a – iaa008c					
−287.9	−97.9	165.4	60.0	−63.5	32.1	18.2	146.7	24.7	236.5
19.0	15.9	11.1	20.3	12.6	10.3	14.1	45.9	19.2	50.7
				aus008a – mao008a					
−277.4	−138.2	158.3	41.5	−71.8	59.6	25.9	134.2	23.2	153.0
16.9	14.1	10.0	18.1	11.1	9.1	12.8	28.5	19.6	41.9
				aus008a – opa008b					
−277.8	−120.3	162.9	33.7	−13.8	7.9	14.4	154.3	25.0	190.3
18.2	15.1	10.6	19.3	11.9	9.7	13.3	55.3	20.5	43.1
				aus008a – usn010b					
−292.9	−85.4	167.9	36.6	−21.1	11.3	26.1	1.0	46.3	226.7
19.1	15.9	11.1	20.3	12.6	10.2	13.8	32.3	19.6	26.7
				aus009a – bkg001a					
−59.4	10.3	−0.4	25.8	20.5	−48.4	18.0	120.6	41.1	166.7
12.4	11.3	8.6	14.6	9.3	8.2	9.7	35.3	14.5	18.5
				aus009a – gsf007b					
−31.1	−13.4	10.2	23.1	16.3	−17.8	14.6	109.1	38.1	167.7
10.7	9.7	7.4	12.6	8.0	7.1	8.5	37.1	12.5	17.2
				aus009a – iaa008c					
−34.7	4.6	18.6	50.4	−10.1	−15.7	7.6	124.3	28.9	192.3
12.0	10.9	8.4	14.1	8.9	8.0	9.4	82.2	13.3	27.0
				aus009a – mao008a					
−23.4	−39.0	2.3	23.7	−17.1	6.6	26.6	111.8	38.7	156.3
10.0	9.2	7.1	11.9	7.5	6.7	8.1	19.6	12.0	15.7
				aus009a – opa008b					
−19.6	−24.4	12.7	23.8	21.9	−26.2	12.9	86.1	38.8	157.6
10.7	9.8	7.5	12.6	8.0	7.1	9.1	40.2	12.7	16.7
				aus009a – usn010b					

Table 8—Continued

$A_1^{\cdot}$	A_2	A_3	D_α	D_δ	B_δ	S_α	φ_α	S_δ	φ_δ
$-39.^{\cdot}4$	18.9	18.4	27.9	6.9	−15.7	36.8	17.8	46.6	198.1
11.6	10.5	8.0	13.6	8.7	7.7	10.2	14.5	12.6	16.4
bkg001a – gsf007b									
29.9	−19.3	14.9	4.0	−3.5	30.0	2.6	257.7	8.4	308.9
6.6	6.1	4.3	7.6	5.3	4.7	5.5	115.2	7.9	49.2
bkg001a – iaa008c									
25.1	−4.2	19.7	24.5	−31.2	34.4	10.8	287.3	19.5	306.8
7.8	7.1	5.2	9.0	6.1	5.4	6.3	35.5	9.2	24.8
bkg001a – mao008a									
36.0	−44.0	5.7	2.0	−37.7	54.8	12.1	120.8	4.6	358.1
10.1	9.3	6.9	11.6	7.8	6.9	7.9	42.9	11.6	140.8
bkg001a – opa008b									
41.4	−29.0	17.8	5.4	2.5	21.2	5.2	323.4	6.9	351.8
6.9	6.4	4.6	7.9	5.5	4.8	5.4	65.5	8.1	63.8
bkg001a – usn010b									
22.9	11.0	22.0	7.2	−11.7	30.6	41.7	351.6	26.7	269.9
7.5	6.8	4.9	8.5	6.0	5.3	6.0	8.4	8.4	18.5
gsf007b – iaa008c									
−5.2	15.2	5.6	22.6	−26.6	3.5	7.7	297.1	11.1	302.6
7.1	6.4	4.9	8.2	5.5	4.9	5.6	46.7	8.3	39.3
gsf007b – mao008a									
7.9	−23.1	−7.1	1.7	−36.2	27.0	13.7	122.5	4.7	71.8
7.3	6.7	5.1	8.4	5.6	5.0	5.8	28.2	8.0	103.7
gsf007b – opa008b									
10.9	−9.5	2.6	0.6	6.0	−8.6	4.5	359.0	5.6	74.7
2.5	2.3	1.7	2.9	1.9	1.7	2.1	26.4	2.7	29.9
gsf007b – usn010b									
−7.1	30.5	7.6	3.9	−7.8	0.9	41.3	355.1	20.9	255.1
4.5	4.1	3.0	5.2	3.6	3.1	3.7	5.2	4.9	14.4
iaa008c – mao008a									
12.4	−38.7	−14.1	−23.8	−7.1	21.7	21.8	119.3	16.3	113.9
9.3	8.5	6.6	10.8	7.1	6.3	7.5	22.4	10.9	35.9
iaa008c – opa008b									
16.6	−25.1	−3.2	−22.1	33.2	−12.7	6.7	79.5	15.3	106.3
7.2	6.6	5.0	8.4	5.5	4.9	6.3	51.3	8.3	30.0
iaa008c – usn010b									
−2.6	15.9	1.9	−18.9	18.0	−2.0	37.4	5.4	16.5	224.5

The results of least square estimation of model parameters are presented in Table 7 and Table 8. Table 7 shows comparison of the combined catalog, maoC08a, with the individual solutions. Mutual comparisons between individual solutions are presented in Table 8. In the tables the first lines for each pair of catalogs present the estimated values, and the second lines present the standard deviations. Parameters A_1, A_2, A_3, B_δ, S_α and S_δ are in units of μas; units for D_α and D_δ are $\mu as/rad$; and phases φ_α and φ_δ are in degrees.

In Table 6 weighted post-fit residuals for each comparison pair are shown. The residuals have been evaluated for each pair of catalogs after removing the estimated systematic effects.

As one can see from the tables, there are significant systematic effects in catalog aus008a. The angles of rotation are about $150 - 300\,\mu$as between aus008a and other individual solutions, while for other individual catalogs (including aus009a) the mutual rotation is about $50\,\mu$as or less. Also, standard deviations of estimated parameters for catalog aus008a are greater than the corresponding deviations of parameters for other solutions by about $2 - 3$ times.

On the other hand, catalog aus009a shows relatively good agreement with the other individual catalogs. Catalogs aus008a and aus009a differ only in the minimum number of observations per source (> 3 for aus008a and > 100 for aus009a, which eliminated many VCS sources). This could indicate the influence of *a priori* information on results in solutions obtained by Geoscience Australia caused either by design of the least squares collocation method or its implementation. In any case, if catalog aus008a is omitted, then the remaining mutual systematic effects between seven individual catalog solutions obtained with four independent software packages do not exceed the $50\,\mu$as level.

Also we note considerably large (up to $40\,\mu$as) angles of rotation between the bkg001a catalog and other individual solutions. The reason of this change in orientation is the absence of one ICRF1 defining source, 1903−802, in the BKG solution. All the other analysis centers included observations of this source and its *a priori* coordinates were used in the no-net-rotation constraints to fix the orientation of the obtained celestial reference frame.

Significant differences in the harmonic oscillation parameters are obtained for the usn010b catalog. Comparing with gsf007b, they are $41 \pm 4\,\mu$as and $21 \pm 5\,\mu$as for Right Ascension and declination respectively. Such deformations could be caused either by the absence of diurnal and semi-diurnal tidal EOP variations or by using an obsolete model of nutation (see Bolotin (2007)).

8.3.2. External Uncertainties

The so-called "external" uncertainties can be evaluated in the following way. For a pair of catalogs we can write (with some assumptions):

$$\overline{d_{12}{}^2} = {\sigma_1}^2 - 2\rho_{12}\sigma_1\sigma_2 + {\sigma_2}^2 \tag{4}$$

where $\overline{d_{12}{}^2}$ is the weighted mean of the squared differences between a pair of catalogs; σ_1 and σ_2 are the "external" uncertainties of the catalogs; and ρ_{12} is the corresponding correlation

coefficient. By writing such equations for three catalogs, it is possible to construct a system of equations and to solve it with respect to σ_1, σ_2 and σ_3. The results of such calculations of external uncertainties are presented in Table 9. In these comparisons the combined solution has been used as third catalog. The calculations were done for all common radio sources in the three catalogs.

Table 8—Continued

$A_1^{\cdot}$	A_2	A_3	D_α	D_δ	B_δ	S_α	φ_α	S_δ	φ_δ
$8^{\cdot}.4$	7.6	5.8	9.7	6.5	5.8	7.2	10.7	8.9	34.3
				mao008a – opa008b					
2.2	13.4	9.2	−2.1	43.8	−37.0	16.4	316.9	1.1	124.7
7.2	6.7	5.1	8.4	5.5	4.9	5.8	23.7	8.6	399.4
				mao008a – usn010b					
−14.7	53.6	15.6	3.6	29.7	−27.0	50.6	342.0	25.3	255.0
8.5	7.8	6.0	9.9	6.6	5.9	7.1	8.6	9.4	22.7
				opa008b – usn010b					
−17.5	39.9	5.1	3.5	−13.6	9.3	37.0	354.1	26.2	255.9
4.4	4.1	3.0	5.1	3.5	3.1	3.7	5.8	4.9	11.4

Table 9. Comparison of catalogs: external uncertainties

Coordinate	index 1	index 2	σ_1 μas	σ_2 μas	σ_3 μas
α	aus008a	aus009a	58	61	6
δ	aus008a	aus009a	73	76	3
α	aus008a	bkg001a	188	89	14
δ	aus008a	bkg001a	220	73	7
α	aus008a	gsf007b	189	22	10
δ	aus008a	gsf007b	223	29	6
α	aus008a	iaa008c	192	64	14
δ	aus008a	iaa008c	219	70	6
α	aus008a	mao008a	199	57	17
δ	aus008a	mao008a	227	62	10
α	aus008a	opa008b	190	20	10
δ	aus008a	opa008b	224	30	6
α	aus008a	usn010b	190	23	11
δ	aus008a	usn010b	223	40	8
α	aus009a	bkg001a	58	24	9
δ	aus009a	bkg001a	77	27	5
α	aus009a	gsf007b	57	15	7
δ	aus009a	gsf007b	75	18	3
α	aus009a	iaa008c	57	33	11
δ	aus009a	iaa008c	76	36	4
α	aus009a	mao008a	56	38	11
δ	aus009a	mao008a	73	42	7
α	aus009a	opa008b	57	15	6
δ	aus009a	opa008b	75	16	3

Table 9—Continued

Coordinate	index		σ_1	σ_2	σ_3
	1	2	μas	μas	μas
α	aus009a	usn010b	57	17	7
δ	aus009a	usn010b	75	30	6
α	bkg001a	gsf007b	88	23	10
δ	bkg001a	gsf007b	115	30	7
α	bkg001a	iaa008c	85	65	14
δ	bkg001a	iaa008c	110	74	8
α	bkg001a	mao008a	94	56	13
δ	bkg001a	mao008a	119	64	9
α	bkg001a	opa008b	92	20	10
δ	bkg001a	opa008b	120	33	7
α	bkg001a	usn010b	89	23	11
δ	bkg001a	usn010b	117	42	8
α	gsf007b	iaa008c	25	64	10
δ	gsf007b	iaa008c	30	73	7
α	gsf007b	mao008a	26	55	12
δ	gsf007b	mao008a	33	62	10
α	gsf007b	opa008b	23	21	10
δ	gsf007b	opa008b	28	32	8
α	gsf007b	usn010b	24	25	11
δ	gsf007b	usn010b	29	41	9
α	iaa008c	mao008a	59	47	15
δ	iaa008c	mao008a	68	53	10
α	iaa008c	opa008b	64	23	10
δ	iaa008c	opa008b	71	32	8

"External" uncertainties for almost all catalogs except bkg001a, aus008a, and aus009a are at the level of 50 μas. For bkg001a they are about twice greater, and for aus009a catalog they are about 1.5 times greater. So, in addition to the systematic effects, these catalogs are also noisier.

8.4. Conclusions

Comparison of individual contributed catalog solutions have showed that the individual catalogs are very close to each other. The systematic effects in general are at the level of 50 μas. The weighted post-fit residuals, evaluated after removing systematic effects for all common sources of pairs of catalogs are at the same level. That indicates good agreement between the different solutions. Considering that the individual catalogs were obtained with four independent software packages, and used slightly different data sets and analysis models, one could conclude that systematic effects and additional random errors in the newly generated celestial reference frame ICRF2 will not exceed $50 - 100\,\mu$as.

9. Determination of Realistic Errors (DM)

The formal uncertainties of source position estimates based on observation noise tend to improve by a factor of $1/\sqrt{N}$ where N is the number of observations. For sources that have a very large number of observations, the formal uncertainties are generally too small. To obtain a more realistic measure of the uncertainty, we have considered three effects: 1) modeling errors, 2) analysis noise, and 3) statistical consistency (validity) of the formal uncertainties. The sensitivities of source position estimates to different modeling choices is discussed in §6 and summarized in Table 2. These sensitivities are less than 20 μas. They should not be interpreted necessarily as errors in analysis but rather as the level of variation associated with improvements of the state-of-the-art analysis. Unmodeled or mis-modeling errors should be at this level. Analysis noise refers to the cumulative effects of data editing and modeling errors. This is quantified by comparing catalogs generated by different analysis centers and is discussed in detail in §8. Differences will result from different analysis software as well as different analysis strategies. Each analysis center may edit data differently or choose different sets of experiment sessions to include in a solution. However, the raw observation data available to all analysis centers are identical. This means that the source position estimates from the different centers will be correlated. Therefore, differences between position estimates from different solutions will not reflect the true noise in either solution. In the following, we consider how to inflate the formal source position estimates to obtain realistic uncertainties.

9.1. Decimation Test

To determine a realistic level of source position errors, we ran a decimation test in which all experiments were ordered chronologically and divided into two sets selected by even or

odd session. This was done for each well-defined session type, where a session type refers to a series of experiments with the same core network of observing stations. This should help ensure that the two full sets of sessions were equivalent in terms of networks and sources observed. The remaining group of sessions not in an obvious category were similarly divided. The source position estimates from the two solutions are independent and the solution position differences provide estimates of the noise of each solution as well as how much the formal uncertainties should be scaled up. In a similar way, Ryan et al. (1993) investigated geodetic solutions to determine the uncertainty of site velocity estimates. Analysis of the differences between site velocities estimated in two terrestrial reference frame solutions that used independent session lists yielded the result that the site velocity component formal errors should be multiplied by a factor of $1.3 - 1.8$.

The differences in source position estimates from the two decimation solutions were scaled by their formal errors and then the standard deviation of the scaled differences was computed. The histograms of the scaled differences are shown in Figure 18. The resulting scaling factors (standard deviations) were 1.6 and 1.5 for declination and right ascension, respectively.

The wrms difference between source position estimates, s_i, from the two solutions after removing biases is

$$\sigma^2 = \left\langle (s_1 - s_2)^2 \right\rangle = \sigma_1^2 + \sigma_2^2 \tag{5}$$

where σ_i^2 are the solution noise variances and the estimates from the two solutions are assumed to be uncorrelated,

$$\langle s_i s_j \rangle = \sigma_i^2 \delta_{ij} \tag{6}$$

If we assume the two solutions have the same noise then we can get an estimate of the noise of each solution

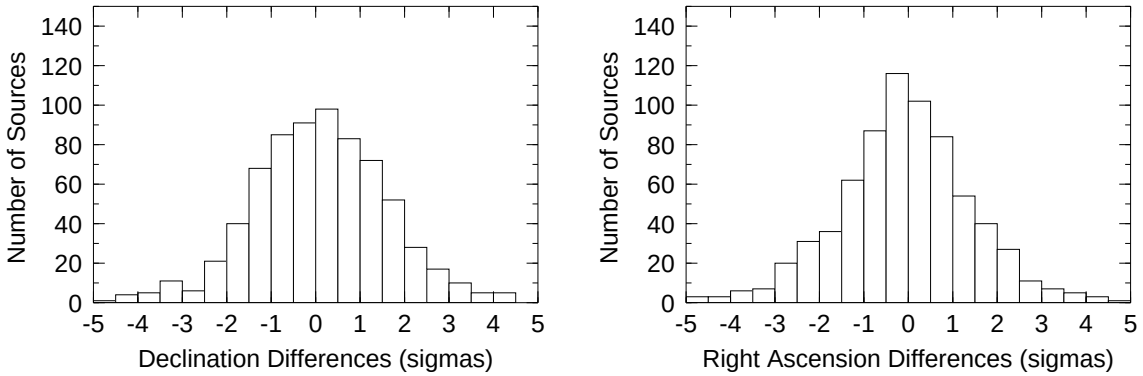

Fig. 18.— Histograms of declination and right ascension differences (scaled by sigmas) between estimates from the two decimation solutions.

Table 9—Continued

Coordinate	index 1	index 2	σ_1 μas	σ_2 μas	σ_3 μas
α	iaa008c	usn010b	64	26	10
δ	iaa008c	usn010b	74	43	8
α	mao008a	opa008b	52	23	12
δ	mao008a	opa008b	59	32	10
α	mao008a	usn010b	56	27	12
δ	mao008a	usn010b	64	45	10
α	opa008b	usn010b	21	24	10
δ	opa008b	usn010b	33	40	9

Table 10: Solution Difference Statistics

Solution difference	Right Ascension wrms (μas)	Right Ascension scale factor	Declination wrms (μas)	Declination scale factor	Number of Sources
Decimation	67	1.6	52	1.54	730
gsf08b -usn10b	39	0.91	32	1.17	1136
gsf08b - iaa008c	55	1.14	38	1.06	1051
gsf08b - mao008a	66	1.37	48	1.31	1031

wrms differences were scaled by $1/\sqrt{2}$.

$$\sigma_i \sim \sigma/\sqrt{2} \tag{7}$$

For comparison, we have computed the wrms differences (scaled by a factor of $1/\sqrt{2}$ between the GSFC solution (gsf008b) and several of the other analysis center solutions (usn010b, iaa008c, and mao008a). VCS sources from these solutions were not included in the comparisons. The average wrms differences (scaled by $1/\sqrt{2}$) for the different analysis center solutions are compared with the differences from the decimation test in Table 1.

9.2. Declination Band Noise

In Figure 19, the noise, σ_i, is shown as a function of declination band. One can see that the right ascension wrms differences for the bands north of $-45°$ declination are about 50 μas. For declination, σ_i are about 50 μas north of 30° declination, but are $60 - 80$ μas between $-45°$ and $-30°$ declination. If the scaling factor is computed for different declination bands, one finds that it has a declination dependence, which is shown in Figure 20. The factor tends to increase with declination because higher declination sources have been observed more frequently.

The differences between the GSFC solution and the other analysis center solutions are shown in Figure 19 and follow the same general trend in declination as for the decimation test difference. The magnitudes of the differences are smaller because each of the analysis center solutions used approximately the same set of data so that the estimates from the two solutions are correlated. The analysis center wrms differences give a measure of analysis noise. The GSFC/USNO differences are generally the smallest since both solutions used the SOLVE analysis software. The MAO and IAA differences tend to be larger probably because these solutions used different analysis software – SteelBreeze for MAO and QUASAR for IAA.

9.3. Dependence of Source Noise on Number of Observing Sessions

The average formal precision of position generally is better as declination increases since observing has been dominated by sites in the Northern hemisphere. However, there is a large range of variation of formal precision in all declination bands. One of the motivations for inflating the position uncertainties is to account for error sources that cannot be averaged down by more frequent observing. If all errors were Gaussian then the uncertainty of position estimates should fall off as $1/\sqrt{N}$ where N is the number of observations. Instead of looking at the dependence of the wrms differences between decimation solutions as a function of declination, we next consider the dependence on the number of sessions that a source was observed. The sources were ordered by the average number of experiment sessions in which a source was observed in the two decimation solutions. The differences in position were analyzed for a running window of 50 sources in this ordered sequence of sources. We computed the wrms difference of positions from the two solutions for each 50 source subset of all the

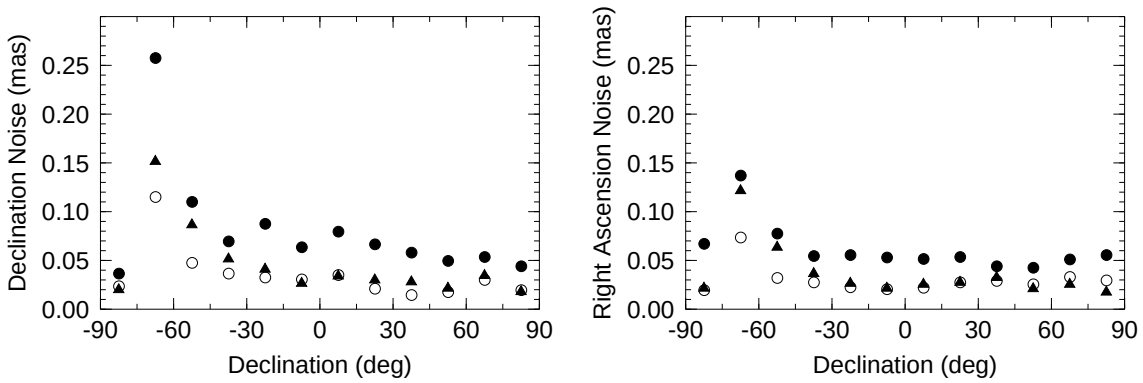

Fig. 19.— Declination and right ascension noise for each 15 degree declination band in each solution derived from differences between positions in the two decimation solutions (solid circles). The average noise for the solution differences gsf08b - usn10b (open circles) and for gsf08b - iaa008c (solid triangles) are shown for comparison.

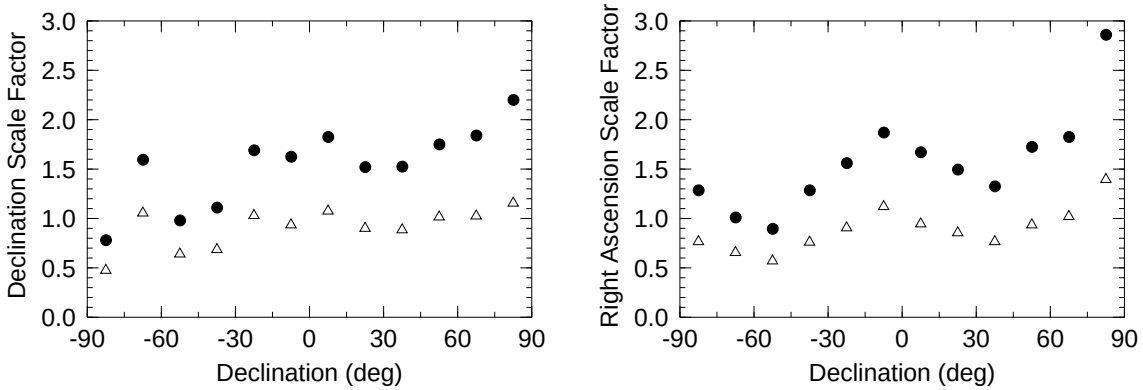

Fig. 20.— Formal error scaling factor for declination and right ascension (solid circles). Also shown is the residual scaling factor after applying a uniform average scaling factor of 1.5 to the formal uncertainties followed by a root-sum-square addition of 40 μas (open triangles).

sources common to both decimation solutions. Figure 21 shows the dependence of the wrms difference (scaled by $1/\sqrt{2}$) as a function of the minimum number of sessions in each subset. This is compared to the median formal uncertainty in the subset. The wrms differences are larger than the median formal errors and both fall off approximately as $1/\sqrt{N}$. The observed minimum error of 25 μas for declination and 15 μas for right ascension is reached for sources that have been observed in more than 200 sessions. If one applies an overall scaling factor of 1.5 based on all source position differences, one still needs to add additional noise to account for residual scaling errors that are as large as 1.5 for sources observed in less than 75 sessions. An additional 40 μas of noise in a root-sum-square sense reduces the residual scaling error to what is shown in Figure 22 at the expense of conservative uncertainties for the most observed sources.

9.4. Summary

For ICRF1, a scaling factor of 1.5 was first applied to the formal uncertainties followed by a root-sum-square increase of 250 μas. From the current decimation test, we get a similar scaling factor when averaging over all sources, but we can see that the scaling factor increases with declination since the formal uncertainties of positions tend to increase with declination. To account for this, we need to then add additional noise. Based on the noise shown in Figure 21, a value of 40 μas is a reasonable upper limit on the noise floor. The residual scale factor after applying first a scale factor of 1.5 to the original formal uncertainties and then adding 40 μas in a root-sum-square sense shown in Figure 20 is flatter and closer to unity as a function of declination. As a function of the number of sessions in which a source is observed, the residual scale factor shown in Figure 22 is generally less than unity. After applying these corrections to the formal errors, the average residual scaling factors are 0.95 for declination and 0.88 for right ascension.

10. External validation (AN, SB2)

In the absence of any superior-quality source position catalogue, a state-of-the-art CRF does not find a data set to which it can be compared to assess its own quality. However, the results of the estimation process of radio source positions always depend on a simultaneous estimate of the whole suite of unknown parameters in the VLBI model. For this reason, the results of site coordinates and velocities as well as of the Earth orientation parameters belong to a certain CRF determination in a consistent way when estimated together. An external validation of a complete VLBI adjustment and of the CRF results can, thus, be carried out through an indirect quality assessment applied to the TRF and the EOP results alone.

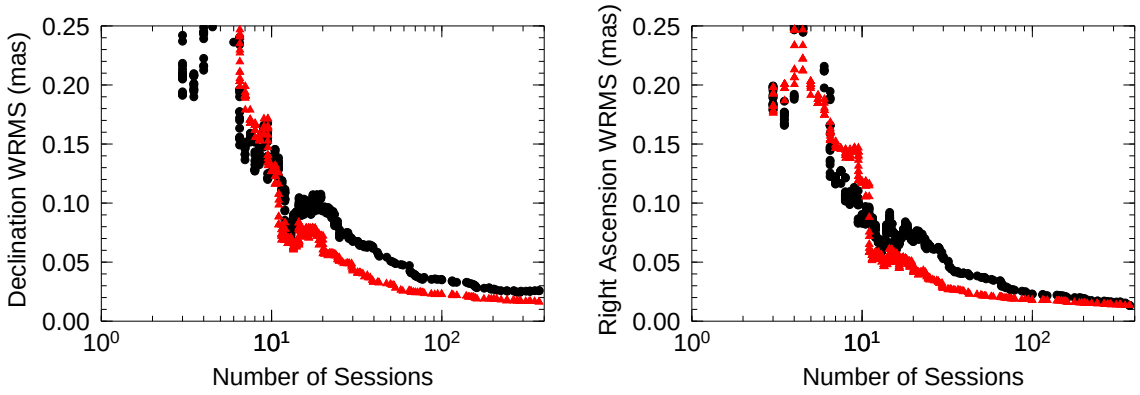

Fig. 21.— Wrms noise (solid circles) for subsets of 50 sources in each solution as a function of the minimum number of sessions a source was observed. The median formal uncertainty (red triangles) in each subset is shown for comparison. These was derived from differences between positions in the two decimation solutions.

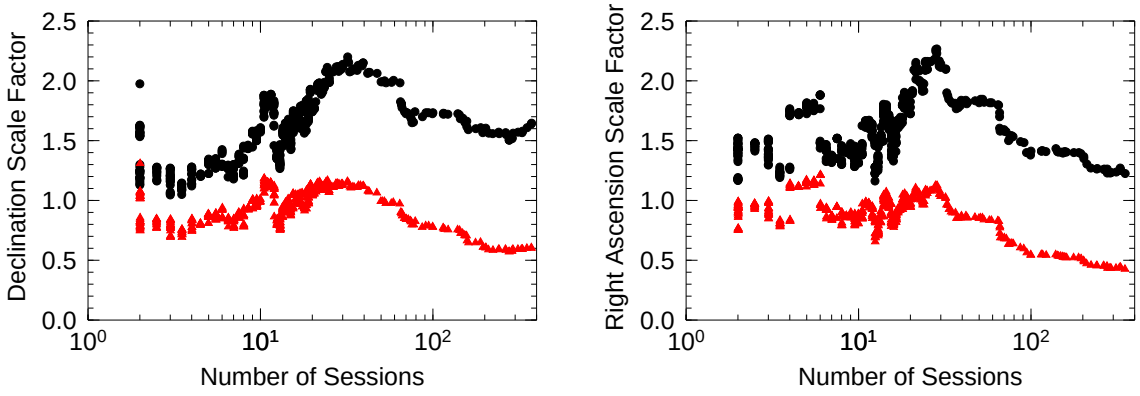

Fig. 22.— Error scaling factor (solid black circles) for each subset of 50 sources in each solution as a function of the minimum number of sessions a source was observed. The residual scaling factor (red triangles) after application of a scale factor of 1.5 to the formal uncertainties followed by a root-sum-square increase of 40 μas.

10.1. Earth Orientation Parameters

For a comparison of the full set of EOP results, i.e., polar motion and UT1−UTC and their time derivatives as well as the offsets in the two nutation angles, it has to be noted that only for the polar motion components an external evaluation is possible through GPS providing a suitable data set with the same or even better quality. The official EOP series (igs00p03.erp) of the International GNSS Service (IGS) was used for the following comparisons. After subtracting a bias and a rate the six solutions considered initially for ICRF2 exhibit a level of agreement of roughly 120 μas in both components (Table 11). Figure 23 and Figure 24 depict the behavior of the pole components in the form of medians calculated every seven days for plus/minus 35 days. Noticeable systematic variations seem to be more prominent in the y component which have been identified to belong to changes in the IVS network constellations (Artz et al. 2008). In general, the scatter of the VLBI results and the systematic network effects are at the same level indicating that the wrms values are representative for the overall agreement.

Table 11: wrms differences of the different VLBI solutions w.r.t. IGS

Analysis Center	X Pole			Y Pole		
	Offset [μas]	Rate [μas]	wrms [μas]	Offset [μas]	Rate [μs]	wrms [μs]
BKG	-87.0 ± 4.3	12.4 ± 1.7	131.0	-125.1 ± 4.1	-13.2 ± 1.6	125.2
GSF	-86.6 ± 3.7	11.4 ± 1.5	111.4	-132.3 ± 3.5	-15.2 ± 1.4	106.7
MAO	-21.3 ± 4.3	6.3 ± 1.7	124.8	-93.9 ± 4.1	-10.1 ± 1.5	120.1
IAA	-140.5 ± 4.1	13.5 ± 1.6	123.5	-137.3 ± 3.9	-17.2 ± 1.5	119.6
OPA	-80.4 ± 3.7	7.6 ± 1.5	115.2	-119.1 ± 3.5	-13.8 ± 1.4	109.1
USN	-79.1 ± 4.0	9.0 ± 1.6	121.3	-141.2 ± 3.8	-12.9 ± 1.5	115.7

The other three components of the standard Earth orientation representation, UT1−UTC and nutation in dX and dY, can only be determined by VLBI observations with sufficient

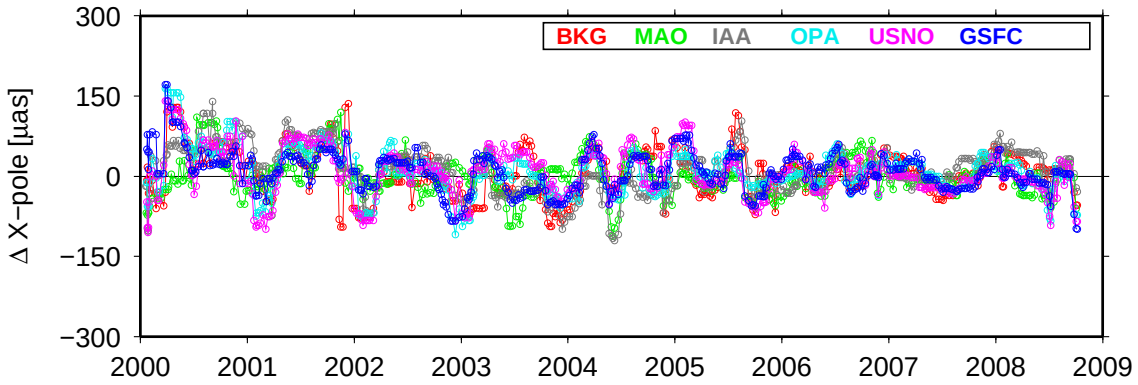

Fig. 23.— 70-day-median smoothed X pole difference w.r.t. IGS (igs00p03.erp)

accuracy. Thus, for these components, no suitable external, i.e. non-VLBI, comparison is available. An evaluation can, thus, only be carried out by inter-comparing the results of the six solutions. This is a valid approach here since the six time series have been generated by three different software packages. In order to subtract a common signal for a better interpretation, the IERS 05C04 EOP series has been used as a reference. It should be mentioned that the wrms differences (Table 12) and the graphs do not show any quality in an absolute sense since the 05C04 series for UT1−UTC and nutation is mainly driven by VLBI results, however computed with different inputs and for a different purpose. For this reason, the quality of these EOP components should only be derived by contemplating the level of relative agreement.

Taking these considerations into account, a first criterion of the quality should be any systematic behavior visible in the plots (Figure 25 and Figure 26). It is easily discernible that the four Calc/Solve solutions and the SteelBreeze solution by MAO do not exhibit strong systematic variations in the 70-day-median representation. However, a very obvious effect with an irregular period is visible in the IAA time series. This effect has been caused by errors in the submitted IAA EOP file. Since the MAO and the IAA time series do not show strong correlations but the MAO rather follows the four Calc/Solve solutions with some excess noise, it can be concluded that the numerical results provide a reliable relative indication of the quality of each input series.

Table 12: wrms differences of the different VLBI solutions w.r.t. IERS 05C04 for nutation

Analysis Center	Nutation dX			Nutation dY		
	Offset [μas]	Rate [μas]	wrms [μas]	Offset [μas]	Rate [μs]	wrms [μs]
BKG	19.0 ± 1.9	-2.0 ± 0.4	76.6	-8.1 ± 2.2	3.4 ± 0.5	93.3
GSF	34.7 ± 1.6	-1.8 ± 0.3	61.9	19.7 ± 1.8	3.9 ± 0.4	75.9
MAO	-14.2 ± 2.6	-1.2 ± 0.6	100.5	-31.1 ± 2.7	2.1 ± 0.7	107.2
IAA	-6.1 ± 3.5	-11.2 ± 0.8	143.8	95.7 ± 3.5	13.5 ± 0.9	147.8
OPA	37.1 ± 1.8	-1.2 ± 0.4	69.8	24.0 ± 1.8	-2.1 ± 0.5	76.3
USN	35.8 ± 1.9	-2.5 ± 0.4	76.7	32.6 ± 2.2	3.3 ± 0.6	92.9

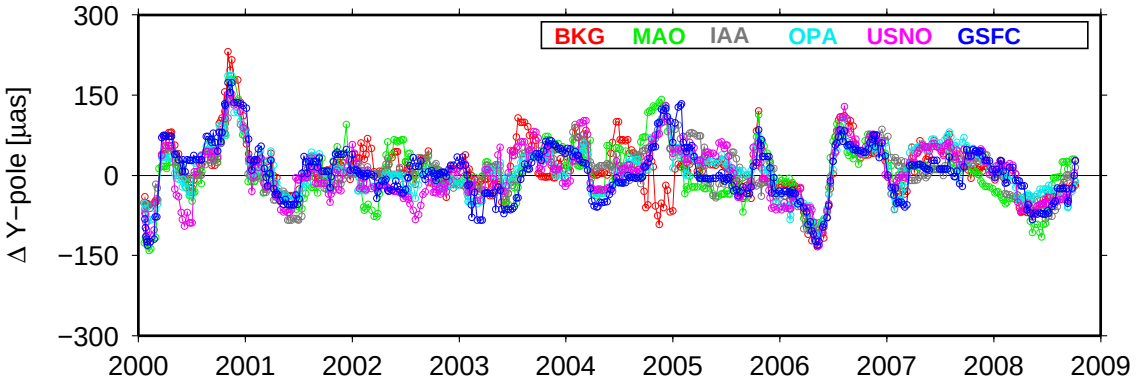

Fig. 24.— 70-day-median smoothed Y pole difference w.r.t. IGS (igs00p03.erp)

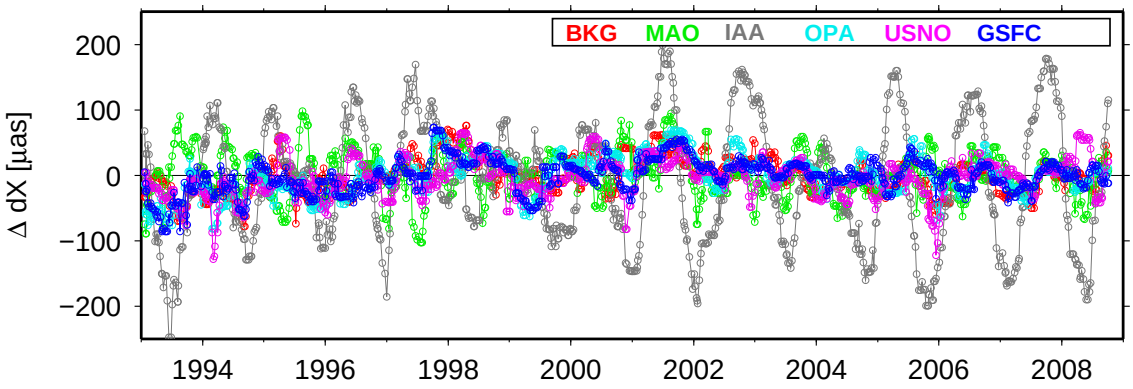

Fig. 25.— 70-day-median smoothed dX nutation differences w.r.t. IERS 05C04

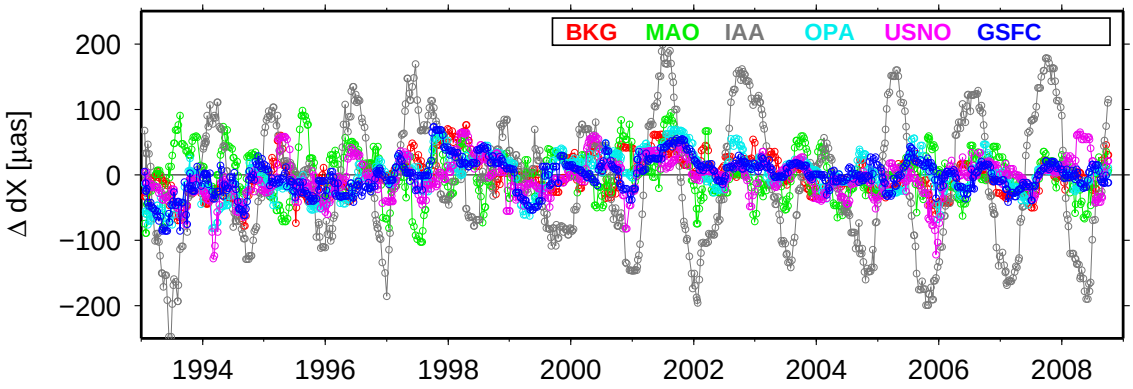

Fig. 26.— 70-day-median smoothed dY nutation differences w.r.t. IERS 05C04

Table 13: wrms differences of the different VLBI solutions w.r.t. IERS 05C04 for UT1−UTC

Analysis Center	UT1−UTC		
	Offset [μs]	Rate [μs]	wrms [μs]
BKG	−4.47 ± 0.23	−0.40± 0.06	9.08
GSF	−3.88 ± 0.21	−0.38± 0.06	8.60
MAO	−0.07 ± 0.24	−0.43± 0.07	9.21
IAA	−0.95 ± 0.21	−0.17± 0.06	8.56
OPA	−4.10 ± 0.21	−0.21± 0.06	8.63
USN	−4.91 ± 0.22	−0.15± 0.06	8.77

In Table 12, the MAO solution agrees with the IERS 05C04 series with 100 and 107 μas in a wrms sense and the Calc/Solve solutions at the level of 60 to 95 μas. Since these time series all agree with the reference series at a similar level, the absolute accuracy of the nutation estimates should not be worse than by a factor of $\sqrt{2}$. This indicates that the nutation accuracy is at the same level than that of polar motion.

A comparison of the six time series for UT1−UTC shows a slightly different problem (Figure 27). The reference series IERS 05C04 exhibits a long term drift after 2002.5. Nevertheless, the VLBI solutions agree with each other at the few μs level. Table 13 provides the wrms differences w.r.t. the reference series at the level of about 9 μs which corresponds to 135 μas. Obviously, this number is driven by the systematic effect in the differences and does not characterize the agreement of the six series as such. This agreement is rather at the level of $4-5$ μs. The level of the agreement of the UT1−UTC results, thus, matches that of the polar motion results and the 100 μas can, therefore, be considered as the upper limit also of this component of Earth rotation.

Biases of the polar motion components of the individual solutions w.r.t. to IERS 05C04 are below the 85 μs. The orientations of the terrestrial axes are, thus, effected at the same level.

From the comparisons of the EOP results, it can be concluded that the solutions initially considered for the computation of ICRF2 agree with each other at the level of better than

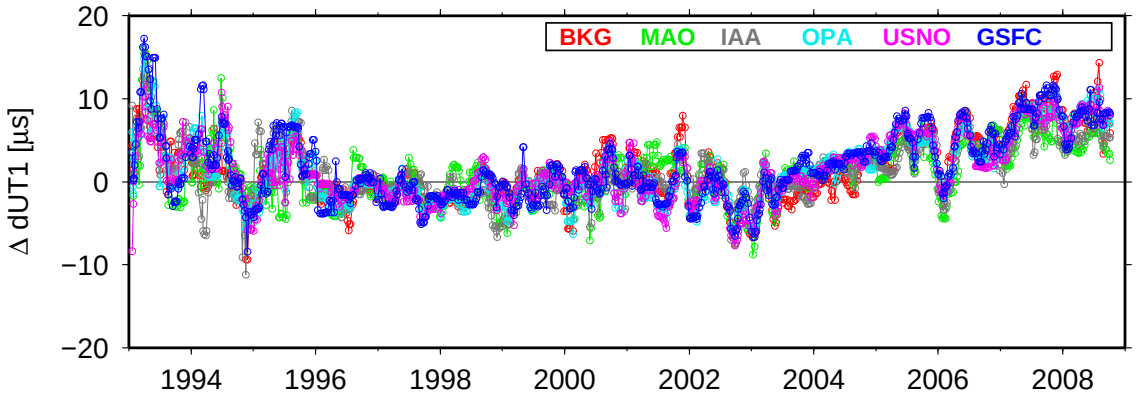

Fig. 27.— 70-day-median smoothed UT1−UTC differences w.r.t. IERS 05C04

100 μas excluding obvious systematic deficiencies. The polar motion results of the solution selected for ICRF2, gsf008a, agree with the IGS GPS results by 111 and 107 μas for the x and y component respectively. Considering that the other EOP components do not exhibit any obvious systematic effects, it can be concluded that their accuracy is at the same level. An upper bound of 110 μas or 3.3 mm at the Earth's surface can thus be inferred for the overall accuracy of each observing session contributing to the determination of ICRF2.

10.2. Terrestrial Reference Frame

A second option for external validations is to investigate what quality the terrestrial reference frame (TRF) has which was estimated in the same process as the CRF was. Since the decision has been made to use the gsf008a solution for ICRF2, the respective TRF has been compared to other TRFs. A comparison of different TRF is most practically being carried out by estimating the parameters of a 14 parameter Helmert transformation and a study of the respective residuals. Ideally, a comparison should be made to the latest realization of the International Terrestrial Reference System, the ITRF2008. Unfortunately, ITRF2008 has not been released at this time. Therefore, VTRF2008 which is the TRF determined from the VLBI input to ITRF2008 is the best independent TRF currently available for this purpose (Böckmann, Nothnagel, & Artz 2009).

VTRF2008 is a TRF combination product from input of several IVS Analysis Centers and should provide a very reliable reference due to the stabilizing effect of the combination. Seven of nine contributions had been accepted after a detailed quality check excluding two solutions which did not match the high quality criteria. Six of the seven ACs accepted had used the program package Calc/Solve and only one other solution by DGFI was generated with an independent software package, OCCAM. Although it would be better to have more solutions from different software packages, the agreement of all the accepted solutions in general and between the software packages of Calc/Solve and OCCAM in particular should exclude any serious deficiencies in the combined TRF.

The second reference TRF to compare the gsf008a TRF to, is ITRF2005 (Altamimi et al. 2007). However, ITRF2005 has a known deficiency due to a flaw in the pole tide modeling of the VLBI input. Due to the pole tide error and the unbalanced distribution of observing sites, any comparisons to ITRF2005 will show a noticeable difference in the scale factor (Altamimi et al. 2007; Böckmann et al. 2007).

The Helmert parameters of the gsf008a solution w.r.t. VTRF2008 and ITRF2005 are listed in Table 14. In the context of ICRF2, the rotations and their time evolution are of particular importance. The gsf008a solution is rotated w.r.t. VTRF2008 by not more than 41 μas and w.r.t. ITRF2005 by not more than 3 μas. The rotation rates are at the level of a few μas/yr with formal errors at the same level. The scale difference and its rate w.r.t. VTRF2008 is so small that it is hardly significant. The well known scale effect of ITRF2005 of 0.4 ppb appears as expected.

The quality of the coordinates and velocities of individual observatories can best be discussed by looking at the post fit residuals of the epoch positions and of the velocities.

Table 14: Helmert parameters of TRF(gsf008a) w.r.t. VTRF2008 and ITRF2005

Helmert Parameter	VTRF2008	σ	ITRF2005	σ	
T_x	−0.69	±0.36	−0.26	±0.94	mm
T_y	−0.22	±0.35	0.00	±0.87	mm
T_z	−0.21	±0.34	0.11	±0.87	mm
R_x	−31.8	±13.9	0.5	±30.0	μas
R_y	−41.2	±13.2	−0.7	±35.3	μas
R_z	15.2	±9.2	2.9	±32.2	μas
ΔS	−0.006	±0.050	−0.406	±0.138	ppb
T_x/dt	−0.06	±0.09	−0.24	±0.14	mm/y
T_y/dt	0.09	±0.09	0.13	±0.15	mm/y
T_z/dt	0.22	±0.09	0.11	±0.14	mm/y
R_x/dt	−4.61	±3.7	−5.50	±5.96	μas/y
R_y/dt	−2.35	±3.5	−7.57	±5.19	μas/y
R_z/dt	−2.52	±3.2	−1.63	±4.83	μas/y
ΔS/dt	−0.009	±0.014	−0.015	±0.022	ppb/y

Observing sites active at the reference epoch of the station positions (2000.0) generally show differences w.r.t. VTRF2008 below 5 mm in the horizontal topocentric positions (Figure 28) with matching discrepancies in the velocity components (Figure 29). Notable exceptions are SYOWA and OHIGGINS in Antarctica, TIGOCONC in Chile and NYALES20 on Spitsbergen with horizontal residuals being slightly larger. However, the vertical differences (Figure 30) of these sites fit to VTRF2008 very well. The other stations with larger residuals are older radio telescopes which have been decommissioned already some time ago.

The comparison with ITRF2005 shows a similar picture (Figure 31 and Figure 32). However, a number of sites did have only a short observing history at that time and differences are, thus, larger. In addition, the error in the 2005 VLBI pole tide model appears as a zonal effect in the differences today. For this reason, ITRF2005 turns out not to be a suitable reference for an external validation of the solution for ICRF2 on an individual site basis.

On the basis of the Helmert parameters of the gsf008a TRF estimates w.r.t. the two reference TRFs (VTRF2008 and ITRF2005) it can be stated that the solution fulfills the requirements in terms of the orientation of the axes. The residuals of horizontal and vertical coordinate components as well as of the velocities confirm the overall accuracy of the gsf008a solution at the level of 3.5 mm.

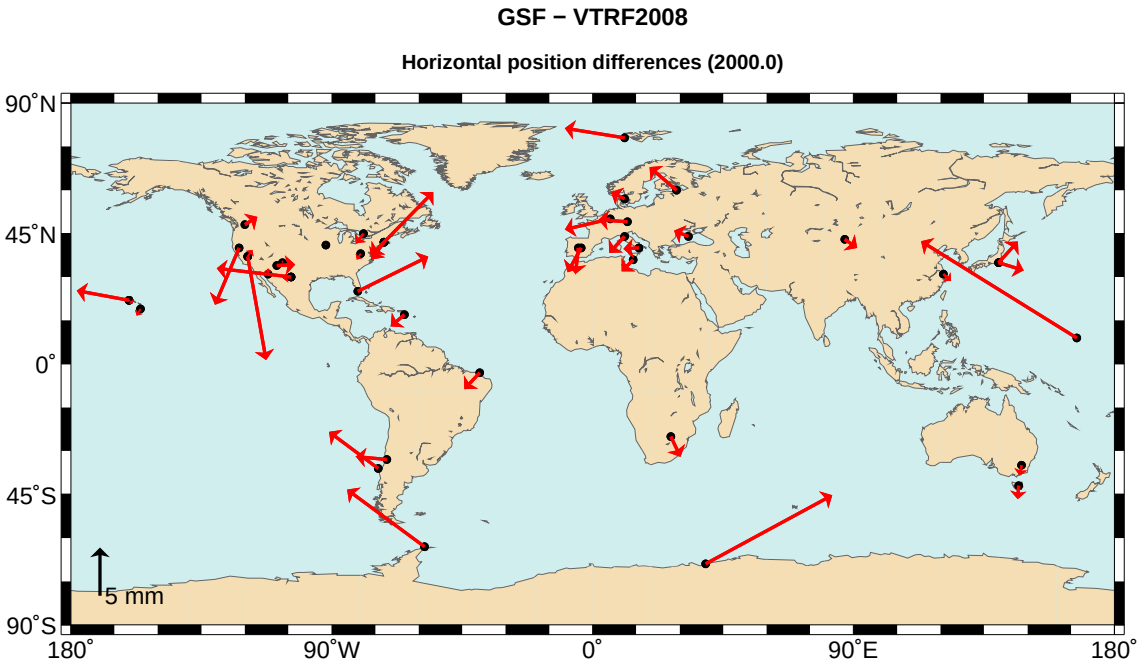

Fig. 28.— Position differences gsf008a−VTRF2008 at epoch 2000.0

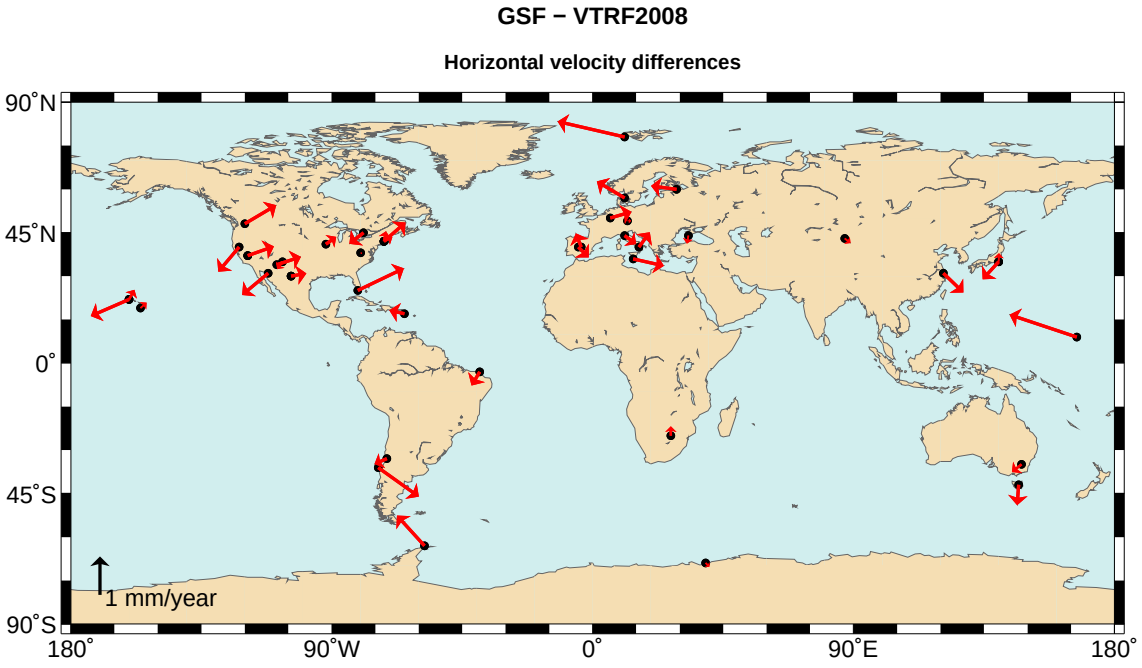

Fig. 29.— Velocity differences gsf008a−VTRF2008

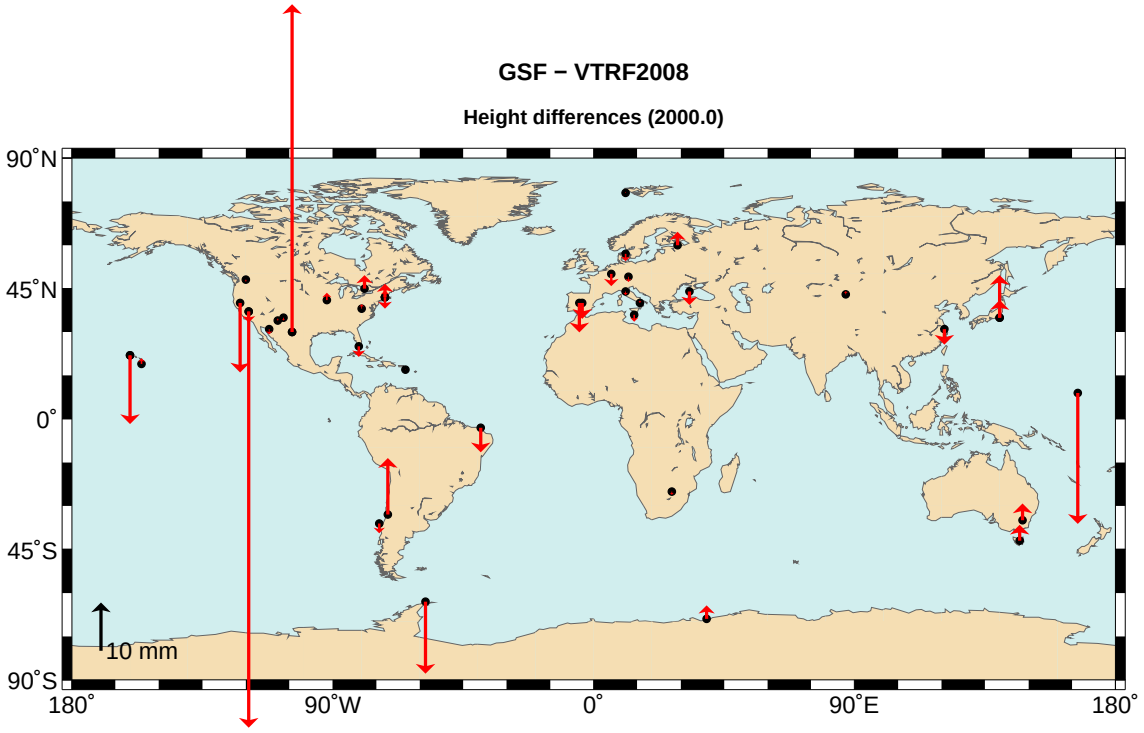

Fig. 30.— Height differences gsf008a−VTRF2008 at epoch 2000.0

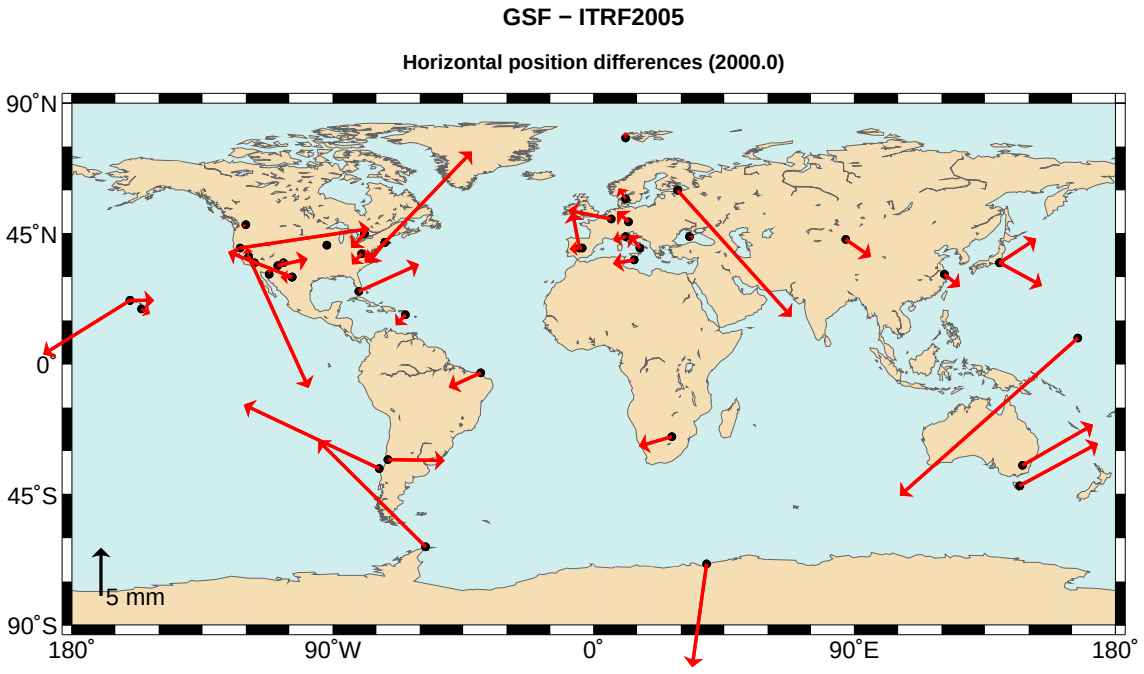

Fig. 31.— Position differences gsf008a−ITRF2005 at epoch 2000.0

10.3. Celestial Reference Frame at 24, 32, and 43 GHz (CJ)

A third method of external validation of the ICRF2 is comparing it to celestial frames at other frequencies.

The original ICRF (Ma et al. 1998), its extensions (Fey et al. 2004) and now the ICRF2 are based on VLBI measurements over the last several decades at radio frequencies of 2.3/8.4 GHz. The deep atmospheric window at these radio frequencies combined with the Gigahertz peaked spectrum nature of many extra-galactic objects facilitates the use of these frequencies for VLBI reference frame work. Historically, the use of these frequencies for radio astronomy at existing antennas contributed to their adoption for use in radio astrometry.

In 1997, as part of the IAU adoption of the original ICRF, resolution B2-d (IAU General Assembly XXIII 1997) was issued encouraging the extension of the ICRF to other frequencies. In response, VLBI global astrometric measurements have now been made at 24, 32, and 43 GHz and thus can provide the independent checks on the ICRF2 source positions that we desire.

10.3.1. High Frequency Data

With that in mind, we now take a closer look at the high frequency data sets.

- At 24 GHz (K-band), 82 000 observations (Lanyi et al. 2008) have produced a frame of 275 sources covering down to about $-40°$ declination.
- At 8.4/32 GHz (X/Ka-band), 9 400 observations (e.g., Jacobs & Sovers (2008)) have produced a frame of 339 sources covering down to $-45°$.
- At 43 GHz (Q-band), 19 000 observations (Lanyi et al. 2008) have produced a frame of 132 sources covering down to roughly $-30°$.

All three of these data sets are much, much smaller than the ICRF2's S/X-band data set. Also all three of these data sets cover only part of the southern hemisphere.

10.3.2. Statistical Agreement

We now examine the agreement of the source positions produced at 24, 32, and 43 GHz with our 2.3/8.4 GHz based ICRF2. Table 15 presents the statistics of the comparison with the three high frequency frames and the ICRF2. N_{src} is the number of overlapping sources considered. After removing a three dimensional rotation, the wrms and mean offset were calculated. The results are tabulated in units of μas.

For all three frequencies the R.A. agreement is better than the declination agreement. For 24 and 43 GHz, this is because of the limited north-south coverage, i.e, the lack of southern stations in the VLBA network, which creates both a geometrical weakness and which leads to sources in the south being systematically observed at lower elevations and

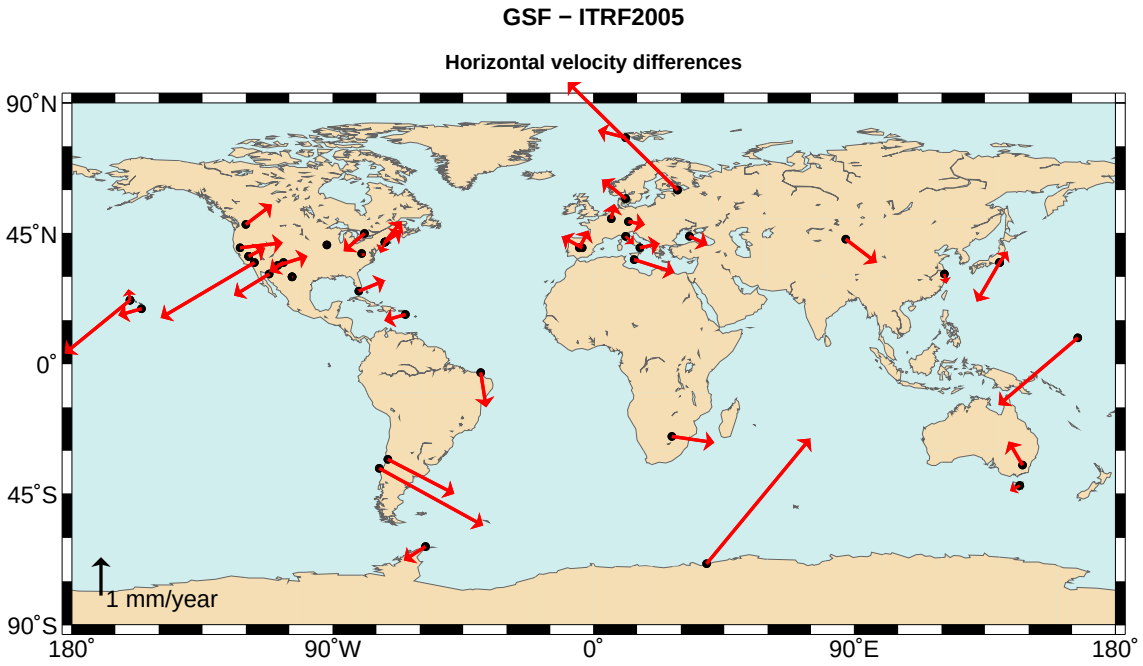

Fig. 32.— Velocity differences gsf008a−ITRF2005

Table 15: Agreement between ICRF2 and frames at 24, 32, and 43 GHz

Frame	N_{src}	$\alpha\cos(\delta)$ wrms	offset	δ wrms	offset
24 GHz	257	115	−2	216	109
32 GHz	320	186	16	261	−8
43 GHz	125	356	20	451	105

thus more susceptible to atmospheric modeling errors. In particular, there were no dual-frequency plasma calibrations for either the 24 or 43 GHz data sets. The ionosphere was only partially corrected using nearby lines of sight observed to GPS satellites. Tropospheric mis-modeling also contributes to the errors.

For 32 GHz, the declination coordinate was weaker because the observations collected using the two-baseline Deep Space Network had far fewer observations on the north-south California-Australia baseline than on the east-west California-Spain baseline.

Both 32 and 43 GHz observations were limited by low SNR. In addition, the 32 GHz sessions lacked instrumental phase calibrations. These factors will limit the level of agreement with the ICRF2. Yet, despite these limitations, the agreement is good. Recall that the ICRF1 imposed a 250 μas noise floor on its positions. Both the 8 vs. 24 GHz and 8 vs. 32 GHz position agreements are close to or better than this floor. Moreover, our experience suggests that once the VLBA's 43 GHz system sensitivity is improved by increasing from $128 - 512$ Mbps sample rates, this band will also agree to ≤ 250 μas.

The most interesting result of this comparison is the 8 vs. 24 GHz wrms agreement in R.A. ($\alpha \cos \delta$) of 115 μas. Given that there is no reason to expect that source structure is systematically different in the declination coordinate and given that a good portion of the scatter is due to thermal and atmospheric errors, this result sets a tight statistical constraint on the core shift and source structure effects between 8 and 24 GHz of $\leq$ 100 μas for the overlapping sources. Because sources which are observable at both 8 and 24 GHz are expected to be more compact than the average S/X-band ICRF2 source, the 100 μas figure given above may be optimistically biased due to the selection effect of requiring the sources be detectable at high frequencies. Thus users are encouraged to consider detectability at high frequency as one attribute of the highest quality sources.

In summary, since the publication of the ICRF1 in 1998, radio frame work has been extended to three new frequencies: 24, 32, and 43 GHz. Comparing the S/X-band ICRF2 to these independent high frequency data sets shows agreement at the $100 - 500$ μas level thus lending further validation to the accuracy of the ICRF2.

11. Selection of ICRF2 Defining Sources (SL1, PC, AMG)

This section reports on the establishment of a preliminary ordered list of sources based on their positional stability, and of the cross-correlation between this preliminary ranking and the list of source structure indices. A list of defining sources for ICRF2 is proposed.

11.1. Positional Stability of Sources

11.1.1. Ranking method

The ranking is based on the data files gsf005a.stats (time series statistics) and gsf008a.cat (non-aligned final ICRF2 catalog), from which the sources considered for special handling

were removed. We keep 593 sources observed in at least ten sessions. All these sources are estimated globally and have an observational history longer than 2 years.

From the former file, one can compute the positional stability as

$$r = \sqrt{\mathrm{wrms}^2_{\alpha\cos\delta}\chi^2_\alpha + \mathrm{wrms}^2_\delta\chi^2_\delta}. \quad (8)$$

From the latter, an overall formal error on the position estimate can be computed as

$$d = \sqrt{\sigma^2_{\alpha\cos\delta} + \sigma^2_\delta + \sigma_{\alpha\cos\delta}\sigma_\delta C(\alpha,\delta)}, \quad (9)$$

where $C(\alpha, \delta)$ is the correlation between estimates of α and δ. Figure 33 displays the values of r and d as functions of the declination.

One could define an overall positional stability as $p = r + d$. However, d appears to be lower than r by a factor of 10, so that p would be dominated by information from time series. Moreover, a ranking based on the above-defined quantities only will obviously reject the southern hemisphere sources.

In the following, we implement a method inspired by Section 3 of Fey et al. (2001).

1. First of all, data are binned by intervals of declination. We chose 4 nodes (−31°, 0°, 18°, and 40°) so that the number of sources in each interval is approximately the same (around 110 sources).

2. In each interval of declination, sources are given a mark between 0 and 10 on the basis of r. Again, the binning is such that the number of sources in each category is approximately the same.

3. Point (ii) is repeated for d.

4. The scaled r and d are summed and normalized to 100: this constitutes the final "quality" index p. The distribution of p is displayed in Figure 34.

It is interesting to note that if one leaves the special handling sources into the input catalog and time series statistics file before doing the ranking, the special handling sources arrive between the 334th place and the 632nd place. Five of them (0235+164, 0607-157, 1611+343, 0637-752, 0528+134) arrive before the 400th place. This indicates that the ranking method can fail to exclude sources known to be of poor quality and that sources ranked after the 300th row must be considered cautiously.

11.1.2. Tests of stability

Method 1: tests on annual catalogs A first test of stability is done using annual reference frames computed from coordinate time series (method explained in Lambert & Gontier (2009)). Results are reported in Figure 35 by the solid, thick line (left scale). The thin line represents a degree-2 polynomial fit. By this method, the stability of the 212 ICRF

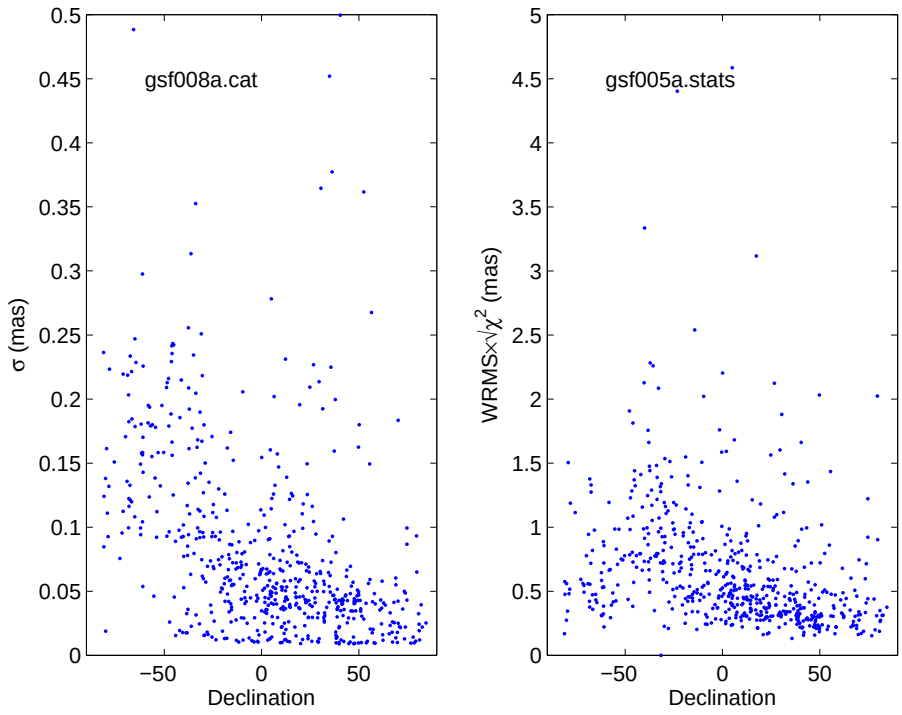

Fig. 33.— Quantities r and d vs. the declination.

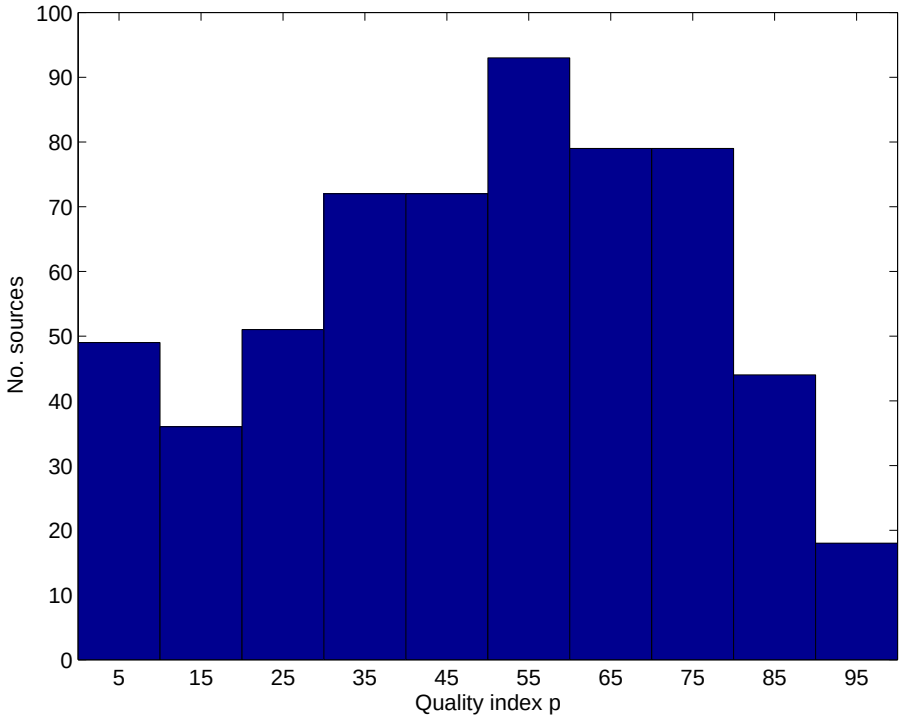

Fig. 34.— Distribution of the final quality index p.

defining sources is close to 25 μas. The red, dashed line (right scale), shows the average declination of the considered set.

Figure 35 indicates that the minimum value of N should be around 200. Taking the first $N > 200$ sources of the ranking would provide a frame definitely more stable than the current 212 ICRF1 defining sources by a factor of two, and would moreover present a much better coverage of both hemispheres. There seems to be an optimal value at N close to 380, after which the stability is degraded.

Method 2: tests on randomly-selected subsets We ran another series of tests of stability similarly to what was proposed in Ma et al. (1998), Section 11. To assess the stability of the axes defined by a set of N sources, we estimate the relative orientation between this set and a reference catalog (e.g., ICRF-Ext.2) on the basis of different subsets of size $N/2$. The scatter of the rotation parameters obtained from the various subsets gives the stability of the axes. The different subsets are randomly selected and are as large as a half of the tested set. The stability of the 212 ICRF1 defining sources checked by this method is $\sim$18 μas, in agreement with the conservative value of $\sim$20 μas mentioned in Ma et al. (1998).

The solid line in Figure 36 (left scale) represents the stability of the frame as a function of the number of defining sources. The stability is computed as the maximum of the respective scatters of the four usual transformation parameters A_1, A_2, A_3, and dz. The horizontal, green line indicates the stability of the 212 ICRF1 defining sources. For example, take a number of defining sources of 200: they are the first 200 lines of the ranking list, i.e, the most stable 200 sources. Among these 200 sources, 100 are selected randomly, and the orientation of these 100 sources is evaluated. The scheme is repeated a thousand times. The obtained stability is close to 10 μas, and the average declination is approximately 5°. (The average declination of the 212 ICRF1 defining sources is around 14°.)

From this method, it seems that taking 200, 400, or more sources is equivalent in terms of stability and sky coverage. However, one must keep in mind that the tests are not done on N sources, but on subsets of $N/2$ sources. For example, the stability for $N = 500$ is computed from subsets of 250 sources. Although containing also 'bad' sources, the axes of such a frame are strongly maintained by the good ones that were selected in the random process.

11.2. Structure Information and Selection of Defining Sources

The final list of defining sources results from the cross-correlation between the ranked list of sources described above, based on positional stability, and the ranked list of sources based on structure indices described in §5. Overall, the two criteria (positional stability and source structure index) show good consistency, with positional stability increasing as the structure index decreases (see Figure 37).

The effect of the cross-correlation was to filter out an initial list of defining sources derived from positional stability only. This initial list comprises a total of 423 sources,

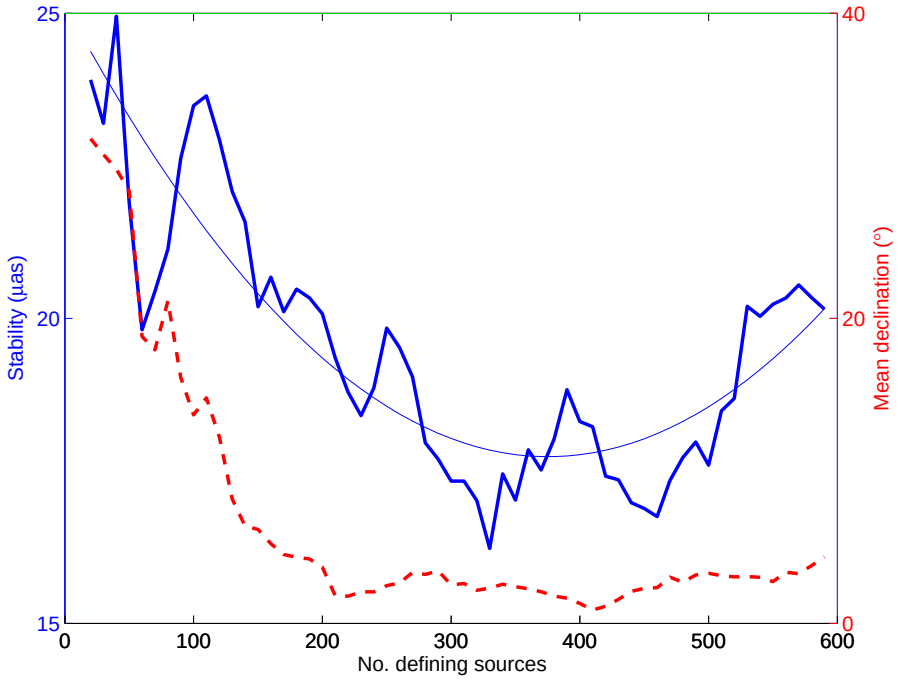

Fig. 35.— Axes stability and average declination of various subsets of sources of increasing size tested on annual catalogs.

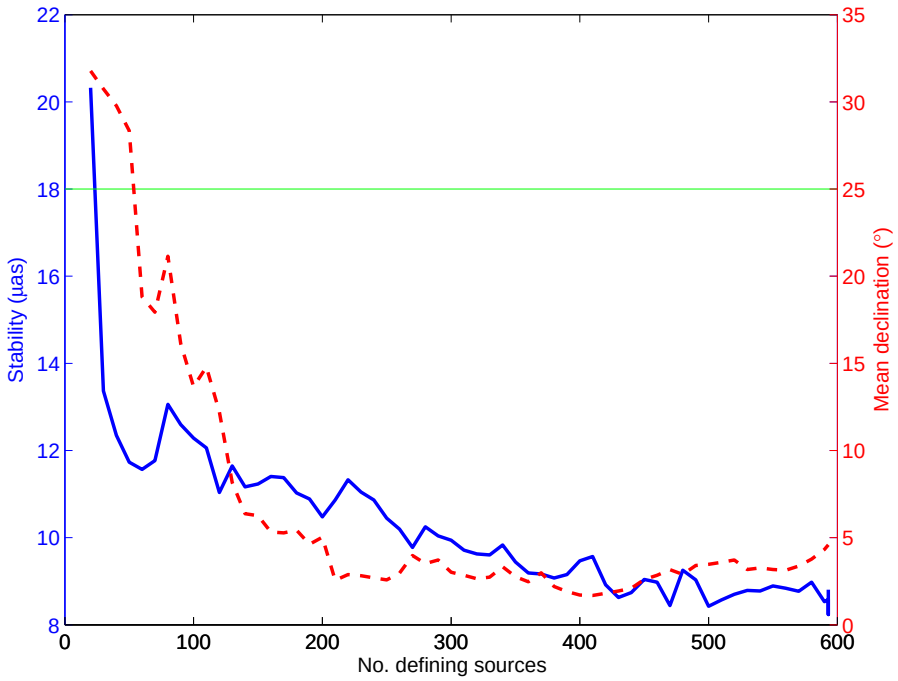

Fig. 36.— Axes stability and average declination of various subsets of sources of increasing size checked on randomly-selected subsets.

corresponding to sources with stability index larger than or equal to 40. Setting the threshold for structure index to 3.0, all sources with structure index values larger than or equal to this threshold were removed from the list, leaving 297 sources. About a quarter of these, mostly in the southern hemisphere, were found to have no structure index. When available, VLBI images from these sources were examined, which led to excluding two additional sources. The other sources (with no structure information available) were kept on the basis of their good positional stability only. Thus, the proposed set of defining sources comprise 295 sources.

The stability of the frame based on these 295 sources is 20 μas using the first method above and 10 μas using the second method, which is satisfactory (the corresponding stability's for the 212 ICRF1 defining sources are 26 μas and 18 μas). The mean declination of the sample is 0.7°. The distributions in declination, in p, and in structure index are shown in Figure 38, with the sky distribution plotted in Figure 39.

Preliminary checks against the ICRF1 revealed that rotation parameters towards the ICRF1 are at the level of $\sim$30 μas. The tilt parameter is negligible as well as the deformation parameters.

12. Alignment of ICRF2 onto ICRS and Axis Stability (AMG, FA, SL1)

12.1. Linking sources

Among the 295 selected defining sources of the ICRF2, only 97 are also defining sources of the ICRF1. Most of them are in the northern hemisphere, making the sample badly distributed for a reliable estimation of rotation angles. To remedy, 41 ICRF2 defining sources (but not defining sources of the ICRF1) preferably taken in the southern hemisphere were added, resulting in 138 common objects for comparison which have been used for the link between the gsf008a catalogue and ICRF-Ext2. The defining sources, the linking sources and the common to both ICRF1 and ICRF2 are displayed in Figure 40. The status in ICRF-Ext.2 of the 41 additional sources is: 24 candidate sources, 16 other, and 1 new. Figure 41 displays the distribution of formal errors of the various subsets of sources before inflation, after inflation (see next paragraph), and of the corresponding errors in the ICRF-Ext.2.

12.2. Rotation

The gsf008a catalogue, wherein the formal errors were inflated following the formula

$$\sigma^2_{\alpha\cos\delta} = (1.5\,\sigma_{\alpha\cos\delta,0})^2 + (0.04\ \mathrm{mas})^2 \quad (10)$$

$$\sigma^2_{\delta} = (1.5\,\sigma_{\delta,0})^2 + (0.04\ \mathrm{mas})^2 \quad (11)$$

was compared to the ICRF-Ext.2 using a 4-parameter transformation in which the coordinate difference is modeled by three rotations of angles A_1, A_2 and A_3, around the X, Y and Z axes of the celestial frame, respectively, and a parameter dz accounting for a global translation of

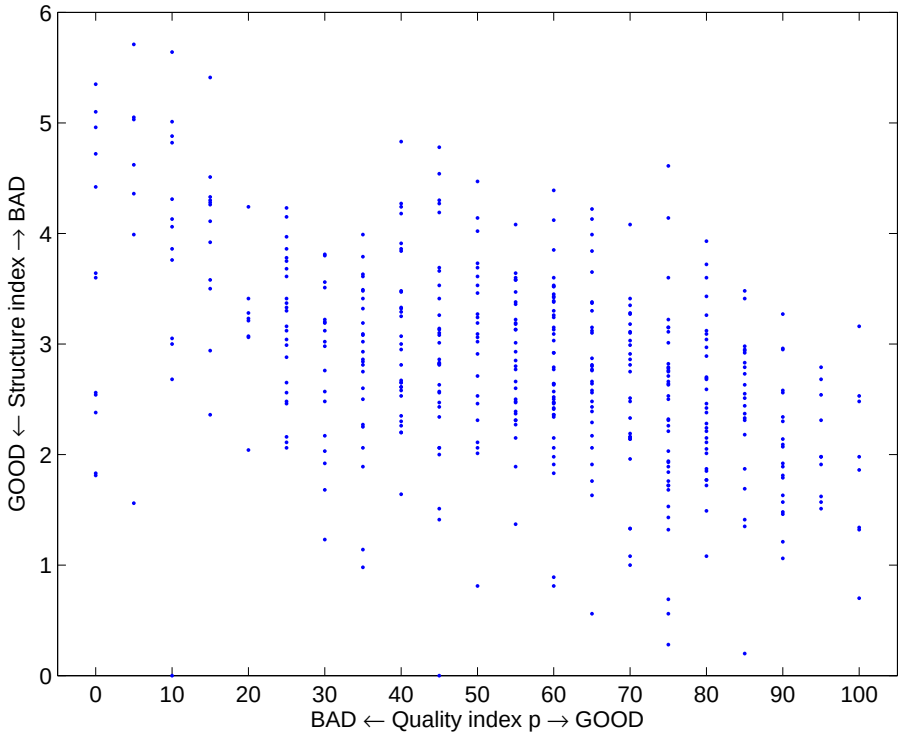

Fig. 37.— Source structure index vs. stability index p.

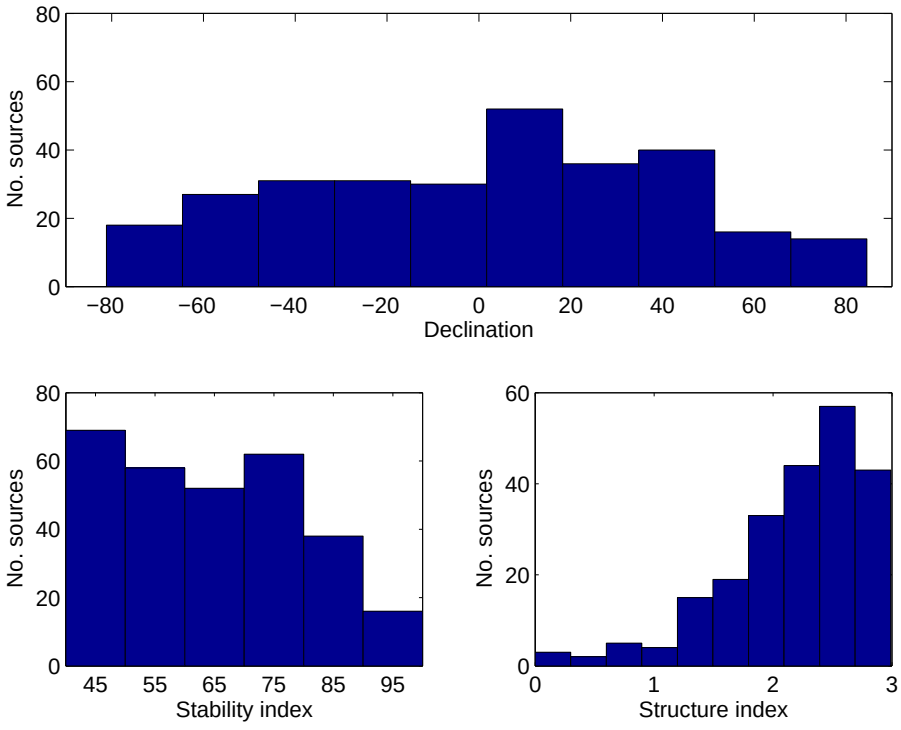

Fig. 38.— Defining sources' distribution in declination (top), in stability index (bottom-left), and in structure index when available (bottom-right).

the source coordinates in declination (see, e.g., IERS (1996) or Feissel-Vernier et al. (2006)):

$$\Delta\alpha = A_1 \tan\delta \cos\alpha + A_2 \tan\delta \sin\alpha - A_3 \quad (12)$$

$$\Delta\delta = -A_1 \sin\alpha + A_2 \cos\alpha + dz \quad (13)$$

The additional two deformation parameters used in the transformation formula for the alignment of the first realization of the ICRF1 (Ma et al. 1998) were found negligible and are not estimated here. Values of parameters are reported in Table 16.

Table 16: Relative orientation and deformation parameter to transform ICRF2 into ICRF-Ext.2. A_1, A_2, A_3 are the small rotation angles between axes of the frames; dz (formerly B_δ) is the bias in declination. All these parameters have been adjusted on the basis of the 138 defining sources in ICRF2 used for the link to ICRF-Ext.2. r_α and r_δ are the wrms residuals in $\alpha\cos\delta$ and δ, respectively. Unit is μas.

A_1	A_2	A_3	dz	r_α	r_δ
23.3	−33.5	7.8	11.2	9.2	12.4
±19.2	±19.5	±18.4	±16.6		

Improvements in the models and procedures applied in the gsf008a catalogue solution resulted in a frame less corrupted by deformations than ICRF-Ext.2, but with a slight misorientation. In the procedure applied to rotate the gsf008a catalogue positions into the ICRS, care was taken not to transfer the deformations of ICRF-Ext.2 to ICRF2. Consequently the radio source coordinates of the gsf008a catalogue were rotated onto the ICRS using only the three rotation angles A_1, A_2, and A_3. The rotated gsf008a catalogue constitutes the ICRF2.

12.3. Axis stability

The stability of the system axes was tested by estimating the relative orientation between ICRF2 and ICRF-Ext.2 on the basis of various subsets of sources (see Table 17). The scatter of the rotation parameters obtained in the different comparisons indicate that the axes are stable to within 10 μas.

13. The ICRF2 Catalogue (AMG, AF)

The ICRF2 catalogue is obtained from gsf008a after inflating the formal errors and aligning it onto the ICRS as discussed in §12.2. It consists of positions of 3414 sources. Of the total number of sources, 2197 sources are observed only in VCS sessions. Among the remaining 1217 sources, 295 have been designated as "defining" sources, i.e., the positions of these 295 sources define the axes of the ICRF2 frame (see §11).

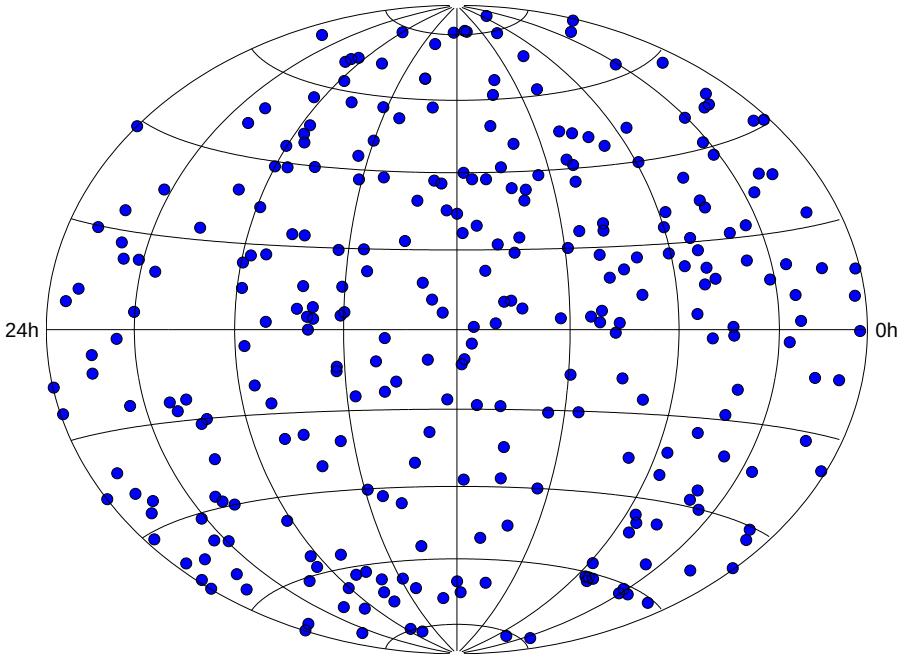

Fig. 39.— Distribution of the defining sources.

Table 17: Axis stability tests: transformation parameters between ICRF2 and ICRF-Ext.2 for various subsets of defining sources. Unit is μas.

	No. sources	A_1	±	A_2	±	A_3	±	dz	±	r_α	r_δ
ICRF2 sources common to ICRF-Ext.2											
All	710	18.2	9.1	−5.6	8.5	8.2	8.3	15.2	8.1	4.52	5.87
North	435	26.7	9.0	−6.2	8.5	5.9	8.8	21.1	8.8	5.18	5.03
South	275	−11.5	23.4	−2.9	21.0	10.9	17.7	1.2	18.2	8.91	13.18
Used for NNR	207	1.0	20.0	4.5	19.7	−14.1	21.0	−2.7	17.5	9.71	13.44
ICRF2 defining sources											
Common to ICRF-Ext.2	245	5.2	11.0	−5.1	10.5	14.0	10.4	22.0	10.0	5.32	7.43
Used for linking	138	−0.0	19.2	0.0	19.5	0.0	18.4	11.1	16.6	9.20	12.44
North	148	17.0	10.7	−1.2	10.4	12.7	10.7	26.1	10.2	6.07	7.51
South	97	−35.4	28.0	−18.6	24.8	11.2	22.3	19.9	22.3	10.46	16.51
Decimation rate = 2	128	−1.9	14.9	15.3	15.7	17.9	14.5	20.1	13.9	7.07	10.66
Decimation rate = 3	166	4.5	11.3	−19.3	10.5	20.2	11.1	13.6	10.5	5.62	7.62
Overall wrms		12.4		7.9		6.8		7.0			

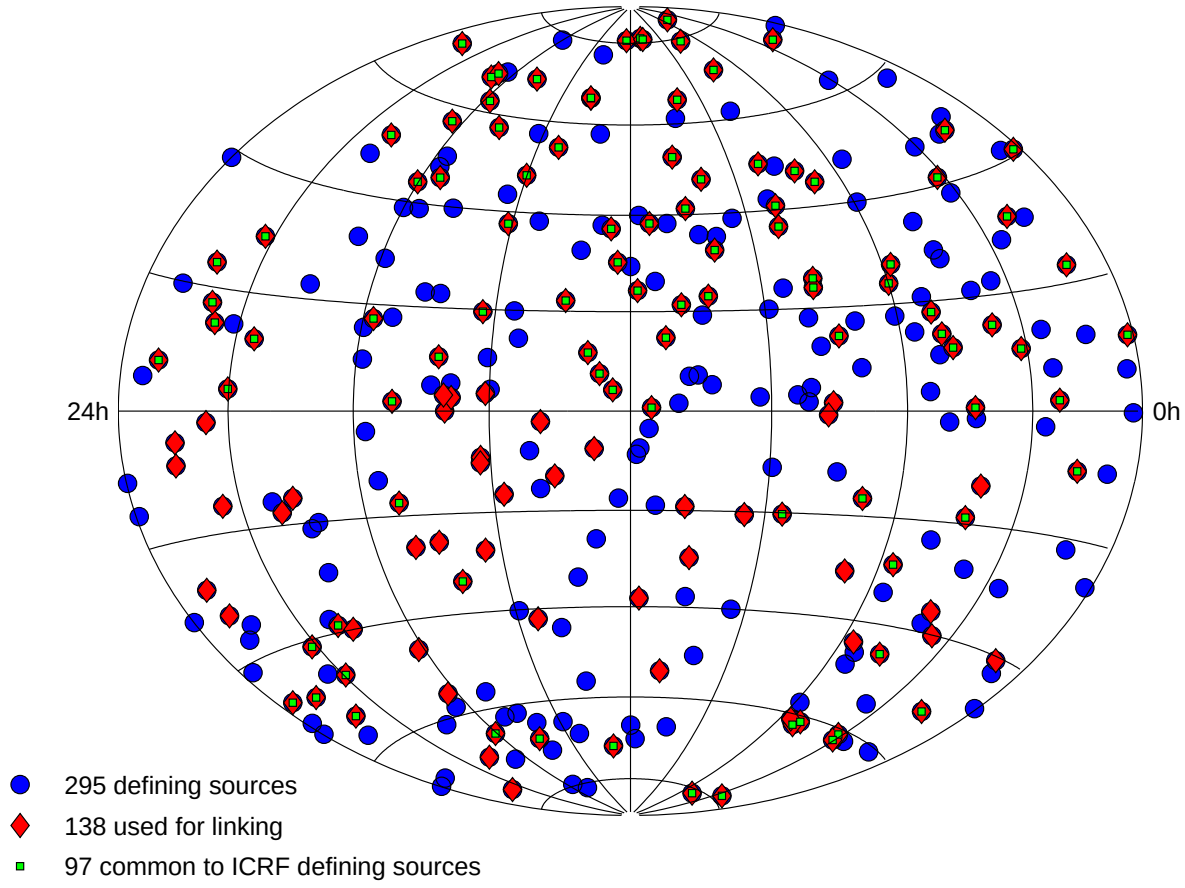

Fig. 40.— Distribution of the 295 defining sources (blue circles), of the 138 used for linking ICRF2 to ICRF-Ext.2 (red diamonds). The 97 ICRF2 defining sources that are also defining sources of the ICRF1 are marked with green squares.

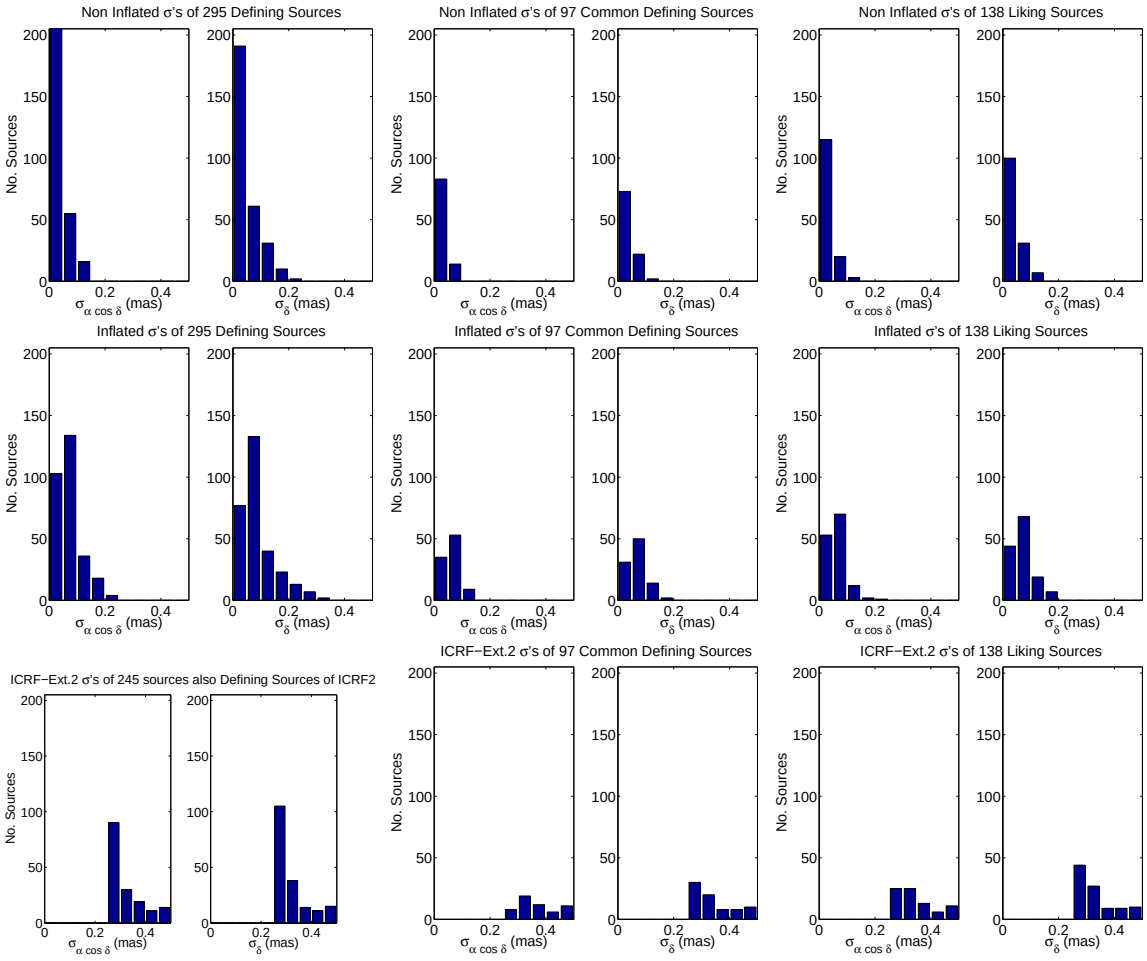

Fig. 41.— Distribution of formal errors of the defining, common and linking sources before inflation, after inflation, and of the corresponding errors in the ICRF-Ext.2.

The coordinates of the 295 ICRF2 defining sources are listed in Table 18. It should be noted that these positions *are not* epoch-dependent and hence no epoch is explicitly stated. However, the listed positions *are* consistent with J2000.0. The coordinates of the 1217 non-VCS sources of the ICRF2 are available at:

- `http://hpiers.obspm.fr/icrs-pc/icrf2/icrf2-non-vcs.dat`.

The coordinates of the 2197 VCS-only sources of the ICRF2 are available at:

- `http://hpiers.obspm.fr/icrs-pc/icrf2/icrf2-vcs-only.dat`.

Note that seven sources from the ICRF-Ext.2 catalogue are not in ICRF2 [0647 − 475, 1020 − 103, 1039 − 474, 1217+295 (NGC 4278), 1329 − 665, 1601+173 (NGC 6034), and 1829 − 106]. The total number of group delay observations for each of these seven sources was less than three, insufficient to derive a reliable position.

14. Statistics of the ICRF2 Catalogue (CJ)

This section will describe the ICRF2 catalogue. The catalogue is taken from a solution named gsf008a which produced angular positions for 3414 sources—more than five times the number of sources in the original ICRF1. However, 1966 sources were observed in only one session with the goal of densifying the catalogue. Hereafter in this section, we will refer to these sources as "survey" sources even though not all of them were observed in specially designed calibrator surveys such as the VLBA Calibrator survey. The remaining sources which were observed in more than one session will be identified as "multi-session" sources.

14.1. Primary Distribution

Figure 42 shows the distribution over the sky of the 1448 sources which have been observed in at least two sessions. The color coding given in the figure's legend signifies the un-inflated 1-σ formal declination uncertainties.

14.2. Survey Distribution

Figure 43 shows the distribution over the sky of the 1966 single-session survey sources. The survey sources median un-inflated formal uncertainties are 406 and 571 μas, in $\alpha\cos(\delta)$ and δ respectively. The survey's median number of group delay observations is 41 and the median epoch of observation is 2004.4.

The rest of this section will focus on the remaining 1448 sources which were observed in at least two sessions. For these sources, we will look at the distribution of sources over the sky, the formal position errors, the number of observing sessions and group delays per source, and the distributions of mean, first and last epochs of observations as well as the total time span of observations per source. In all these ways we will characterize the ICRF2 observations.

14.3. Un-inflated formal uncertainties

Figure 44 shows the distribution of the un-inflated 1-σ formal uncertainties in Right Ascension arc-length for which the median is $\sigma_{\alpha\cos(\delta)} = 100$ μas. Figure 45 shows the distribution of the un-inflated 1-σ formal uncertainty in declination for which the median is $\sigma_\delta = 175$ μas. Both figures show $\log_{10}(\sigma)$ vs. $\log_{10}(N_{obs})$. A slope of -0.5 corresponds to the un-inflated formal uncertainties scaling as $1/\sqrt{N_{obs}}$ as one would expect from averaging white noise limited measurements. However, for small numbers of observations the observed slopes are steeper than -0.5 and become shallower as the numbers of observations increase. For sources with the largest numbers of observations the slope is nearly flat with a $\sigma \approx 10$ μas.

14.4. Number of observations

Figure 46 shows the distribution of the number of observing sessions per source for sources with a minimum of two sessions. The median number of sessions for these sources is 7. Note that over 400 sources have been observed in only a few sessions.

Figure 47 shows the distribution of the number of group delay measurements per source plotted on a log scale. The median number of delay observations per multi-session source is 156. Note the strong peak near 100 observations.

Some sources that have long been used for geodetic and earth orientation sessions have more than 10,000 observations and a few even have more than 100,000 observations. The unevenness in the distributions of both sessions and delay observations results from the ICRF2 database being built in large part from programs whose primary goals were not building a celestial frame, but rather measuring plate tectonics or earth orientation. Programs to densify the ICRF1 have been very successful as was seen in Figs. 42 and 43, but the densification programs typically are resource limited to observe each source in only a few sessions.

14.5. Observing Epochs

Figure 48 shows the distribution of the mean epoch of observation for the 1448 multi-session sources. The median mean epoch is 2001 with the vast majority of the source mean epochs being between 1994 and 2007. Figure 49 shows the distribution of the first epoch of observation for the 1448 multi-session sources . The median first epoch is 1995.5. Figure 50 shows the distribution of the last epoch of observation for the 1448 multi-session sources. The median last epoch is 2008. About half of the 1448 sources have been observed within the last few years and the vast majority of the sources have been observed since 1995 – the data cutoff date for the original ICRF1.

Finally, Figure 51 shows the distribution of observing span in years for the 1448 multi-session sources. As just explained the distribution of observations is very uneven. From this figure we note that about 250 sources have spans of about a year or less. At the other extreme, there are a few sources that were used in early geodetic and earth orientation programs that have 23–30 year spans. After the mid-1980s the Mark III observing system

increased sensitivity resulting in more sources being observed. We see this reflected the increase in the distribution height for sources with spans less than 23 years.

15. Conclusions and Future Work (DG)

Through an international effort, we have produced a celestial reference frame of 3414 compact radio sources using nearly 30 years of VLBI observations. This new catalog is expected to become the second realization of the International Celestial Reference Frame (ICRF2). Compared to the first ICRF, the second ICRF has more than 5 times as many sources, is roughly 5-6 times more accurate, and is nearly twice as stable.

In preparation for ICRF2, we generated and studied catalog solutions from 7 different VLBI analysis centers made with 4 different analysis software packages. A combined catalog was also constructed. Inter-comparisons between the individual catalogs and with the combined catalog indicate agreement at the $\sim$50μas level. Internal and external tests and comparisons were made to determine a formal error scaling factor of $\sim$1.5 and a conservative estimate of the noise floor of $\sim$40μas.

The final ICRF2 catalog is based on a single solution, made after some final tweeking of the sessions and the solution configuration. This final solution was aligned with the first ICRF by using 138 stable sources common with ICRF-Ext2. Some 295 sources were selected to be the ICRF2 "defining" sources, based on their positional stability and a lack of any known extensive source structure. Their stability and the fact that they are very evenly distributed over the northern and southern hemispheres eliminates the two largest weaknesses of the first ICRF. The 295 ICRF2 defining sources will be used to define the ICRF2 frame for all future maintenance or extensions of the ICRF2.

The ICRF2 catalog is extremely diverse, with over half the sources being observed in only one session. As such, it is split into two parts. The 'multi-session' sources (1448 sources) are those sources in two or more sessions; and the 'survey' sources (1966 sources) are those in only one session, mostly VLBA Calibrator Survey sources.

It is not certain whether any future extensions will be made to ICRF2, but the VLBI geodetic/astrometric programs will continue. Reference frame work will continue in several areas. The southern hemisphere CRF sessions should continue, and perhaps new antennas can be used and/or new collaborations in the southern hemisphere can be developed. Attempts should be made to re-observe many of the noisiest sources to improve their positions, particularly after an expected doubling of the recorded bit rates for some sessions are accomplished. And attempts to observe the optically brightest quasars, even though they may be weak in the radio region, should be begun, for future alignment with Gaia optical positions.

The research described in this paper was performed in part at: Geoscience Australia, Canberra, ACT, Australia (AUS); Laboratoire d′Astrophysique de Bordeaux, University of Bordeaux, CNRS, Floirac, France; Bundesamt für Kartographie und Geodäsie, Frankfurt am Main, Germany (BKG); Goddard Space Flight Center, Greenbelt, MD, USA (GSF); Institute of Astronomy and Astrophysics of the Russian Academy of Sciences, St. Petersburg, Russia

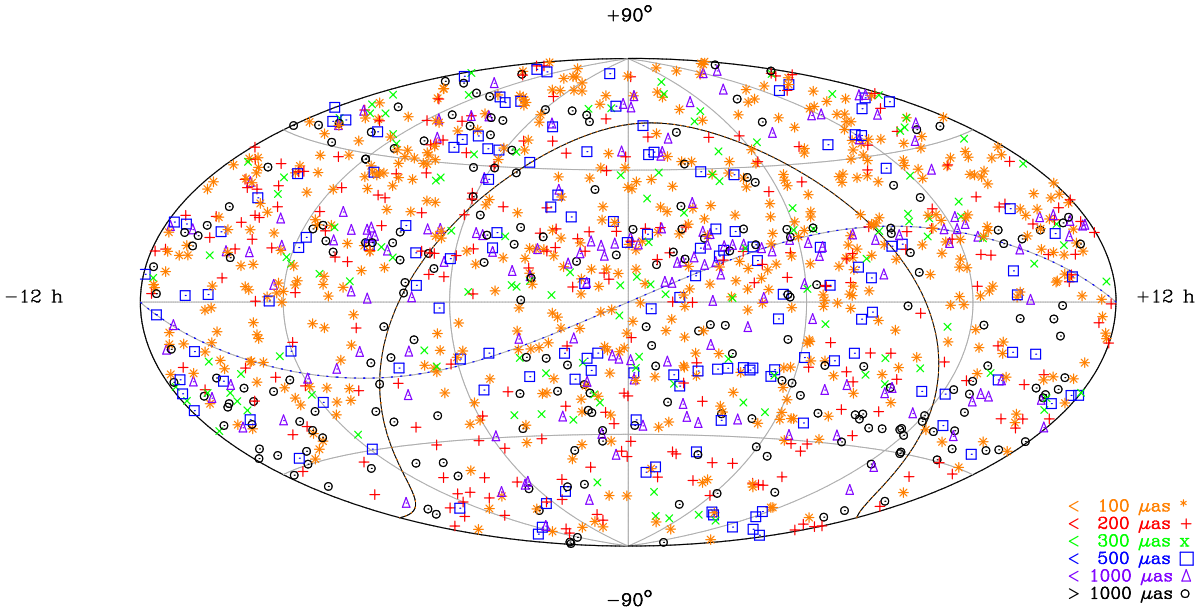

Fig. 42.— gsf008a distribution of 1448 multi-session sources (at least 2 observing sessions). The un-inflated 1-σ formal declination errors are color coded according to the legend in the figure. The median σ_δ = 175 μas. The center is $(\alpha, \delta) = (0, 0)$. The Galactic plane is the roughly Ω-shaped line surrounding the center. The ecliptic plane is the dashed line. The single-session survey sources used to densify are shown in the next figure, Figure 43.

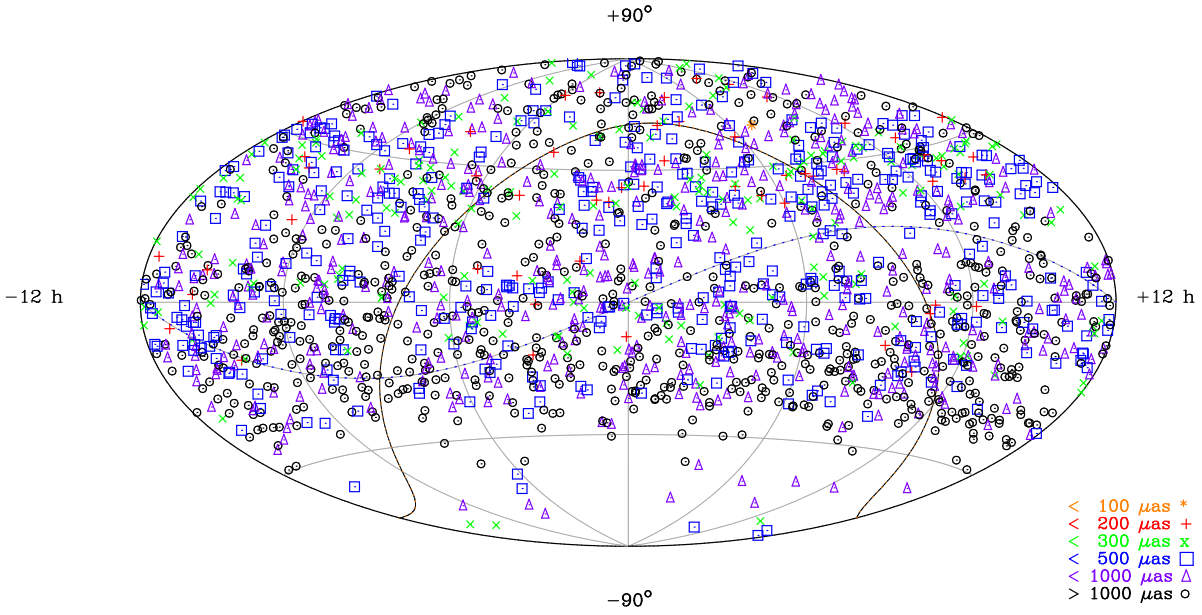

Fig. 43.— gsf008a survey distribution of 1966 single-session sources. The un-inflated 1-σ formal declination errors are color coded according to the legend in the figure. The median σ_δ = 751 μas. The center is (α,δ)=(0,0). The Galactic plane is the roughly Ω-shaped line surrounding the center. The ecliptic plane is the dashed line.

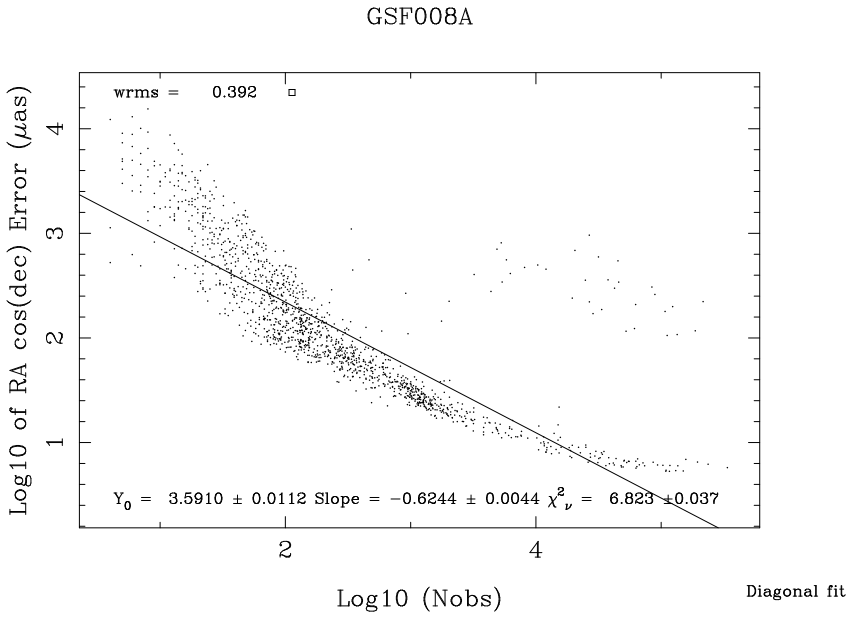

Fig. 44.— gsf008a catalogue's dependence of un-inflated $\sigma_{\alpha\cos(\delta)}$ on the number of observations for sources observed in at least two sessions. A slope of -0.5 would correspond to $1/\sqrt{N_{obs}}$ averaging of white noise. Calibrator survey's ≈ 2000 single-session densifying sources are not shown.

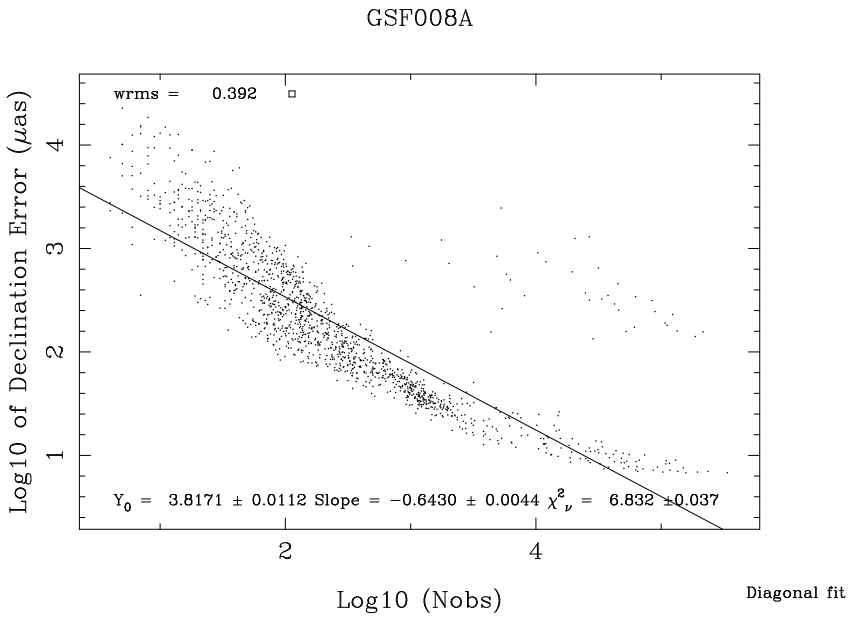

Fig. 45.— gsf008a catalogue's dependence of un-inflated σ_δ on the number of observations for sources observed in at least two sessions. A slope of -0.5 would correspond to $1/\sqrt{N_{obs}}$ averaging of white noise. Calibrator survey's ≈ 2000 single-session densifying sources are not shown.

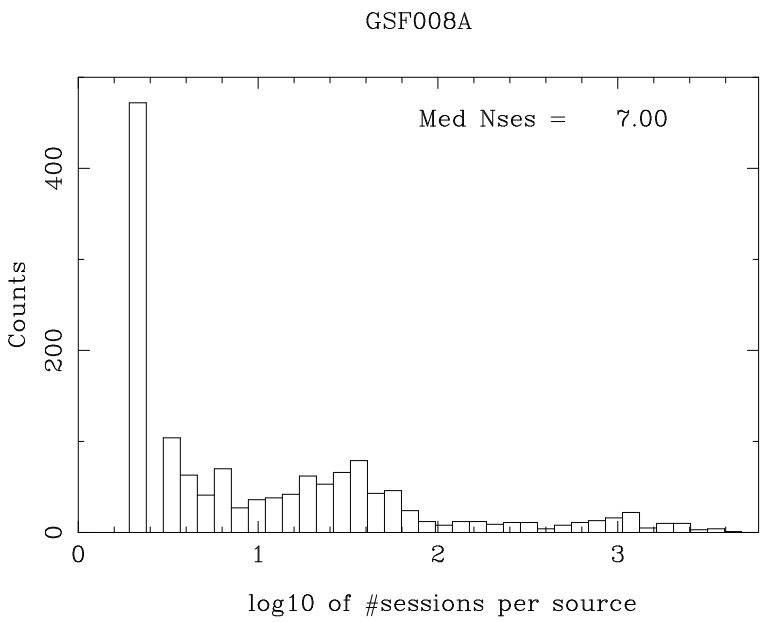

Fig. 46.— gsf008a catalogue's distribution of the number of observing sessions per source for sources with at least two sessions. The median number of sessions per source is 7 excluding the set of ≈ 2000 single-session densifying sources (not shown) from calibrator surveys.

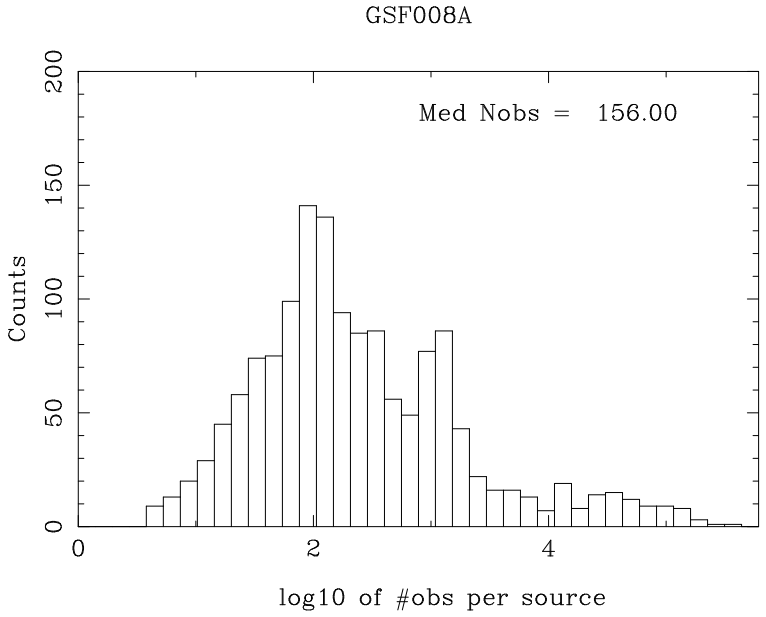

Fig. 47.— gsf008a catalogue's distribution of the number of group delay measurements plotted on a log scale for sources observed in at least two sessions. Note the strong peak near 100 observations. Calibrator survey's ≈ 2000 single-session densifying sources are not shown.

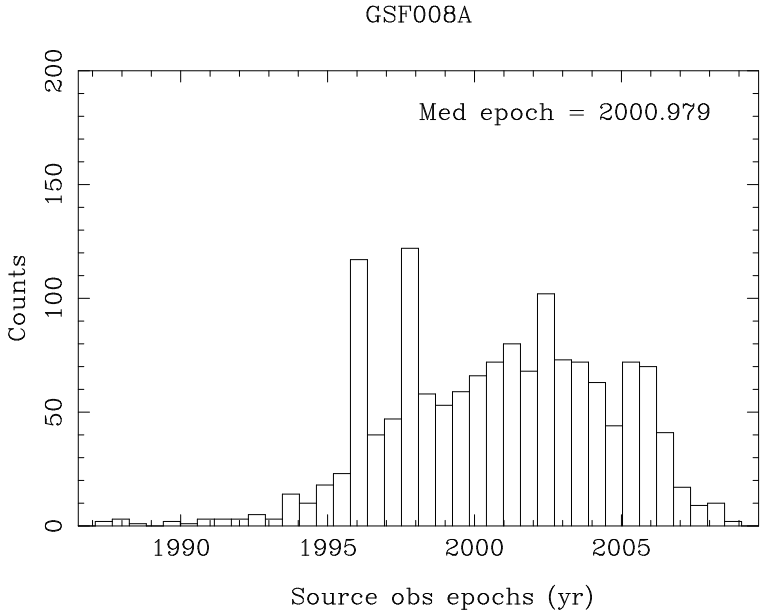

Fig. 48.— gsf008a catalogue's distribution of mean observing epoch for sources observed in at least two sessions. Calibrator survey's ≈ 2000 single-session densifying sources are not shown.

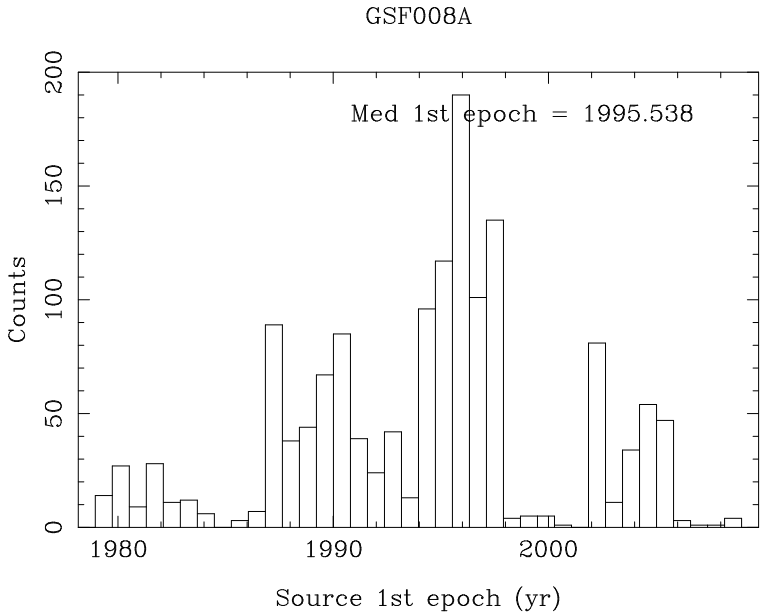

Fig. 49.— gsf008a catalogue's distribution of first observing epoch for sources observed in at least two sessions. Calibrator survey's ≈ 2000 single-session densifying sources are not shown.

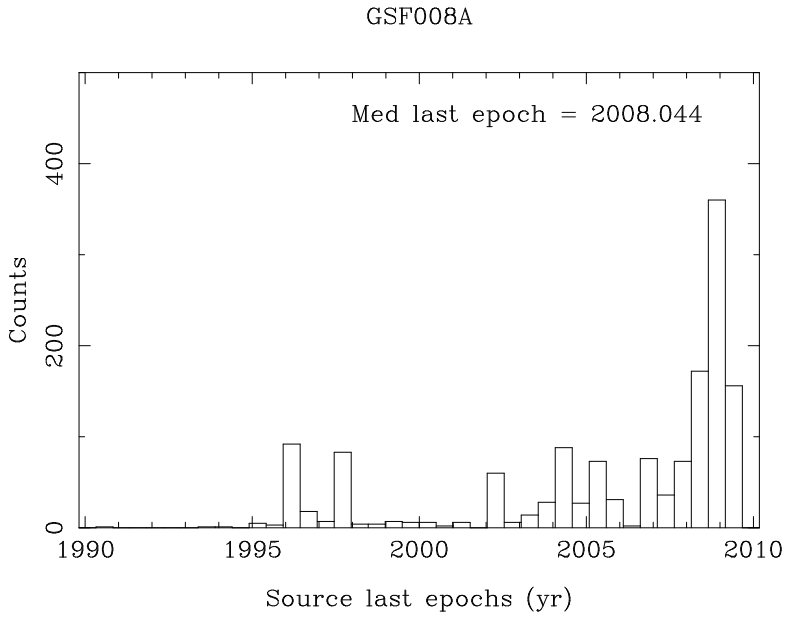

Fig. 50.— gsf008a catalogue's distribution of last observing epoch for sources observed in at least two sessions. Calibrator survey's ≈ 2000 single-session densifying sources are not shown.

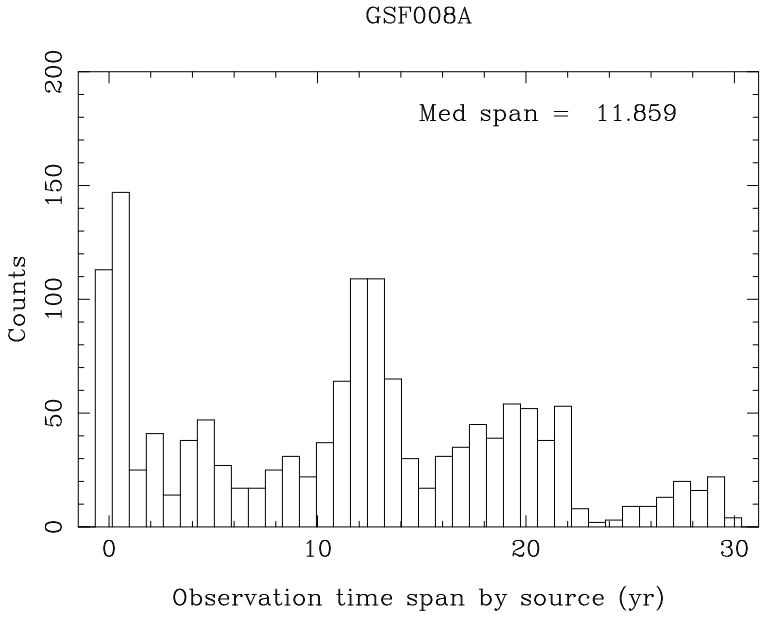

Fig. 51.— gsf008a catalogue's distribution of observing span for each source which was observed in at least two sessions. The observation spans are very unevenly distributed from zero to 30 years with a median of about 12 years Calibrator survey's ≈ 2000 single-session densifying sources are not shown.

(IAA); Jet Propulsion Laboratory of the California Institute of Technology, Pasadena, CA, USA, under a contract with the National Aeronautics and Space Administration; Main Astronomical Observatory of the National Academy of Sciences of Ukraine, Kyiv, Ukraine (MAO); Pulkovo Observatory, St. Petersburg, Russia; l′Observatoire de Paris, CNRS, Paris, France (OPA); and the U.S. Naval Observatory, Washington, DC, USA (USN).

APPENDIX A

IERS/IVS Working Group

Charter: The purpose of the working group is to generate the second realization of the ICRF from VLBI observations of extragalactic radio sources, consistent with the current realization of the ITRF and EOP data products. The working group will apply state-of-the-art astronomical and geophysical models in the analysis of the entire relevant S/X astrometric and geodetic VLBI data set. The working group will carefully consider the selection of defining sources and the mitigation of source position variations to improve the stability of the ICRF. The goal is to present the second ICRF to relevant authoritative bodies, e.g. IERS and IVS, and submit the revised ICRF to the IAU Division I working group on the second realization of the ICRF for adoption at the 2009 IAU general assembly.

Goal: Produce ICRF2 for IERS/IVS consideration and for submission to the IAU Working Group.

Active: 2006 – 2009

Membership:

- O. Titov, Australia
- R. Heinkelmann, Austria
- G. Wang, China
- F. Arias, France
- P. Charlot, France
- A.-M. Gontier, France
- S. Lambert, France
- J. Souchay, France
- G. Engelhardt, Germany
- A. Nothnagel, Germany
- V. Tesmer, Germany
- G. Bianco, Italy
- S. Kurdubov, Russia
- Z. Malkin, Russia
- E. Skurikhina, Russia
- J. Sokolova, Russia
- V. Zharov, Russia
- S. Bolotin, Ukraine
- D. Boboltz, USA
- A. Fey, USA
- R. Gaume, USA
- C. Jacobs, USA
- C. Ma, USA (Chair)
- L. Petrov, USA
- O. Sovers, USA

APPENDIX B

IAU Working Group – Division I

Charter The purpose of the working group is to oversee the generation of the second realization of the ICRF from VLBI observations of extragalactic radio sources. The reference frame will apply state-of-the-art astronomical and geophysical models in the analysis of the entire relevant S/X astrometric and geodetic VLBI data set. The working group will ensure the selection of defining sources and the mitigation of source position variations and the consistency with the ITRF and the IERS EOP to improve the stability of the ICRF. The goal is to present the second ICRF at the 2009 IAU general assembly.

Goal: Oversee generation, validation and utility of ICRF2; engage in formulation of resolutions of adoption by IAU.

Active: 2006 – 2009

Membership:

- Alexandre Andrei, Brazil
- Felicitas Arias, France
- Bob Campbell, Netherlands
- Patrick Charlot, France
- Alan Fey, USA
- Ed Fomalont, USA
- Ralph Gaume, USA
- Chopo Ma, USA (Chair)
- Jean Souchay, France
- Yaroslav Yatskiv, Ukraine
- Norbert Zacharias, USA

REFERENCES

Altamimi, Z., X. Collilieux, J. Legrand, B. Garayt, C. Boucher, "ITRF2005: A new release of the International Terrestrial Reference Frame based on time series of station positions and Earth Orientation Parameters," Journal of Geophysical Research, Vol. 112, B09401, doi:10.1029/2007/JB004949, Sep. 2007.
http://www.agu.org/journals/jb/jb0709/2007JB004949/

Artz, T., Böckmann S., Nothnagel A., Tesmer V., "Comparison and Validation of VLBI Derived Polar Motion Estimates," In: International VLBI Service for Geodesy and Astrometry, Measuring the Future, Proceedings of the Fifth IVS General Meeting; A. Finkelstein and Dirk Behrend (eds.); pp 324 - 328, Nauka, Saint Petersburg, ISBN 978-5-02-025332-2, 2008.
ftp://ivscc.gsfc.nasa.gov/pub/general-meeting/2008/pdf/artz.pdf

Beasley, A. J., D. Gordon, A. B. Peck, L. Petrov, D. S. McMillan, E. B. Fomalont, C. Ma, "The VLBA Calibrator Survey-VCS1," Astrophys. J., Supp., vol. 141, p.13-21, 2002.
http://www.iop.org/EJ/abstract/0067-0049/141/1/13/

Biermann, G.J., 1977, 'Factorization Methods for Discrete Sequential Estimation', V128, Mathematics in Science and Engineering Series, Academic Press.

Böckmann, S., T. Artz, A. Nothnagel, V. Tesmer, "Comparison and combination of consistent VLBI solutions," Geowissenschaftliche Mitteilungen, Schriftenreihe Vermessung und Geoinformation der TU Wien, Heft 79, 82 - 87, 2007.

Böckmann, S., Nothnagel A., Artz, T., "VLBI terrestrial reference frame contributions to ITRF2008," J. Geod, in preparation, 2009.

Böhm, J., B. Werl, H. Schuh, "Troposphere mapping functions for GPS and very long baseline interferometry from European Centre for Medium-Range Weather Forecasts operational analysis data," Journal of Geophysical Research, Volume 111, Issue B2, CiteID B02406, 2006.

Bolotin S., "Influence of different strategies in VLBI data analysis on realizations of ICRF" In.: Proc. of the Journées 2007 "Systèmes de Référence Spatio-Temporels", Paris, September 2007, p .20-23.

Bolotin S., Lytvyn S., "Comparison of Radio Source Positions from Individual Solutions," In: International VLBI Service for Geodesy and Astrometry, *Measuring the Future*, Proceedings of the Fifth IVS General Meeting; A. Finkelstein and D. Behrend (eds.); pp 270–274, Nauka, Saint Petersburg, ISBN 978-5-02-025332-2, 2008.
ftp://ivscc.gsfc.nasa.gov/pub/general-meeting/2008/pdf/bolotin.pdf

Charlot, P., "Radio Source Structure in Astrometric and Geodetic Very Long Baseline Interferometry", 1990, AJ, 99, 1309–1326.

Charlot, P., D. A. Boboltz, A. L. Fey, E. B. Fomalont, B. J. Geldzahler, D. Gordon, C. S. Jacobs, G. .E. Lanyi, C. Ma, C. J. Naudet, J. D. Romney, O. J. Sovers, and L. D. Zhang, "The Celestial Reference Frame at Higher Radio Frequencies II. VLBA Imaging at 24 and 43 GHz," submitted to AJ, 21 Nov 2008.
http://www.iop.org/EJ/journal/aj

Clark, T. A, D. Gordon, W. E. Himwich, C. Ma, A. Mallama, J. W. Ryan, "Determination of Relative Site Motions in the Western United States Using Mark III Very Long Baseline Interferometry," J. Geophysical Research, vol. 92, no. B12, p.12741-12750, 10 Nov. 1987.
http://www.agu.org/journals/jb/v092/iB12/JB092iB12p12741/JB092iB12p12741.pdf

Feissel-Vernier, M., Ma, C., Gontier, A.-M., & Barache, C. 2006, A&A, 452, 1107

Fey, A. L., Clegg, A. W., Fomalont, E. B., "VLBA Observations of Radio Reference Frame Sources. I", 1996, ApJS, 105, 299–330.

Fey, A. L., Charlot, P., "VLBA Observations of Radio Reference Frame Sources. II. Astrometric Suitability Based on Observed Structure", 1997, ApJS, 111, 95–142.

Fey, A. L., Charlot, P., "VLBA Observations of Radio Reference Frame Sources. III. Astrometric Suitability of an Additional 225 Sources", 2000, ApJS, 128, 17–83.

Fey, A. L., Boboltz, D. A., Gaume, R. A., Eubanks, T. M., & Johnston, K. J., "Extragalactic Radio Source Selection for Use in Directly Linking Optical Astrometric Observations to the Radio Reference Frame," 2001, AJ, 121, 1741

Fey, A. L., C. Ma, E. F. Arias, P. Charlot, M. Feissel-Vernier, A.-M. Gontier, C. S. Jacobs, J. Li, and D. S. MacMillan, "The Second Extension of the ICRF: ICRF-Ext.2," AJ, vol. 127, no. 6, pp. 3587-3608, June 2004.
http://www.iop.org/EJ/article/1538-3881/127/6/3587/204010.html

Fomalont. E. B., L. Petrov, D. S. McMillan, D. Gordon, C. Ma, "The second VLBA Calibrator Survey: VCS2," Astronomical Journal, vol. 126 (N5), p. 2562-2566, 2003.
http://www.iop.org/EJ/article/1538-3881/126/5/2562/203233.html

Fricke, W., Schwan, H., Lederle, T., 1988, 'Fifth Fundamental Catalogue (FK5), Part I, Veroff. Astron. Rechen Inst 32, Heidelberg.

Gontier, A.-M., M. Feissel, C. Ma, 'The Contribution of VLBI to the Realization of a Celestial Reference System, in IERS Technical Note 23, 'Definition and Realization of the International Celestial Reference System by VLBI Astrometry of Extragalactic Objects', Ma, C. and M. Feissel (editors), June 1997, Observatoire de Paris.

Gordon, D., "VLBA Impact on Geodesy and Astronomy," International VLBI Service for Geodesy and Astrometry, 2004 General Meeting Proceedings, Ottawa, Canada, 2004.
http://ivscc.gsfc.nasa.gov/publications/gm2004/gordon1/

IAU General Assembly XXIII, Resolution B2-d, Kyoto, Japan, August 1997.
http://iau.org/static/resolutions/IAU1997_French.pdf

IERS 1996, International Earth Rotation Service Annual Report 1995 (Observatoire de Paris), II-19

Jacobs, C.S., & O. J. Sovers, "Extending the ICRF to Higher Radio Frequencies: Global Astrometric Results at 32/8 GHz," In: International VLBI Service for Geodesy and Astrometry, *Measuring the Future*, Proceedings of the Fifth IVS General Meeting; A. Finkelstein and D. Behrend (eds.); pp 284–288, Nauka, Saint Petersburg, ISBN 978-5-02-025332-2, 2008.
ftp://ivscc.gsfc.nasa.gov/pub/general-meeting/2008/pdf/jacobs.pdf

Kovalev, Y. Y., L. Petrov, E. B. Fomalont, D. Gordon, "The Fifth VLBA Calibrator Survey - VCS5," Astronomical Journal, vol. 133, pp. 1236-1242, April 2007.
http://www.iop.org/EJ/article/1538-3881/133/4/1236/205496.html

Kur′yanova A. N., Yatskiv, Ya. S., "The compiled catalog of positions of extragalactic radio sources RSC(GAO UA) 91 C 01," Kinematics Phys. Celest. Bodies, Vol. 9, No. 2, p. 12–21, 1993.
http://adsabs.harvard.edu/abs/1993KPCB....9Q..12K

Lambert, S.B., & Gontier, A.-M. 2009, "On radio source selection to define a stable celestial frame," Astron. Astrophys., 193, 317

Lanyi, G. E. ; E. B. Fomalont, P. Charlot, B. Geldzahler, D. Gordon, C. S. Jacobs, C. Ma, C. J. Naudet, J. Romney, O. J. Sovers, L. D. Zhang, and the K-Q VLBI Survey Collaboration, "Extragalactic Celestial Reference Frames at 24 and 43 GHz: Global Astrometric Results from the VLBA," AJ, submitted 21 Nov 2008.
http://www.iop.org/EJ/journal/aj

Ma C., J.M. Sauber, L.J. Bell, T.A. Clark, D. Gordon, W.E. Himwich, J.W Ryan, "Measurement of horizontal motions in Alaska using very long baseline interferometry," J. Geophys. Res., vol. 95, p. 21991-22011, 1990.

Ma, C., E.F. Arias, T.M. Eubanks, A.L. Fey, A.-M. Gontier, C.S. Jacobs, O.J. Sovers, B.A. Archinal, P. Charlot, "The International Celestial Reference Frame Realized by VLBI," in IERS Technical Note 23, 'Definition and Realization of the International Celestial Reference System by VLBI Astrometry of Extragalactic Objects', Ma, C. and M. Feissel (editors), June 1997, Observatoire de Paris.

Ma, C., E. F. Arias, T. M. Eubanks, A. L. Fey, A.-M. Gontier, C. S. Jacobs, O. J. Sovers, B. A. Archinal, and P. Charlot, "The International Celestial Reference Frame as Realized by Very Long Baseline Interferometry," AJ, 116, 1, pp. 516-546, July 1998.
http://www.iop.org/EJ/abstract/1538-3881/116/1/516

McCarthy, D.D. and G. Petit (editors), "IERS Conventions (2003)," IERS Technical Note, No. 32, Verlag des Bundesamtes fur Kartographie und Geodesie, Frankfurt am Main, 2004.

MacMillan, D.S., C. Ma, "Atmospheric Gradients and the VLBI terrestrial and celestial reference frames," Geophys. Res. Lett., vol. 24, issue 4, p.453-456, 15 Feb. 1997. http://www.agu.org/journals/gl/gl9704/97GL00143.pdf

Niell, A.E., "Global mapping functions for the atmosphere delay at radio wavelengths," J. Geophys. Res., vol. 101, no. B2, p. 3227-3246, 1996. http://www.agu.org/journals/jb/jb9602/95JB03048.pdf

Nothnagel, A., "Conventions on thermal expansion modeling of radio telescopes for geodetic and astrometric VLBI," J. of Geod., doi: 10.1007/s00190-008-0284-z, 15 Nov 2008. http://www.springerlink.com/content/k235683l1t031728/

Ojha, R., Fey, A. L., Johnston, K. J., Jauncey, D. L., Reynolds, J. E., Tzioumis, A. K., Quick, J. F . H., Nicolson, G. D., Ellingsen, S. P., Dodson, R. G., McCulloch, P. M., "VLBI Observations of Southern Hemisphere ICRF Sources. I." 2004, AJ, 127, 3609–3621.

Ojha, R., Fey, A. L., Charlot, P., Jauncey, D. L., Johnston, K. J., Reynolds, J. E., Tzioumis, A. K. , Quick, J. F. H., Nicolson, G. D., Ellingsen, S. P., McCulloch, P. M., Koyama, Y., "VLBI Observations of Southern Hemisphere ICRF Sources. II. Astrometric Suitability Based on Intrinsic Structure", 2005, AJ, 130, 2529–2540.

Petrov, L., Y. Y. Kovalev, E. Fomalont, D. Gordon, "The Third VLBA Calibrator Survey: VCS3," Astronomical Journal, vol. 129, p. 1163–1170, Feb. 2005. http://www.iop.org/EJ/article/1538-3881/129/2/1163/204415.html

Petrov, L., Y. Y. Kovalev, E. Fomalont, D. Gordon, "The Fourth VLBA Calibrator Survey: VCS4," Astronomical Journal, vol. 131, pp. 1872-1879, March 2006. http://www.iop.org/EJ/article/1538-3881/131/3/1872/204973.html

Petrov, L., Y. Y. Kovalev, E. B. Fomalont, D. Gordon, "The Sixth VLBA Calibrator Survey: VCS6," Astronomical Journal, vol. 136, pp. 580585, 2 July 2008. http://www.iop.org/EJ/article/1538-3881/136/2/580/aj_136_2_580.html

Petrov, L., D. Gordon, J. Gipson, D. MacMillan, C. Ma, E. Fomalont, R.C. Walker, C. Carabajal, "Precise Geodesy with the Very Long Baseline Array," Journal of Geodesy, 28 Feb 2009. http://www.springerlink.com/content/ul417881xj8485gm/

Petrov, L., J.-P. Boy, "Study of the atmospheric pressure loading signal in very long baseline interferometry observations," Journal of Geophys. Res.,vol. 109, B03405,

doi:10.1029/2003JB002500, 2004.
http://www.agu.org/journals/jb/jb0403/2003JB002500/

Ryan, J. W., T. A. Clark, C. Ma, D. Gordon, D. S. Caprette, W. E. Himwich, "Global Scale Tectonic Plate Motions Measured with CDP Data," in Contributions of Space Geodesy to Geodynamics: Crustal Dynamics, D.E. Smith and D.L. Turcotte (eds), American Geophysical Union,Washington D.C., Geodynamics Series 23, p. 37-49, 1993.

Tesmer, V., "Effect of various analysis options on VLBI determined CRF," in Proceedings of 18th European VLBI for Geodesy and Astrometry (EVGA) Working Meeting, Vienna, Austria, 2007
http://mars.hg.tuwien.ac.at/∼evga/proceedings/S42_Tesmer.pdf

Titov, O., Tesmer, V., Boehm, J., 2004, OCCAM v.6.0 software for VLBI data analysis, In International VLBI Service for Geodesy and Astrometry 2004 General Meeting Proc (eds. Vandenberg N. V. and Baver, K. D.) NASA/CP-2004-212255, pp. 267–271.

Titov, O. 2004, Construction of a celestial coordinate reference frame from VLBI data, Astron. Rep. 48, 941.

Table 18. Coordinates of 295 ICRF2 Defining Sources at S/X-band

Designation [a]	Source [b]	α	δ	σ_α (s)	σ_δ ($''$)	$C_{\alpha-\delta}$	Epoch of Observation Mean	First	Last	$N_{\rm exp}$	$N_{\rm obs}$
ICRF J000435.6 − 473619	0002 − 478	00 04 35.65550384	−47 36 19.6037899	0.00001359	0.0002139	0.383	52501.0	49330.5	54670.7	28	129
ICRF J001031.0 + 105829	0007 + 106	00 10 31.00590186	10 58 29.5043827	0.00000491	0.0000930	−0.187	53063.9	47288.7	54803.7	29	559
ICRF J001101.2 − 261233	0008 − 264	00 11 01.24673846	−26 12 33.3770171	0.00000660	0.0000936	−0.183	52407.5	47686.1	54768.6	45	592
ICRF J001331.1 + 405137	0010 + 405	00 13 31.13020334	40 51 37.1441040	0.00000482	0.0000683	−0.139	51619.2	48434.7	54713.7	22	1083
ICRF J001611.0 − 001512	0013 − 005	00 16 11.08855479	−00 15 12.4453413	0.00000435	0.0001005	−0.235	50403.0	47394.1	51492.8	67	716
ICRF J001945.7 + 732730	0016 + 731	00 19 45.78641940	73 27 30.0174396	0.00000989	0.0000424	−0.050	49249.8	44343.6	54865.7	458	25038
ICRF J002232.4 + 060804	0019 + 058	00 22 32.44120914	06 08 04.2690807	0.00000439	0.0000956	−0.237	52705.8	47394.1	54880.7	42	800
ICRF J003824.8 + 413706	0035 + 413	00 38 24.84359231	41 37 06.0003032	0.00000499	0.0000613	−0.035	52262.4	49422.9	54887.7	18	1024
ICRF J005041.3 − 092905	0048 − 097	00 50 41.31738756	−09 29 05.2102688	0.00000278	0.0000428	−0.030	51323.1	44773.8	54816.7	1802	41482
ICRF J005109.5 − 422633	0048 − 427	00 51 09.50182012	−42 26 33.2932480	0.00000932	0.0001177	0.013	53857.8	52306.7	54907.7	31	315
ICRF J010245.7 + 582411	0059 + 581	01 02 45.76238248	58 24 11.1366009	0.00000523	0.0000414	0.009	52030.9	48720.9	54880.7	1864	236989
ICRF J010645.1 − 403419	0104 − 408	01 06 45.10796851	−40 34 19.9602291	0.00000376	0.0000455	0.016	52201.3	47640.2	54903.8	1175	11531
ICRF J010915.4 − 604948	0107 − 610	01 09 15.47520598	−60 49 48.4599686	0.00001744	0.0001750	0.108	53933.9	52780.7	54726.7	24	102
ICRF J011205.8 + 224438	0109 + 224	01 12 05.82471754	22 44 38.7863909	0.00000379	0.0000653	−0.007	51836.0	48434.7	54872.7	37	1851
ICRF J011327.0 + 494824	0110 + 495	01 13 27.00680344	49 48 24.0431742	0.00000597	0.0000727	−0.135	52989.4	49422.9	54781.7	20	759
ICRF J011857.2 − 214130	0116 − 219	01 18 57.26216666	−21 41 30.1399986	0.00000683	0.0001138	−0.058	52128.2	50632.3	54768.6	19	289
ICRF J012141.5 + 114950	0119 + 115	01 21 41.59504339	11 49 50.4131012	0.00000279	0.0000429	−0.018	52622.1	47394.1	54901.7	1151	36167
ICRF J013305.7 − 520003	0131 − 522	01 33 05.76255607	−52 00 03.9457209	0.00001218	0.0001605	0.251	52621.9	48162.4	54901.7	28	126
ICRF J013658.5 + 475129	0133 + 476	01 36 58.59480585	47 51 29.1000445	0.00000407	0.0000414	0.014	52890.7	44343.6	54907.7	1307	117353
ICRF J013708.7 + 312235	0134 + 311	01 37 08.73362970	31 22 35.8553611	0.00000553	0.0001012	0.044	53105.6	50219.8	54901.7	13	550
ICRF J014125.8 − 092843	0138 − 097	01 41 25.83215547	−09 28 43.6741894	0.00000455	0.0000878	−0.020	52777.3	46875.8	54768.6	34	1008
ICRF J015456.2 + 474326	0151 + 474	01 54 56.28988783	47 43 26.5395732	0.00000530	0.0000654	−0.014	53123.2	49750.8	54657.8	21	1395
ICRF J020333.3 + 723253	0159 + 723	02 03 33.38496841	72 32 53.6672938	0.00001231	0.0000546	0.052	52872.5	47011.4	54907.7	35	1482
ICRF J020504.9 + 321230	0202 + 319	02 05 04.92536007	32 12 30.0954538	0.00000367	0.0000520	−0.038	52311.3	45466.3	54852.7	62	2357
ICRF J021748.9 + 014449	0215 + 015	02 17 48.95475182	01 44 49.6990704	0.00000348	0.0000673	−0.120	51978.4	48919.9	54837.7	37	1200
ICRF J022428.4 + 065923	0221 + 067	02 24 28.42819659	06 59 23.3415393	0.00000382	0.0000683	−0.214	52153.5	47394.1	54662.7	68	1173
ICRF J022934.9 − 784745	0230 − 790	02 29 34.94659358	−78 47 45.6017972	0.00003546	0.0001073	0.032	52873.3	47626.5	54726.7	49	247
ICRF J023145.8 + 132254	0229 + 131	02 31 45.89405431	13 22 54.7162668	0.00000281	0.0000422	−0.006	49841.4	44773.8	54844.7	2537	66911
ICRF J023631.1 − 295355	0234 − 301	02 36 31.16942057	−29 53 55.5402759	0.00000978	0.0001544	−0.032	53761.6	53126.1	54741.8	16	135
ICRF J023653.2 − 613615	0235 − 618	02 36 53.24574589	−61 36 15.1834250	0.00002197	0.0001688	0.249	53734.9	52861.2	54670.7	17	106
ICRF J023752.4 + 284808	0234 + 285	02 37 52.40567732	28 48 08.9900231	0.00000313	0.0000421	−0.023	49361.6	44447.0	54664.7	1199	53070
ICRF J023945.4 − 023440	0237 − 027	02 39 45.47226775	−02 34 40.9144020	0.00000359	0.0000672	−0.090	52760.9	49253.8	54901.7	36	1437
ICRF J030335.2 + 471616	0300 + 470	03 03 35.24222254	47 16 16.2754406	0.00000417	0.0000433	−0.048	48470.0	44343.6	54844.7	757	25008
ICRF J030350.6 − 621125	0302 − 623	03 03 50.63134799	−62 11 25.5498711	0.00001499	0.0001135	0.150	51436.6	48162.4	54726.7	44	248
ICRF J030642.6 + 624302	0302 + 625	03 06 42.65954796	62 43 02.0241642	0.00000833	0.0000613	−0.047	52280.3	48614.0	54662.7	37	1334
ICRF J030903.6 + 102916	0306 + 102	03 09 03.62350016	10 29 16.3409599	0.00000415	0.0000770	−0.209	52036.1	47394.1	54768.6	76	952

Table 18—Continued

Designation [a]	Source [b]	α	δ	σ_α (s)	σ_δ ($''$)	$C_{\alpha-\delta}$	Epoch of Observation			$N_{\rm exp}$	$N_{\rm obs}$
							Mean	First	Last		
ICRF J030956.0 − 605839	0308 − 611	03 09 56.09915397	−60 58 39.0561502	0.00000861	0.0000726	0.169	50431.8	47626.5	54907.7	121	1152
ICRF J031049.8 + 381453	0307 + 380	03 10 49.87992951	38 14 53.8378720	0.00000642	0.0001107	−0.044	53283.0	49939.8	54901.7	11	347
ICRF J031301.9 + 412001	0309 + 411	03 13 01.96212305	41 20 01.1835585	0.00000480	0.0000642	−0.147	52400.3	47165.8	54818.7	47	1138
ICRF J032536.8 + 222400	0322 + 222	03 25 36.81435154	22 24 00.3655873	0.00000389	0.0000695	−0.141	51716.8	50085.5	54907.7	32	1171
ICRF J033413.6 − 400825	0332 − 403	03 34 13.65451358	−40 08 25.3978415	0.00001125	0.0001211	−0.345	51855.9	47640.2	54893.7	25	212
ICRF J033553.9 − 543025	0334 − 546	03 35 53.92484162	−54 30 25.1146727	0.00001704	0.0002055	0.355	52901.7	48388.4	54706.7	31	113
ICRF J034506.4 + 145349	0342 + 147	03 45 06.41654424	14 53 49.5582021	0.00000446	0.0000837	−0.094	51563.2	47394.1	54676.7	47	894
ICRF J034838.1 − 274913	0346 − 279	03 48 38.14457723	−27 49 13.5655526	0.00000599	0.0000929	−0.157	53999.3	50688.3	54901.7	11	372
ICRF J040145.1 + 211028	0358 + 210	04 01 45.16607260	21 10 28.5870359	0.00000639	0.0001325	−0.026	52184.0	50085.5	54887.7	15	396
ICRF J040353.7 − 360501	0402 − 362	04 03 53.74989835	−36 05 01.9131085	0.00000359	0.0000487	0.161	52084.5	47415.7	54887.7	857	7648
ICRF J040534.0 − 130813	0403 − 132	04 05 34.00338957	−13 08 13.6907083	0.00000397	0.0001030	−0.146	51867.0	47176.5	54112.8	20	745
ICRF J040659.0 − 382628	0405 − 385	04 06 59.03533560	−38 26 28.0423567	0.00000423	0.0000575	−0.147	53096.5	48162.4	54882.8	286	2087
ICRF J041636.5 − 185108	0414 − 189	04 16 36.54445140	−18 51 08.3400284	0.00000471	0.0000851	−0.100	52136.7	46840.8	54803.7	39	930
ICRF J042315.8 − 012033	0420 − 014	04 23 15.80072776	−01 20 33.0654034	0.00000279	0.0000450	−0.037	48415.7	44773.8	54893.7	1290	30117
ICRF J042446.8 + 003606	0422 + 004	04 24 46.84206092	00 36 06.3293676	0.00000385	0.0000768	−0.082	52464.8	46976.8	54887.7	31	1013
ICRF J042952.9 + 272437	0426 + 273	04 29 52.96076804	27 24 37.8762939	0.00000428	0.0000790	0.059	52851.0	50219.8	54802.7	35	984
ICRF J043337.8 + 290555	0430 + 289	04 33 37.82985993	29 05 55.4770346	0.00000372	0.0000576	−0.044	51901.2	50043.8	54901.7	52	1948
ICRF J043900.8 − 452222	0437 − 454	04 39 00.85466883	−45 22 22.5628657	0.00001180	0.0001577	−0.108	52776.1	48766.9	54670.7	35	269
ICRF J044331.6 + 344106	0440 + 345	04 43 31.63520255	34 41 06.6640222	0.00000445	0.0000642	−0.049	50605.8	47718.4	51967.7	37	1454
ICRF J044907.6 + 112128	0446 + 112	04 49 07.67110088	11 21 28.5964577	0.00000341	0.0000603	−0.082	53331.6	47394.1	54845.7	41	1722
ICRF J045005.4 − 810102	0454 − 810	04 50 05.44020132	−81 01 02.2313228	0.00004163	0.0000967	0.064	51639.5	47626.5	54726.7	49	342
ICRF J045703.1 − 232452	0454 − 234	04 57 03.17922863	−23 24 52.0201418	0.00000299	0.0000428	−0.026	51444.2	46440.9	54903.8	2533	55475
ICRF J050112.8 − 015914	0458 − 020	05 01 12.80988366	−01 59 14.2562534	0.00000273	0.0000424	−0.068	51137.5	44773.8	54907.7	2150	48225
ICRF J050145.2 + 135607	0458 + 138	05 01 45.27082031	13 56 07.2204176	0.00000539	0.0001288	−0.026	52136.0	47394.1	54201.7	28	619
ICRF J050643.9 − 610940	0506 − 612	05 06 43.98872791	−61 09 40.9937940	0.00001524	0.0001190	0.113	52511.7	48110.9	54880.7	41	182
ICRF J050842.3 + 843204	0454 + 844	05 08 42.36345199	84 32 04.5440155	0.00003335	0.0000494	−0.108	52914.6	44343.6	54889.8	165	4081
ICRF J050927.4 + 101144	0506 + 101	05 09 27.45706864	10 11 44.6000396	0.00000378	0.0000826	−0.113	52566.7	47394.1	54872.7	42	1174
ICRF J051002.3 + 180041	0507 + 179	05 10 02.36912982	18 00 41.5816534	0.00000404	0.0000610	−0.075	51714.9	47605.1	54713.7	62	1182
ICRF J051644.9 − 620705	0516 − 621	05 16 44.92616793	−62 07 05.3892036	0.00001331	0.0001157	0.112	51882.1	48749.6	54726.7	37	218
ICRF J051803.8 + 205452	0515 + 208	05 18 03.82450329	20 54 52.4974899	0.00000620	0.0001535	−0.037	52114.2	50085.5	54907.7	11	428
ICRF J052234.4 − 610757	0522 − 611	05 22 34.42547880	−61 07 57.1335242	0.00002109	0.0001653	0.322	52851.2	47626.5	54706.7	20	90
ICRF J052531.4 − 455754	0524 − 460	05 25 31.40015013	−45 57 54.6848636	0.00001684	0.0001861	0.000	52412.0	49750.8	54726.7	28	161
ICRF J052616.6 − 483036	0524 − 485	05 26 16.67131064	−48 30 36.7915470	0.00001592	0.0002543	0.400	53913.6	53223.4	54726.7	11	68
ICRF J052732.7 + 033131	0524 + 034	05 27 32.70544796	03 31 31.5166429	0.00000484	0.0000871	−0.074	53092.2	49914.7	54893.7	12	441
ICRF J053315.8 + 482252	0529 + 483	05 33 15.86578266	48 22 52.8076620	0.00000506	0.0000584	−0.035	54311.3	50306.3	54852.7	13	1348
ICRF J053435.7 − 610607	0534 − 611	05 34 35.77248961	−61 06 07.0730607	0.00002193	0.0001790	0.082	53715.3	50182.6	54670.7	19	81

Table 18—Continued

Designation [a]	Source [b]	α	δ	σ_α (s)	σ_δ ($''$)	$C_{\alpha-\delta}$	Epoch of Observation			$N_{\rm exp}$	$N_{\rm obs}$
							Mean	First	Last		
ICRF J053628.4 − 340111	0534 − 340	05 36 28.43237520	−34 01 11.4684150	0.00001027	0.0001610	0.218	53790.6	52306.7	54907.7	34	341
ICRF J053850.3 − 440508	0537 − 441	05 38 50.36155219	−44 05 08.9389165	0.00000392	0.0000442	0.010	52847.7	47305.8	54903.8	1085	18435
ICRF J053942.3 + 143345	0536 + 145	05 39 42.36599103	14 33 45.5616993	0.00000370	0.0000640	−0.147	51944.2	47394.1	54901.7	73	1202
ICRF J053954.2 − 283955	0537 − 286	05 39 54.28147645	−28 39 55.9478122	0.00000515	0.0000782	−0.036	52718.2	48573.8	54872.7	58	995
ICRF J054734.1 + 272156	0544 + 273	05 47 34.14892109	27 21 56.8425667	0.00000412	0.0000700	−0.101	51906.5	47394.1	54858.7	65	1421
ICRF J055009.5 − 573224	0549 − 575	05 50 09.58018296	−57 32 24.3965304	0.00001696	0.0002398	0.372	53796.1	53223.4	54670.7	10	64
ICRF J055530.8 + 394849	0552 + 398	05 55 30.80561150	39 48 49.1649664	0.00000355	0.0000413	0.001	51012.9	44090.5	54901.7	4068	337322
ICRF J055932.0 + 235353	0556 + 238	05 59 32.03313165	23 53 53.9267683	0.00000305	0.0000445	−0.020	52323.5	47394.1	54887.7	590	11999
ICRF J060309.1 + 174216	0600 + 177	06 03 09.13026176	17 42 16.8105604	0.00000479	0.0000799	−0.379	52205.7	47394.1	54664.7	46	829
ICRF J064632.0 + 445116	0642 + 449	06 46 32.02599463	44 51 16.5901237	0.00000386	0.0000413	−0.014	53168.5	45466.3	54903.8	1211	103287
ICRF J064814.0 − 304419	0646 − 306	06 48 14.09647071	−30 44 19.6596827	0.00000692	0.0000939	−0.154	52092.0	47640.2	54887.7	40	601
ICRF J065024.5 − 163739	0648 − 165	06 50 24.58185521	−16 37 39.7251917	0.00000350	0.0000578	−0.066	53236.8	46875.8	54907.7	60	1791
ICRF J065917.9 + 081330	0656 + 082	06 59 17.99603428	08 13 30.9533022	0.00000302	0.0000590	−0.377	53670.1	49914.7	54903.8	401	4840
ICRF J070001.5 + 170921	0657 + 172	07 00 01.52553646	17 09 21.7014901	0.00000308	0.0000490	−0.113	51827.5	47655.8	54907.7	183	4503
ICRF J071046.1 + 473211	0707 + 476	07 10 46.10487679	47 32 11.1427167	0.00000527	0.0000642	−0.057	51517.3	44343.6	54837.7	25	1162
ICRF J072153.4 + 712036	0716 + 714	07 21 53.44846336	71 20 36.3634253	0.00000948	0.0000470	−0.032	52163.3	44343.6	54893.7	136	2799
ICRF J072516.8 + 142513	0722 + 145	07 25 16.80776128	14 25 13.7466902	0.00000366	0.0000615	−0.102	52580.8	47394.1	54522.7	45	1266
ICRF J072611.7 + 791131	0718 + 792	07 26 11.73524096	79 11 31.0162085	0.00001488	0.0000415	0.002	52440.4	48223.7	54887.7	1251	34947
ICRF J073019.1 − 114112	0727 − 115	07 30 19.11247420	−11 41 12.6005110	0.00000278	0.0000422	−0.022	51578.1	45259.2	54903.8	3261	109457
ICRF J073918.0 + 013704	0736 + 017	07 39 18.03389693	01 37 04.6178588	0.00000337	0.0000580	−0.122	52409.0	44773.8	54845.7	63	1624
ICRF J074202.7 + 490015	0738 + 491	07 42 02.74894651	49 00 15.6089340	0.00000593	0.0000688	−0.037	53155.0	49750.8	54823.7	18	1156
ICRF J074554.0 − 004417	0743 − 006	07 45 54.08232111	−00 44 17.5398546	0.00000384	0.0000971	−0.089	51189.3	46527.7	53068.7	30	731
ICRF J074625.8 + 254902	0743 + 259	07 46 25.87417871	25 49 02.1347553	0.00000305	0.0000422	−0.054	53817.2	47407.6	54903.8	671	26091
ICRF J074836.1 + 240024	0745 + 241	07 48 36.10927469	24 00 24.1100315	0.00000349	0.0000542	−0.072	51144.2	47620.8	54810.7	159	2550
ICRF J075052.0 + 123104	0748 + 126	07 50 52.04573519	12 31 04.8281766	0.00000299	0.0000475	−0.125	52767.7	44773.8	54816.7	145	3819
ICRF J080248.0 + 180949	0759 + 183	08 02 48.03196182	18 09 49.2493958	0.00000519	0.0001104	−0.110	52214.7	50085.5	54872.7	12	494
ICRF J080518.1 + 614423	0800 + 618	08 05 18.17956846	61 44 23.7002968	0.00000740	0.0000609	−0.147	54532.8	52409.7	54887.7	10	981
ICRF J080757.5 + 043234	0805 + 046	08 07 57.53857015	04 32 34.5310021	0.00001020	0.0002069	−0.168	51371.7	49914.7	54664.7	14	174
ICRF J080839.6 + 495036	0804 + 499	08 08 39.66628353	49 50 36.5304035	0.00000426	0.0000414	−0.047	51488.4	44343.6	54893.7	1406	86324
ICRF J080856.6 + 405244	0805 + 410	08 08 56.65203923	40 52 44.8888616	0.00000366	0.0000425	−0.014	51735.0	48720.9	54901.7	575	18706
ICRF J081126.7 + 014652	0808 + 019	08 11 26.70731189	01 46 52.2202616	0.00000289	0.0000456	−0.024	52826.7	46977.9	54818.7	221	5330
ICRF J081525.9 + 363515	0812 + 367	08 15 25.94485739	36 35 15.1488917	0.00000449	0.0000725	−0.028	52354.7	45775.8	54657.8	21	973
ICRF J081815.9 + 422245	0814 + 425	08 18 15.99960470	42 22 45.4149140	0.00000486	0.0000575	−0.080	49202.0	44343.6	53051.1	149	2383
ICRF J082550.3 + 030924	0823 + 033	08 25 50.33835429	03 09 24.5200730	0.00000273	0.0000430	−0.029	51407.8	45466.3	54907.7	1365	49660
ICRF J083052.0 + 241059	0827 + 243	08 30 52.08619070	24 10 59.8204032	0.00000354	0.0000544	−0.131	51630.9	47023.7	54655.7	82	1980
ICRF J083639.2 − 201659	0834 − 201	08 36 39.21525294	−20 16 59.5040953	0.00000559	0.0001054	−0.121	52587.9	46840.8	54741.8	33	626

Table 18—Continued

Designation [a]	Source [b]	α	δ	σ_α (s)	σ_δ ($''$)	$C_{\alpha-\delta}$	Epoch of Observation			$N_{\rm exp}$	$N_{\rm obs}$
							Mean	First	Last		
ICRF J085448.8 + 200630	0851 + 202	08 54 48.87492702	20 06 30.6408861	0.00000290	0.0000416	−0.039	50426.4	44342.2	54907.7	3449	149927
ICRF J085641.8 − 110514	0854 − 108	08 56 41.80414812	−11 05 14.4301901	0.00000512	0.0000778	−0.109	54477.1	53552.8	54858.7	15	344
ICRF J091437.9 + 024559	0912 + 029	09 14 37.91343166	02 45 59.2469393	0.00000329	0.0000601	−0.001	53574.1	47407.6	54865.7	30	1838
ICRF J092246.4 − 395935	0920 − 397	09 22 46.41826064	−39 59 35.0683561	0.00000431	0.0000859	−0.167	51602.8	47686.1	54907.7	227	3181
ICRF J092314.4 + 384939	0920 + 390	09 23 14.45293105	38 49 39.9101375	0.00000432	0.0000594	−0.003	52287.9	49736.9	54845.7	64	1567
ICRF J092751.8 − 203451	0925 − 203	09 27 51.82431596	−20 34 51.2324031	0.00000467	0.0000749	−0.146	52818.4	47777.3	54887.7	71	1010
ICRF J095232.0 + 351252	0949 + 354	09 52 32.02616656	35 12 52.4030592	0.00000524	0.0000893	−0.044	52576.8	50242.8	54887.7	16	483
ICRF J095819.6 + 472507	0955 + 476	09 58 19.67163931	47 25 07.8424347	0.00000404	0.0000414	−0.054	52388.7	48720.9	54907.7	2006	135716
ICRF J095820.9 + 322402	0955 + 326	09 58 20.94963113	32 24 02.2095353	0.00000390	0.0000580	−0.101	52606.9	47761.7	54657.8	29	1915
ICRF J095847.2 + 653354	0954 + 658	09 58 47.24510127	65 33 54.8180587	0.00000701	0.0000444	−0.117	49883.0	44343.6	54901.7	284	11507
ICRF J100614.0 − 501813	1004 − 500	10 06 14.00931618	−50 18 13.4706757	0.00001340	0.0001922	0.270	53837.6	49535.0	54795.7	22	105
ICRF J101447.0 + 230116	1012 + 232	10 14 47.06545658	23 01 16.5708649	0.00000413	0.0000634	−0.086	52012.0	47407.6	54712.7	34	1656
ICRF J101603.1 + 051302	1013 + 054	10 16 03.13646769	05 13 02.3414482	0.00000383	0.0000735	−0.020	54066.5	49914.7	54893.7	13	903
ICRF J101725.8 + 611627	1014 + 615	10 17 25.88757718	61 16 27.4966664	0.00000843	0.0000596	0.069	50914.9	49422.9	53153.2	22	1224
ICRF J101810.9 + 354239	1015 + 359	10 18 10.98809086	35 42 39.4408279	0.00000525	0.0001043	0.024	53327.1	50242.8	54880.7	10	493
ICRF J102343.5 − 664648	1022 − 665	10 23 43.53319996	−66 46 48.7177526	0.00002040	0.0001359	0.165	53658.5	52780.7	54670.7	27	153
ICRF J102444.8 + 191220	1022 + 194	10 24 44.80959508	19 12 20.4156249	0.00000354	0.0000619	−0.036	51418.7	47783.2	54803.7	41	2343
ICRF J103303.7 + 411606	1030 + 415	10 33 03.70786817	41 16 06.2329177	0.00000481	0.0000627	0.024	52634.8	47019.9	54818.7	29	1178
ICRF J103334.0 + 071126	1030 + 074	10 33 34.02429130	07 11 26.1477035	0.00000426	0.0000745	−0.080	52507.6	50855.8	54627.7	154	1220
ICRF J103653.4 − 374415	1034 − 374	10 36 53.43960199	−37 44 15.0656721	0.00001205	0.0001597	−0.102	53991.0	53223.4	54741.8	13	138
ICRF J103716.0 − 293402	1034 − 293	10 37 16.07973476	−29 34 02.8133345	0.00000324	0.0000444	−0.047	51514.0	46440.9	54903.8	1887	21896
ICRF J104146.7 + 523328	1038 + 528	10 41 46.78163764	52 33 28.2313168	0.00000517	0.0000524	0.029	51279.1	48524.8	54852.7	199	3040
ICRF J104423.0 + 805439	1039 + 811	10 44 23.06254789	80 54 39.4430277	0.00002013	0.0000478	−0.051	51808.6	47288.7	54788.7	53	2150
ICRF J104455.9 + 065538	1042 + 071	10 44 55.91124593	06 55 38.2626553	0.00000708	0.0001883	−0.211	51442.2	47777.3	52711.7	13	289
ICRF J104806.6 − 190935	1045 − 188	10 48 06.62060701	−19 09 35.7266240	0.00000394	0.0000869	−0.154	52670.5	47176.5	54858.7	33	1130
ICRF J105148.7 + 211952	1049 + 215	10 51 48.78907490	21 19 52.3138145	0.00000422	0.0000685	−0.088	51671.0	47931.6	54746.7	28	1229
ICRF J105811.5 + 811432	1053 + 815	10 58 11.53537962	81 14 32.6751819	0.00001836	0.0000420	0.003	52489.6	47453.0	54880.7	675	18890
ICRF J105829.6 + 013358	1055 + 018	10 58 29.60520747	01 33 58.8237691	0.00000300	0.0000526	−0.221	49266.2	44773.8	54601.7	307	6161
ICRF J110352.2 − 535700	1101 − 536	11 03 52.22167171	−53 57 00.6966293	0.00000939	0.0001166	0.232	50525.9	47626.5	54706.7	54	398
ICRF J110427.3 + 381231	1101 + 384	11 04 27.31394136	38 12 31.7990644	0.00000359	0.0000444	−0.101	51979.0	49519.8	54763.8	528	11654
ICRF J111358.6 + 144226	1111 + 149	11 13 58.69508359	14 42 26.9525965	0.00000484	0.0000982	−0.073	51713.1	47005.8	54789.7	42	779
ICRF J112553.7 + 261019	1123 + 264	11 25 53.71192285	26 10 19.9786840	0.00000360	0.0000544	−0.138	50804.2	46977.9	54907.7	165	2248
ICRF J112704.3 − 185717	1124 − 186	11 27 04.39244958	−18 57 17.4416582	0.00000292	0.0000432	0.009	52704.6	46875.8	54903.8	1087	27242
ICRF J113053.2 + 381518	1128 + 385	11 30 53.28261193	38 15 18.5469933	0.00000348	0.0000417	−0.044	51787.2	45775.8	54903.8	1227	63954
ICRF J113320.0 + 004052	1130 + 009	11 33 20.05579171	00 40 52.8372903	0.00000472	0.0000956	−0.129	51426.8	47019.9	54852.7	50	850
ICRF J113624.5 − 033029	1133 − 032	11 36 24.57693290	−03 30 29.4964694	0.00000509	0.0001256	−0.038	53907.2	50576.2	54845.7	10	474

Table 18—Continued

Designation [a]	Source [b]	α	δ	σ_α (s)	σ_δ ($''$)	$C_{\alpha-\delta}$	Epoch of Observation Mean	First	Last	$N_{\rm exp}$	$N_{\rm obs}$
ICRF J114553.6 − 695401	1143 − 696	11 45 53.62417065	−69 54 01.7977922	0.00002802	0.0001945	0.377	53671.0	52872.9	54706.7	14	72
ICRF J114658.2 + 395834	1144 + 402	11 46 58.29791629	39 58 34.3045026	0.00000392	0.0000483	−0.067	50262.3	45138.8	54872.7	177	4823
ICRF J114701.3 − 381211	1144 − 379	11 47 01.37070177	−38 12 11.0234199	0.00000362	0.0000456	−0.014	52592.2	47654.0	54907.7	928	10954
ICRF J114751.5 − 072441	1145 − 071	11 47 51.55402876	−07 24 41.1410887	0.00000294	0.0000529	−0.170	51567.1	47176.5	54713.7	161	7586
ICRF J115019.2 + 241753	1147 + 245	11 50 19.21217405	24 17 53.8353207	0.00000401	0.0000671	−0.100	52721.4	48720.9	54893.7	20	1262
ICRF J115217.2 − 084103	1149 − 084	11 52 17.20951537	−08 41 03.3138824	0.00000432	0.0000688	−0.021	54046.7	50576.2	54893.7	15	517
ICRF J115918.3 − 663539	1156 − 663	11 59 18.30544873	−66 35 39.4272186	0.00002870	0.0002008	0.313	53993.0	52872.9	54726.7	14	90
ICRF J115931.8 + 291443	1156 + 295	11 59 31.83390975	29 14 43.8268741	0.00000313	0.0000420	−0.038	52031.0	46977.9	54880.7	1312	47905
ICRF J121546.7 − 173145	1213 − 172	12 15 46.75176110	−17 31 45.4029502	0.00000377	0.0000745	−0.055	52572.7	46840.8	54907.7	54	1267
ICRF J121752.0 + 300700	1215 + 303	12 17 52.08196139	30 07 00.6359190	0.00000533	0.0000920	−0.089	51708.3	48434.7	54683.7	20	890
ICRF J122222.5 + 041315	1219 + 044	12 22 22.54962080	04 13 15.7761797	0.00000275	0.0000435	−0.070	51119.4	48378.8	54907.7	1241	31223
ICRF J122340.4 + 804004	1221 + 809	12 23 40.49373854	80 40 04.3404390	0.00002117	0.0000540	−0.006	51486.2	48022.7	54803.7	35	2145
ICRF J122847.4 + 370612	1226 + 373	12 28 47.42367744	37 06 12.0958631	0.00000471	0.0000705	0.003	51946.9	48378.8	54830.7	31	1147
ICRF J123924.5 + 073017	1236 + 077	12 39 24.58832517	07 30 17.1892686	0.00000389	0.0000729	−0.063	52779.9	48378.8	54601.7	28	960
ICRF J124251.3 + 375100	1240 + 381	12 42 51.36907635	37 51 00.0252447	0.00000504	0.0000664	−0.188	52701.2	49429.9	54818.7	18	1258
ICRF J124604.2 − 073046	1243 − 072	12 46 04.23210358	−07 30 46.5745473	0.00000407	0.0000811	−0.168	51744.3	47176.5	54684.7	69	1034
ICRF J124646.8 − 254749	1244 − 255	12 46 46.80203492	−25 47 49.2887900	0.00000375	0.0000587	−0.209	51956.8	46875.8	54880.7	131	1989
ICRF J125438.2 + 114105	1252 + 119	12 54 38.25561161	11 41 05.8951798	0.00000445	0.0000826	−0.094	52027.5	46977.9	54830.7	54	914
ICRF J125459.9 − 713818	1251 − 713	12 54 59.92144870	−71 38 18.4366697	0.00002216	0.0001076	0.122	50743.2	47626.5	54726.7	38	258
ICRF J130252.4 + 574837	1300 + 580	13 02 52.46527568	57 48 37.6093180	0.00000515	0.0000415	−0.005	52953.0	49422.9	54844.7	942	71553
ICRF J131059.4 + 323334	1308 + 328	13 10 59.40272936	32 33 34.4496333	0.00000376	0.0000557	−0.016	52791.2	49706.7	54865.7	55	2153
ICRF J131607.9 − 333859	1313 − 333	13 16 07.98593995	−33 38 59.1725057	0.00000370	0.0000587	−0.134	51699.5	47415.7	54657.8	334	4738
ICRF J132700.8 + 221050	1324 + 224	13 27 00.86131377	22 10 50.1629729	0.00000320	0.0000496	−0.073	53314.8	48429.0	54901.7	74	3162
ICRF J132901.1 − 560802	1325 − 558	13 29 01.14492878	−56 08 02.6657428	0.00001797	0.0002042	0.409	53671.8	52676.7	54670.7	27	126
ICRF J133739.7 − 125724	1334 − 127	13 37 39.78277768	−12 57 24.6932620	0.00000280	0.0000428	−0.018	51396.0	46840.8	54903.8	2674	73758
ICRF J134345.9 + 660225	1342 + 662	13 43 45.95957134	66 02 25.7451011	0.00000768	0.0000472	0.002	53694.5	47783.2	54887.7	31	3135
ICRF J134408.6 + 660611	1342 + 663	13 44 08.67966687	66 06 11.6438846	0.00000872	0.0000537	−0.015	51630.0	44343.6	54803.7	57	2123
ICRF J135256.5 − 441240	1349 − 439	13 52 56.53494294	−44 12 40.3875227	0.00001113	0.0001047	−0.392	52338.6	48110.9	54706.7	45	301
ICRF J135406.8 − 020603	1351 − 018	13 54 06.89532213	−02 06 03.1904447	0.00000278	0.0000479	−0.007	52358.7	48573.8	54901.7	882	15317
ICRF J135711.2 − 152728	1354 − 152	13 57 11.24497976	−15 27 28.7867232	0.00000356	0.0000600	−0.140	52510.7	46875.8	54818.7	136	1964
ICRF J135755.3 + 764321	1357 + 769	13 57 55.37153147	76 43 21.0510512	0.00001195	0.0000413	0.015	52397.9	47011.4	54903.8	1786	194975
ICRF J140856.4 − 075226	1406 − 076	14 08 56.48120036	−07 52 26.6664200	0.00000357	0.0000682	−0.147	52583.4	47176.5	54657.8	59	1385
ICRF J141946.5 + 542314	1418 + 546	14 19 46.59740212	54 23 14.7871875	0.00000474	0.0000419	−0.022	52721.5	45138.8	54907.7	697	32547
ICRF J141946.6 + 382148	1417 + 385	14 19 46.61376070	38 21 48.4750925	0.00000355	0.0000430	−0.009	53418.9	49750.8	54713.7	271	12066
ICRF J142455.5 − 680758	1420 − 679	14 24 55.55739563	−68 07 58.0945205	0.00002421	0.0002266	0.289	53830.0	52872.9	54723.8	15	76
ICRF J142549.0 + 142456	1423 + 146	14 25 49.01801632	14 24 56.9019040	0.00000659	0.0001657	−0.007	51188.2	50085.5	53690.7	15	334

Table 18—Continued

Designation [a]	Source [b]	α	δ	σ_α (s)	σ_δ ($''$)	$C_{\alpha-\delta}$	Epoch of Observation			$N_{\rm exp}$	$N_{\rm obs}$
							Mean	First	Last		
ICRF J142756.2 − 420619	1424 − 418	14 27 56.29756536	−42 06 19.4375991	0.00000389	0.0000464	0.032	52594.1	47305.8	54907.7	886	8609
ICRF J143439.7 + 195200	1432 + 200	14 34 39.79335525	19 52 00.7358213	0.00000452	0.0000813	0.103	52140.7	48863.2	54907.7	29	1099
ICRF J144553.3 − 162901	1443 − 162	14 45 53.37628643	−16 29 01.6189137	0.00000690	0.0000981	−0.433	52430.8	47941.3	54741.8	35	499
ICRF J145239.6 − 650203	1448 − 648	14 52 39.67924989	−65 02 03.4333591	0.00003553	0.0002790	0.196	53586.2	52887.6	54726.7	13	53
ICRF J145432.9 − 401232	1451 − 400	14 54 32.91235921	−40 12 32.5142375	0.00000696	0.0001251	0.067	51860.3	47640.2	54732.7	54	684
ICRF J145859.3 + 041613	1456 + 044	14 58 59.35621201	04 16 13.8206019	0.00000546	0.0001029	−0.025	53225.9	49914.7	54893.7	15	426
ICRF J150048.6 + 475115	1459 + 480	15 00 48.65422191	47 51 15.5381838	0.00000554	0.0000616	0.003	51760.8	47459.8	54844.7	25	1739
ICRF J150424.9 + 102939	1502 + 106	15 04 24.97978142	10 29 39.1986151	0.00000298	0.0000496	−0.111	48555.5	44447.0	54664.7	623	13963
ICRF J150506.4 + 032630	1502 + 036	15 05 06.47715917	03 26 30.8126616	0.00000351	0.0000636	−0.099	53031.1	48853.8	54872.7	29	1503
ICRF J150609.5 + 373051	1504 + 377	15 06 09.52996778	37 30 51.1325044	0.00000466	0.0000660	−0.001	51732.7	46977.9	54614.7	32	1267
ICRF J151002.9 + 570243	1508 + 572	15 10 02.92236464	57 02 43.3759071	0.00000681	0.0000621	0.099	50741.0	49541.8	53153.2	53	1572
ICRF J151250.5 − 090559	1510 − 089	15 12 50.53292491	−09 05 59.8295878	0.00000310	0.0000560	−0.160	49643.6	44773.8	54713.7	354	5184
ICRF J151344.8 − 101200	1511 − 100	15 13 44.89341390	−10 12 00.2644930	0.00000437	0.0001068	−0.251	51598.7	46875.8	53153.2	34	718
ICRF J151656.7 + 193212	1514 + 197	15 16 56.79616342	19 32 12.9920178	0.00000391	0.0000712	−0.111	52149.3	48434.7	54858.7	33	1269
ICRF J152149.6 + 433639	1520 + 437	15 21 49.61387985	43 36 39.2681562	0.00000567	0.0000873	0.088	53679.3	50242.8	54901.7	11	367
ICRF J152237.6 − 273010	1519 − 273	15 22 37.67598872	−27 30 10.7854174	0.00000320	0.0000444	0.010	53348.7	46875.8	54887.7	659	11666
ICRF J154929.4 + 023701	1546 + 027	15 49 29.43684301	02 37 01.1634197	0.00000310	0.0000599	−0.135	53012.2	47005.8	54907.7	64	2191
ICRF J155035.2 + 052710	1548 + 056	15 50 35.26924162	05 27 10.4484262	0.00000314	0.0000557	−0.050	48158.6	44773.8	53609.2	254	6518
ICRF J155751.4 − 000150	1555 + 001	15 57 51.43397128	−00 01 50.4137075	0.00000324	0.0000624	−0.267	51279.0	44773.8	54901.7	235	2087
ICRF J155850.2 − 643229	1554 − 643	15 58 50.28436339	−64 32 29.6374071	0.00002934	0.0002738	0.200	53611.1	52861.2	54670.7	15	58
ICRF J155930.9 + 030448	1557 + 032	15 59 30.97261545	03 04 48.2568829	0.00000418	0.0000783	−0.066	51808.0	49541.8	54732.7	42	835
ICRF J160734.7 − 333108	1604 − 333	16 07 34.76234480	−33 31 08.9133114	0.00000993	0.0001104	−0.483	52916.8	48393.7	54741.8	49	506
ICRF J160846.2 + 102907	1606 + 106	16 08 46.20318554	10 29 07.7758300	0.00000277	0.0000419	0.014	51950.0	45138.8	54903.8	2259	116280
ICRF J161630.6 − 710831	1611 − 710	16 16 30.64155980	−71 08 31.4545422	0.00004268	0.0002293	0.353	53791.6	52887.6	54670.7	13	62
ICRF J161637.5 + 045932	1614 + 051	16 16 37.55681502	04 59 32.7367495	0.00000353	0.0000670	−0.181	51528.0	47605.1	54657.8	158	1619
ICRF J161914.8 + 224747	1617 + 229	16 19 14.82461057	22 47 47.8510784	0.00000540	0.0001014	−0.217	52327.2	50085.5	54901.7	11	542
ICRF J162418.4 − 680912	1619 − 680	16 24 18.43700573	−68 09 12.4965314	0.00002085	0.0001461	0.128	51926.5	47626.5	54706.7	30	167
ICRF J162546.8 − 252738	1622 − 253	16 25 46.89164010	−25 27 38.3267989	0.00000307	0.0000439	−0.017	51255.1	46840.8	54903.8	2182	33914
ICRF J162854.6 − 615236	1624 − 617	16 28 54.68982354	−61 52 36.3978862	0.00002301	0.0002064	0.231	53863.5	52861.2	54726.7	15	73
ICRF J163813.4 + 572023	1637 + 574	16 38 13.45629705	57 20 23.9790727	0.00000548	0.0000463	0.045	49616.1	44343.6	54907.7	324	7675
ICRF J164029.6 + 394646	1638 + 398	16 40 29.63277180	39 46 46.0285033	0.00000356	0.0000416	0.024	51119.1	44343.6	54852.7	1177	93554
ICRF J164125.2 + 225704	1639 + 230	16 41 25.22756501	22 57 04.0327611	0.00000376	0.0000698	−0.133	53216.0	50085.5	54907.7	31	1283
ICRF J164207.8 + 685639	1642 + 690	16 42 07.84850549	68 56 39.7564973	0.00000785	0.0000428	0.017	51281.4	44090.5	54614.7	194	13165
ICRF J164257.3 − 810835	1633 − 810	16 42 57.34565318	−81 08 35.0701687	0.00009167	0.0002633	0.274	53711.6	52861.2	54670.7	15	50
ICRF J170053.1 − 261051	1657 − 261	17 00 53.15406129	−26 10 51.7253457	0.00000377	0.0000665	−0.205	52210.7	46875.8	54887.7	99	2558
ICRF J170144.8 − 562155	1657 − 562	17 01 44.85811384	−56 21 55.9019532	0.00001398	0.0001933	0.313	53753.0	52676.7	54723.8	29	142

Table 18—Continued

Designation [a]	Source [b]	α	δ	σ_α (s)	σ_δ ($''$)	$C_{\alpha-\delta}$	Epoch of Observation			$N_{\rm exp}$	$N_{\rm obs}$
							Mean	First	Last		
ICRF J170336.5 − 621240	1659 − 621	17 03 36.54124564	−62 12 40.0081704	0.00001844	0.0001686	0.408	53741.4	52780.7	54726.7	22	111
ICRF J170734.4 + 014845	1705 + 018	17 07 34.41527100	01 48 45.6992837	0.00000342	0.0000736	−0.138	51738.7	48194.7	54858.7	65	1498
ICRF J170934.3 − 172853	1706 − 174	17 09 34.34539327	−17 28 53.3649724	0.00000453	0.0000943	−0.337	52211.4	48093.0	54741.8	149	900
ICRF J171913.0 + 174506	1717 + 178	17 19 13.04848160	17 45 06.4373011	0.00000372	0.0000702	0.009	52556.6	47011.4	54830.7	29	1476
ICRF J172727.6 + 453039	1726 + 455	17 27 27.65080470	45 30 39.7313444	0.00000392	0.0000417	0.034	51622.9	48720.9	54798.5	1342	54791
ICRF J173302.7 − 130449	1730 − 130	17 33 02.70578476	−13 04 49.5481484	0.00000313	0.0000540	−0.112	47785.2	45259.2	53609.2	635	15034
ICRF J173340.7 − 793555	1725 − 795	17 33 40.70027819	−79 35 55.7166934	0.00005617	0.0001818	0.213	53897.2	52887.6	54723.8	14	80
ICRF J173420.5 + 385751	1732 + 389	17 34 20.57853662	38 57 51.4430746	0.00000447	0.0000596	−0.049	51811.4	46977.9	54858.7	62	1455
ICRF J173927.3 + 495503	1738 + 499	17 39 27.39049252	49 55 03.3684410	0.00000608	0.0000725	0.013	52608.9	49422.9	54901.7	18	986
ICRF J173957.1 + 473758	1738 + 476	17 39 57.12907360	47 37 58.3615566	0.00000538	0.0000643	0.071	51602.7	47288.7	54713.7	29	1261
ICRF J174358.8 − 035004	1741 − 038	17 43 58.85613396	−03 50 04.6166450	0.00000273	0.0000422	0.021	51323.2	44773.8	54903.8	3318	130762
ICRF J174535.2 + 172001	1743 + 173	17 45 35.20817083	17 20 01.4236878	0.00000393	0.0000762	−0.162	51587.7	46977.9	54657.8	52	1059
ICRF J174614.0 + 622654	1745 + 624	17 46 14.03413721	62 26 54.7383903	0.00000601	0.0000420	0.066	51974.3	48916.8	54893.7	925	27177
ICRF J175132.8 + 093900	1749 + 096	17 51 32.81857318	09 39 00.7284829	0.00000276	0.0000419	0.031	51989.2	44447.0	54907.7	2635	108967
ICRF J175342.4 + 284804	1751 + 288	17 53 42.47364429	28 48 04.9388841	0.00000361	0.0000544	−0.091	52901.8	47005.8	54901.7	44	1608
ICRF J175653.1 + 153520	1754 + 155	17 56 53.10213624	15 35 20.8265328	0.00000522	0.0001064	0.132	53639.4	52306.7	54893.7	11	491
ICRF J180024.7 + 384830	1758 + 388	18 00 24.76536125	38 48 30.6975330	0.00000414	0.0000540	−0.037	52081.0	49429.9	54907.7	42	1570
ICRF J180045.6 + 782804	1803 + 784	18 00 45.68391641	78 28 04.0184502	0.00001378	0.0000413	0.023	50587.1	44343.6	54907.7	2295	157326
ICRF J180132.3 + 440421	1800 + 440	18 01 32.31482108	44 04 21.9003219	0.00000421	0.0000505	0.050	53394.6	48194.7	54845.7	39	2759
ICRF J180323.4 − 650736	1758 − 651	18 03 23.49666700	−65 07 36.7612094	0.00001681	0.0001262	0.198	52673.9	48043.8	54706.7	30	175
ICRF J180957.8 − 455241	1806 − 458	18 09 57.87175020	−45 52 41.0139197	0.00001886	0.0001793	−0.382	53146.2	49629.6	54726.7	37	182
ICRF J181945.3 − 552120	1815 − 553	18 19 45.39951849	−55 21 20.7453785	0.00000818	0.0000552	0.025	51665.2	47626.5	54903.8	334	1726
ICRF J182332.8 + 685752	1823 + 689	18 23 32.85390304	68 57 52.6125919	0.00001275	0.0000816	0.009	53891.4	49827.5	54901.7	10	419
ICRF J182407.0 + 565101	1823 + 568	18 24 07.06837771	56 51 01.4908371	0.00000529	0.0000448	0.034	51440.8	44343.6	54887.7	205	6364
ICRF J182912.4 − 581355	1824 − 582	18 29 12.40237320	−58 13 55.1616899	0.00002140	0.0002150	0.403	54023.5	53223.4	54726.7	10	58
ICRF J183728.7 − 710843	1831 − 711	18 37 28.71493799	−71 08 43.5545891	0.00002405	0.0001336	0.012	49334.4	47626.5	52971.6	23	229
ICRF J184233.6 + 680925	1842 + 681	18 42 33.64168915	68 09 25.2277840	0.00000865	0.0000490	−0.099	51888.8	44343.6	54830.7	26	2463
ICRF J184822.0 + 321902	1846 + 322	18 48 22.08858135	32 19 02.6037429	0.00000451	0.0000830	−0.018	53653.9	50219.8	54865.7	10	573
ICRF J184916.0 + 670541	1849 + 670	18 49 16.07228978	67 05 41.6802978	0.00000753	0.0000445	0.029	52094.0	48649.8	54713.7	148	5045
ICRF J191109.6 − 200655	1908 − 201	19 11 09.65289198	−20 06 55.1089891	0.00000298	0.0000476	−0.081	52233.4	46840.8	54865.7	852	14482
ICRF J192332.1 − 210433	1920 − 211	19 23 32.18981466	−21 04 33.3330547	0.00000424	0.0000794	−0.384	51790.5	47407.6	54858.7	93	999
ICRF J192451.0 − 291430	1921 − 293	19 24 51.05595514	−29 14 30.1210524	0.00000319	0.0000448	0.006	50176.4	45259.2	54903.8	1744	33365
ICRF J193006.1 − 605609	1925 − 610	19 30 06.16009446	−60 56 09.1841517	0.00002042	0.0002039	0.159	52356.8	47626.5	54706.7	26	120
ICRF J193124.9 + 224331	1929 + 226	19 31 24.91678444	22 43 31.2586209	0.00000381	0.0000665	−0.040	52878.8	48614.0	54907.7	36	2062
ICRF J193716.2 − 395801	1933 − 400	19 37 16.21735166	−39 58 01.5529907	0.00000832	0.0001018	−0.356	51868.7	47640.2	54810.7	53	371
ICRF J193926.6 − 152543	1936 − 155	19 39 26.65774750	−15 25 43.0584183	0.00000343	0.0000646	−0.171	52436.9	47176.5	54901.7	86	1763

Table 18—Continued

Designation [a]	Source [b]	α	δ	σ_α (s)	σ_δ ($''$)	$C_{\alpha-\delta}$	Epoch of Observation			$N_{\rm exp}$	$N_{\rm obs}$
							Mean	First	Last		
ICRF J194025.5 − 690756	1935 − 692	19 40 25.52820104	−69 07 56.9714945	0.00002282	0.0001647	0.148	52017.0	47626.5	54726.7	31	128
ICRF J195542.7 + 513148	1954 + 513	19 55 42.73826837	51 31 48.5461210	0.00000538	0.0000539	−0.117	51522.9	45775.8	54818.7	58	2260
ICRF J195759.8 − 384506	1954 − 388	19 57 59.81927470	−38 45 06.3557585	0.00000365	0.0000457	−0.074	52549.4	48766.9	54907.7	849	12512
ICRF J200057.0 − 174857	1958 − 179	20 00 57.09044485	−17 48 57.6725440	0.00000291	0.0000433	0.011	51879.7	46875.8	54903.8	1320	29536
ICRF J200210.4 + 472528	2000 + 472	20 02 10.41825568	47 25 28.7737223	0.00000479	0.0000519	0.006	54513.2	50306.3	54880.7	16	1457
ICRF J200555.0 − 372341	2002 − 375	20 05 55.07090025	−37 23 41.4778536	0.00001226	0.0002700	0.185	53301.1	52306.7	54684.7	14	107
ICRF J201115.7 − 154640	2008 − 159	20 11 15.71093257	−15 46 40.2536652	0.00000349	0.0000676	−0.146	51615.5	46840.8	54907.7	116	1447
ICRF J203154.9 + 121941	2029 + 121	20 31 54.99427114	12 19 41.3403129	0.00000349	0.0000596	0.016	52328.2	47019.9	54788.7	46	1719
ICRF J205616.3 − 471447	2052 − 474	20 56 16.35981874	−47 14 47.6276461	0.00000463	0.0000516	−0.204	53381.0	48162.4	54903.8	285	3243
ICRF J210138.8 + 034131	2059 + 034	21 01 38.83416420	03 41 31.3209577	0.00000357	0.0000696	−0.036	52596.7	48434.7	54907.7	57	1569
ICRF J210841.0 + 143027	2106 + 143	21 08 41.03215158	14 30 27.0123177	0.00000467	0.0001236	−0.076	51110.8	50085.5	53355.7	12	605
ICRF J210933.1 − 411020	2106 − 413	21 09 33.18859195	−41 10 20.6053191	0.00000750	0.0001219	0.027	52594.7	47626.5	54880.7	55	520
ICRF J211529.4 + 293338	2113 + 293	21 15 29.41345556	29 33 38.3669657	0.00000317	0.0000432	0.011	53066.6	46977.9	54907.7	527	19303
ICRF J212630.7 − 460547	2123 − 463	21 26 30.70426484	−46 05 47.8920231	0.00001556	0.0003044	0.328	53732.0	53223.4	54706.7	13	46
ICRF J212912.1 − 153841	2126 − 158	21 29 12.17589777	−15 38 41.0413097	0.00000302	0.0000532	−0.015	53235.2	47176.5	54903.8	720	6058
ICRF J213410.3 − 015317	2131 − 021	21 34 10.30959643	−01 53 17.2387909	0.00000366	0.0000719	−0.230	51782.1	47176.5	54768.6	92	1317
ICRF J213901.3 + 142335	2136 + 141	21 39 01.30926937	14 23 35.9922096	0.00000282	0.0000421	−0.010	53139.2	45466.3	54837.7	947	42224
ICRF J214712.7 − 753613	2142 − 758	21 47 12.73062415	−75 36 13.2248179	0.00004159	0.0001621	0.175	52936.3	47626.5	54670.7	19	84
ICRF J215224.8 + 173437	2150 + 173	21 52 24.81939953	17 34 37.7950583	0.00000368	0.0000638	−0.098	52151.9	47005.8	54648.7	45	1763
ICRF J220743.7 − 534633	2204 − 540	22 07 43.73330411	−53 46 33.8197226	0.00001054	0.0001418	0.231	52590.7	48110.9	54726.7	43	235
ICRF J221205.9 + 235540	2209 + 236	22 12 05.96631138	23 55 40.5438272	0.00000304	0.0000428	0.011	53642.5	48194.7	54788.7	227	13321
ICRF J222305.9 − 345547	2220 − 351	22 23 05.93057815	−34 55 47.1774281	0.00001175	0.0003101	0.226	53774.6	53223.4	54741.8	20	128
ICRF J222547.2 − 045701	2223 − 052	22 25 47.25929302	−04 57 01.3907581	0.00000275	0.0000425	−0.009	53301.4	44773.8	54844.7	947	38566
ICRF J222940.0 − 083254	2227 − 088	22 29 40.08434003	−08 32 54.4353948	0.00000359	0.0000661	−0.181	51961.7	45466.3	54852.7	86	1127
ICRF J223036.4 + 694628	2229 + 695	22 30 36.46970494	69 46 28.0768954	0.00000853	0.0000443	0.010	54249.0	47459.8	54907.7	48	3820
ICRF J223513.2 − 483558	2232 − 488	22 35 13.23657712	−48 35 58.7945006	0.00000978	0.0001159	−0.018	52833.6	48162.4	54670.7	51	389
ICRF J223912.0 − 570100	2236 − 572	22 39 12.07592367	−57 01 00.8393966	0.00001773	0.0002127	0.312	53973.7	53223.4	54670.7	10	54
ICRF J224703.9 − 365746	2244 − 372	22 47 03.91732284	−36 57 46.3039624	0.00001209	0.0001214	−0.324	53586.9	52676.7	54741.8	24	254
ICRF J224838.6 − 323552	2245 − 328	22 48 38.68573771	−32 35 52.1879540	0.00001173	0.0001555	−0.641	50937.3	47394.1	53126.1	36	286
ICRF J225307.3 + 194234	2250 + 190	22 53 07.36917339	19 42 34.6287472	0.00000348	0.0000624	−0.079	52833.3	50085.5	54845.7	42	2828
ICRF J225717.3 + 074312	2254 + 074	22 57 17.30312249	07 43 12.3024770	0.00000391	0.0000828	−0.001	52174.3	47011.4	54601.7	52	1007
ICRF J225805.9 − 275821	2255 − 282	22 58 05.96288481	−27 58 21.2567425	0.00000320	0.0000455	0.175	50766.7	46875.8	54907.7	1559	19519
ICRF J230343.5 − 680737	2300 − 683	23 03 43.56462053	−68 07 37.4429706	0.00002212	0.0001313	0.071	53693.5	49650.8	54706.7	19	91
ICRF J232044.8 + 051349	2318 + 049	23 20 44.85659790	05 13 49.9525567	0.00000281	0.0000437	−0.082	53208.0	47019.9	54889.8	807	12205
ICRF J232917.7 − 473019	2326 − 477	23 29 17.70435026	−47 30 19.1148404	0.00000929	0.0001188	0.117	51685.6	47305.8	54726.7	64	346
ICRF J233633.9 − 411521	2333 − 415	23 36 33.98509655	−41 15 21.9839279	0.00001435	0.0002856	−0.017	53888.7	53223.4	54726.7	15	61

Table 18—Continued

Designation [a]	Source [b]	α	δ	σ_α (s)	σ_δ ($''$)	$C_{\alpha-\delta}$	Epoch of Observation Mean	First	Last	$N_{\rm exp}$	$N_{\rm obs}$
ICRF J234719.8 − 511036	2344 − 514	23 47 19.86409462	−51 10 36.0654829	0.00001458	0.0002418	0.368	54063.7	53223.4	54723.8	14	85
ICRF J235430.1 − 151311	2351 − 154	23 54 30.19518762	−15 13 11.2130207	0.00000576	0.0001319	−0.484	50462.3	47394.1	51282.8	39	451
ICRF J235600.6 − 682003	2353 − 686	23 56 00.68140587	−68 20 03.4717084	0.00001928	0.0001166	0.044	52861.1	48162.4	54723.8	33	178
ICRF J235753.2 − 531113	2355 − 534	23 57 53.26608808	−53 11 13.6893562	0.00001476	0.0001888	0.270	51084.2	47626.5	54706.7	40	181
ICRF J235810.8 − 102008	2355 − 106	23 58 10.88240761	−10 20 08.6113211	0.00000326	0.0000545	−0.155	52378.0	47394.1	54893.7	196	2707
ICRF J235933.1 + 385042	2356 + 385	23 59 33.18079739	38 50 42.3182943	0.00000359	0.0000436	−0.048	53220.2	49519.8	54907.7	813	10501
ICRF J235935.4 − 313343	2357 − 318	23 59 35.49154293	−31 33 43.8242510	0.00000861	0.0002660	0.051	53392.9	52409.7	54872.7	9	257

[a]ICRF Designations, constructed from the source coordinates with the format ICRF JHHMMSS.s+DDMMSS or ICRF JHHMMSS.s-DDMMSS; they follow the recommendations of the IAU Task Group on Designations.

[b]IERS Designations, previously constructed from B1950 coordinates; the complete format, including acronym and epoch in addition to the coordinates, is IERS BHHMM+DDd or IERS BHHMM-DDd.